Universiteit Antwerpen
Faculteit Wetenschappen
Departement Biologie
Onderzoeksgroep Polaire Ecologie, Limnologie en Geomorfologie

Tidal channel development and the role of vegetation: fundamental insights and application for tidal marsh restoration

Ontwikkeling van getijdengeulen en de rol van vegetatie: fundamentele kennis en toepassing voor schorherstel

Proefschrift voorgelegd tot het behalen van de graad
Doctor in de Wetenschappen
aan de Universiteit Antwerpen
door

Wouter Vandenbruwaene

Promotor: Prof. Dr. Stijn Temmerman
Copromotor: Prof. Dr. Patrick Meire

Antwerpen 2011

Table of contents

Dankwoord

Het is ondertussen meer dan 4 jaar geleden toen ik voor het eerst op de campus Drie Eiken toekwam. Reden was een sollicitatie, over een onderwerp waar ik eigenlijk niet zo veel van af wist, maar wat me wel erg boeide: de morfologie van getijdengebieden. Gewapend met deze interesse trok ik op gesprek, en zoals gehoopt liep alles vlot en was het gevoel goed. Toen PM me op het einde van het gesprek de gevleugelde woorden meegaf: “je moet wel beseffen dat een doctoraat geen nine to five job maar een five to nine job is”, en ST instemmend knikte, wist ik dat mijn lot bezegeld was.

In de eerste plaats wil ik mijn promotor Stijn Temmerman bedanken. Hij was mijn gids doorheen de wondere wereld van slikken, schorren, getijdengeulen, stromingen en andere *Spartinas*. Ik kon steeds bij hem terecht met mijn talloze vragen, wat vaak uitmondde in inspirerende brainstormsessies. Samen met de no-nonsense aanpak van mijn co-promotor Patrick Meire zorgde dit voor de nodige sturing om dit doctoraat tot een goed einde te brengen.

Al de mensen die geholpen hebben tijdens de vele veldcampagnes. Niet enkel voor de geboden hulp maar ook voor de vele leute tijdens en na het veldwerk. Ik denk hierbij in de eerste plaats aan Jean. Hij heeft vele uren moeten doorbrengen in geulen, nog half opgevuld met water, en dit door weer en wind. De Lippenbroekbuddies van het eerste uur: Sander, Johnny, Olivier en Tom. Werken in hetzelfde studiegebied schept een band, zeker als er 13-uurs metingen aan te pas komen. Iedereen die meegegaan is naar de veldsite in Saeftinghe, het waren serieuze ondernemingen! Tenslotte alle onderzoekers die betrokken waren bij de hydralab experimenten in Delft. Het is een zege om aan een dergelijk grootschalig project te kunnen meewerken.

Merci aan Louis Beyens, Marijke, Andrey, Alexandra, Annick, Lucie en Frans voor de leuke en goede samenwerking binnen de PLG-groep. Floor en Lotte voor de inspirerende gesprekken op vrijdag na het werk. En alle overige collega’s binnen de PLG en ECOBE onderzoeksgroepen die direct of eerder indirect hun steentje hebben bijgedragen.

Als laatste wil ik mijn familie en vrienden bedanken, voor hun onvoorwaardelijke steun, zeker tijdens de laatste drukke en hectische maanden van mijn doctoraat. Ik heb nu eindelijk wat meer tijd voor jullie.

Summary

Tidal channel networks play an essential role in tidal ecosystem functioning since they are the major flow paths for water, sediments, nutrients and biota between the intertidal zone and the subtidal estuarine or coastal area. Understanding their morphogenesis and evolution is crucial for (1) the evolution of natural tidal flats and marshes under the influence of environmental changes such as sea-level rise, and (2) the restoration of tidal marshes on formerly embanked land.

The thesis can be subdivided into two large parts. Part 1 (chapters 2, 3 and 4) focuses on the natural tidal environment and studies the role of vegetation in the morphogenesis and evolution of tidal channel networks (objective 1). This part of the thesis can be considered as fundamental research on tidal channel networks. Part 2 (chapters 5 and 6) handles the morphodynamic evolution of a de-embankment site (objective 2), and incorporates fundamental research on tidal channel networks (part 1) within a perspective of tidal marsh restoration. While most studies on the morphogenesis and evolution of tidal channel networks are based on modeling work, this PhD provides new insights based upon field and empirical data.

During the evolution of an unvegetated tidal flat towards a vegetated tidal marsh, the intertidal landscape becomes colonized by dynamic vegetation patches. Chapter 2 explores the flow acceleration around these dynamic vegetation patches (*Spartina anglica*) in a large-scale flow facility, and discusses the implications for the evolution of the intertidal landscape. Results demonstrate that the amount of flow acceleration next to vegetation patches, and the distance from the patch where maximum flow acceleration occurs, increase with increasing patch size. In between the patches, the accelerated flow pattern starts to interact as soon as the ratio patch size (D) / inter-patch distance (d) $\geq$ 0.43-0.67. As the patches grow further, the flow acceleration increases until D/d $\geq$ 6.67-10, from which the flow acceleration between the patches becomes suppressed, and the two patches start to act as one.

Chapter 3 relates the long term evolution of tidal channels to the observed changes on the intertidal platform, i.e., establishment of vegetation and the reduction of tidal prism. Tidal channels properties were hereby determined by use of aerial photographs. This chapter demonstrates that there is a strong impact of intertidal vegetation on the evolution of channel network dimensions, while the role of tidal prism changes is of minor importance.

Chapter 4 compares the flow hydrodynamics of an unvegetated tidal flat with the flow hydrodynamics of a vegetated tidal marsh, and assesses the effect of vegetation on the observed tidal channel properties. Flow patterns were determined by measuring water levels, flow velocities

and flow directions. Results show that during the flood and ebb phase flow patterns in a vegetated tidal marsh are clearly routed through the tidal channel network, whereas on an unvegetated tidal flat the platform floods and drains more like a sheet flow. This results in larger channel widths and channel depths in the tidal marsh compared to the tidal flat (for comparable watershed areas), and the presence of a levee-basin topography on the vegetated marsh platform, which is absent on bare tidal flats.

Chapters 5 and 6 focus on the morphological evolution of a de-embankment site after introducing a daily tidal regime and compare the results with a nearby natural tidal marsh. Chapter 5 hereby handles the morphological evolution of the platform of the de-embankment site by measuring platform elevation changes at locations with different inundation heights. Based on these measurements a model was built which predicts long-term (75 years) elevation changes under different scenarios of mean high water level (MHWL) rise. In the de-embankment site (CRT) the MHWL follows the increase in CRT surface elevation (for details see chapter 5). Under a scenario of no MHWL rise in the estuary, this results after 75 years in a 2-2.5 times larger elevation gain in the CRT marsh, and a faster reduction of spatial elevation differences compared to the natural tidal marsh. Under a scenario of constant MHWL rise the equilibrium elevation is lower in the CRT marsh and is reached almost 2 times faster. Under a scenario of accelerated MHWL a CRT marsh is much less able to keep up with the MHWL rise.

Chapter 6 assesses the channel initiation and channel development in the de-embankment site. Channel network properties were determined based on topographical surveys. Results demonstrate that several tidal channel properties develop quickly: after 2 to 3 years the cross-sectional area of the former ditches is in equilibrium with the corresponding watershed areas, and moreover there is a rapid headward growth of newly forming channels and tributary channel formation near the channel heads. Newly formed channels preferentially develop in the low elevated zones, however the overall channel drainage density and channel cross-sectional area of the newly formed channels is after 4 years still lower compared to the natural tidal marsh, indicating that further channel network extension and continued channel deepening must be expected during the coming years.

Samenvatting

Getijdengeulnetwerken vervullen een essentiële rol in het functioneren van getijdenecosystemen vermits ze de belangrijkste stroompaden vormen voor water, sedimenten, nutriënten, en biota tussen de intergetijdenzone en de subtidale estuariene gebieden of de kustgebieden. Inzicht in hun morfogenese en evolutie is cruciaal voor (1) de evolutie van natuurlijke slikken en schorren onder invloed van omgevingsveranderingen zoals zeespiegelstijging, en (2) het herstel van schorren op eerder ingepolderd land.

De thesis kan onderverdeeld worden in twee grote delen. Deel 1 (hoofdstukken 2, 3 en 4) richt zich op de natuurlijke getijdengebieden en bestudeert de rol van vegetatie in het proces van morfogenese en evolutie van getijdengeulnetwerken (doelstelling 1). Dit deel van de thesis kan beschouwd worden als fundamenteel onderzoek op getijdengeulnetwerken. Deel 2 (hoofdstukken 5 en 6) behandelt de morfodynamische evolutie van een ontpolderingssite (doelstelling 2) en implementeert hierbij fundamenteel onderzoek op getijdengeulnetwerken (deel 1) in een context van schorreherstel. Terwijl de meeste studies met betrekking tot de morfogenese en evolutie van getijdengeulnetwerken gebaseerd zijn op modeleerwerk, geeft dit doctoraat nieuwe inzichten gebruik makende van velddata en empirische data.

Het intergetijdenlandschap wordt tijdens de evolutie van een niet-begroeid slik naar een begroeid schor gekoloniseerd door dynamische vegetatiepatches. Hoofdstuk 2 onderzoekt de stroomversnelling rond deze dynamische vegetatiepatches (*Spartina anglica*) in een grootschalige stroomfaciliteit, en bespreekt de implicaties voor de evolutie van het intergetijdenlandschap. Resultaten tonen aan dat de hoeveelheid stroomversnelling naast de vegetatiepatches, en de locatie waar maximale stroomversnelling naast de patch plaatsvindt, toeneemt met toenemende patchgrootte. Het versneld stroompatroon tussen de patches begint te interageren vanaf een verhouding patchgrootte (D) / patch tussenafstand (d) $\geq$ 0.43-0.67. Met toenemende patchgroei neemt ook de stroomversnelling verder toe. Vanaf een waarde D/d $\geq$ 6.67-10 wordt de stroomversnelling tussen de patches echter onderdrukt en beginnen de twee patches zich te gedragen als één patch.

Hoofdstuk 3 linkt de lange termijn evolutie van getijdengeulen aan de waargenomen veranderingen op het intergetijdenplatform (i.e. de vestiging van vegetatie en de reductie van het getijprisma). De eigenschappen van de getijdengeulen werden bepaald gebruik makende van luchtfoto's. Hoofdstuk 3 toont aan dat er een sterke impact is van intergetijdenvegetatie op de evolutie van de geulnetwerkdimensies, terwijl de rol van het getijprisma van minder belang is.

Hoofdstuk 4 vergelijkt de stroomhydrodynamica van een niet-begroeid slik met de stroomhydrodynamica van een begroeid schor, en beoordeelt het effect van vegetatie op de geobserveerde getijdengeulnetwerken. Stroompatronen werden bepaald door waterhoogtes, stroomsnelheden en stroomrichtingen te meten. Resultaten tonen aan dat tijdens vloed en eb, stroompatronen in een begroeid schor duidelijk doorheen het getijdengeulnetwerk stromen, terwijl op een niet-begroeid slik het platform eerder als een 'sheet flow' draineert en irrigeert. Dit resulteert in grotere geulbreedtes en –dieptes voor het schor (voor vergelijkbare toestroomgebieden met het slik), en de aanwezigheid van een 'levee-basin' topografie op het begroeide schorreplatform.

Deel 2 (hoofdstukken 5 en 6) richt zich op de morfologische evolutie van een ontpolderingssite na introductie van een dagelijks getijregime, en vergelijkt de resultaten met een nabijgelegen natuurlijk schor. Hoofdstuk 5 onderzoekt hierbij de morfologische evolutie van het platform door hoogteveranderingen te meten op locaties met verschillende overstromingsdieptes. Gebaseerd op deze metingen werd een model gemaakt dat de lange termijn (75 jaar) hoogteveranderingen voorspelt, en dit voor verschillende scenario's in stijging van 'mean high water level' (MHWL). Belangrijk hierbij is dat in de ontpolderingssite een hoogtetoename van het CRT oppervlak resulteert in een toename van het CRT MHWL. Voor een modelscenario zonder stijging in MHWL resulteert dit na 75 jaar in een 2-2.5 maal grotere hoogtetoename in het CRT schor en een snellere reductie van de ruimtelijke hoogteverschillen in vergelijking met het natuurlijk schor. Voor een scenario met constante stijging in MHWL is de evenwichtshoogteligging lager in het CRT schor en wordt dit niveau bijna 2 maal zo snel bereikt. Voor een scenario met versnelde stijging in MHWL blijkt een CRT schor minder in staat te zijn om de stijging in MHWL te volgen.

Hoofdstuk 6 beoordeelt de beginnende, en de verdere geulontwikkeling in de ontpolderingssite. De eigenschappen van de geulnetwerken werden bepaald op basis van topografische metingen. Resultaten tonen aan dat sommige eigenschappen van getijdengeulen snel ontwikkelen. Zo is na 2 tot 3 jaar de dwarsdoorsnede van de vroegere grachten in evenwicht met de bijhorende toestroomgebieden, groeien de 'hoofden' van de nieuwe geulen snel, en is er ontwikkeling van aftakkingen nabij de geulhoofden. Nieuwgevormde geulen ontwikkelen zich bij voorkeur in de laaggelegen zones. Desalniettemin zijn de algemene geuldichtheid (volledige gebied) en de dwarsdoorsneden van de nieuwgevormde geulen na 4 jaar nog steeds lager in vergelijking met een natuurlijk schor. Dit toont aan dat de komende jaren een verdere uitbreiding van het geulnetwerk en een verdere geulverdieping kan verwacht worden.

Chapter 1:

Introduction

W. Vandenbruwaene

1.1 Estuaries and low elevated coastal areas

Estuaries and low elevated coastal areas form the transition zone between the land and the marine environment. The intertidal zone, which is the zone between low and high water level, is occupied by lower-lying non-vegetated tidal flats and higher-lying vegetated tidal marshes (Figure 1.1). The tidal flats and marshes provide a number of valuable ecosystem services (Costanza et al., 1997). Due to the shallow water depths and the presence of vegetation, they have an important function in the dissipation of tidal energy and storm surges, and hence play a crucial role in the protection of surrounding land against flooding (Costanza et al., 2008; Mitsch and Gosselink, 2000; Wamsley et al., 2010). Tidal flats and marshes are further essential for the deposition of sediments (e.g., Temmerman et al., 2004b), the cycling of nutrients (e.g., Gribsholt et al., 2005; Jacobs et al., 2008; Struyf et al., 2006), and the primary production of biomass within the larger-scale estuarine and coastal system (Mitsch, 2000; McLusky and Elliot, 2004).

Figure 1.1 Higher-lying vegetated tidal marsh and lower-lying non-vegetated tidal flat (Paulina marsh, Westerschelde estuary, SW Netherlands). In this case the transition between tidal marsh and tidal flat is formed by a cliff and the tidal flat is partly colonized by vegetation.

Despite these valuable ecosystem functions, estuaries and coastal areas are the last decades characterized by a global loss in tidal flat and marsh area (Lotze et al., 2006), mainly induced by human activities such as embankment and harbor construction. Due to climate change and the increasing threat of sea-level rise and increased storm intensity and frequency (Intergovernmental Panel on Climate Change IPCC, 2007), several countries have now plans to restore tidal marshes on formerly embanked land, or have executed such plans rather recently (Bakker et al., 2002; Cox et al., 2006; French, 2006; Maris et al., 2007; Pethick, 2002; Williams and Faber, 2001; Wolters et al., 2005).

Whether or not de-embankment and the restoration of tidal marsh ecosystem functions will be successful is largely dependent on the induced sedimentation and erosion processes. On the one hand will an increase in surface elevation by sediment deposition affect the water storage capacity of a de-embanked area and hence its buffering effect on flooding. On the other hand is sediment deposition crucial for the colonization and evolution of tidal flats and marsh ecosystems.

1.2 Tidal channel networks

The generally flat platforms of tidal flats and marshes are typically dissected by branched networks of tidal channels (Figure 1.2). These tidal channel networks play an essential role in tidal ecosystem functioning since they are the major flow paths for water, sediments, nutrients and biota between the intertidal zone and the subtidal estuarine or coastal area. Understanding their morphogenesis and evolution is crucial for (1) the evolution of natural tidal flats and marshes under the influence of environmental changes such as sea-level rise, and (2) the restoration of tidal marshes on formerly embanked land.

The morphogenesis of tidal channel networks has been studied mainly through morphodynamic modeling (e.g., Fagherazzi and Furbish, 2001; Fagherazzi and Sun, 2004; D'Alpaos et al., 2005; Marciano et al., 2005; Temmerman et al., 2007; Kirwan and Murray 2007; D'Alpaos et al., 2007b). Existing models typically considered the initial formation of tidal channel networks as a quick morphodynamic process (e.g., Fagherazzi and Sun, 2004; D'Alpaos et al., 2005). After the rapid network initiation, slower, more long-term (10-100 years) processes are considered to take place during which the tidal network evolution interacts with the morphodynamic and ecological evolution of the surrounding intertidal platform (e.g., Kirwan and Murray, 2007; D'Alpaos 2007). First, an intertidal platform may evolve by sediment accretion from an initially unvegetated tidal flat, low in the tidal frame, towards a higher elevation, where colonization by marsh vegetation takes place. Subsequently, continued mineral and organic sediment accumulation direct the vegetated marsh platform towards a high equilibrium position in

the tidal frame (e.g., Allen, 1990; Allen, 2000; Pethick, 1981; Temmerman et al., 2003a). During this process the increase in platform elevation thus results in (1) vegetation establishment at a certain point in time, and (2) a gradual decrease in flooding frequency and tidal prism (which is the volume of water that floods and drains from the intertidal basin). Typical long-term changes in channel properties that are considered, are the gradual channel infilling as the tidal prism decreases due to platform accretion (D'Alpaos et al., 2006), and the meandering of tidal channels (Marani et al., 2002).

Figure 1.2 (a-b) Oblique aerial photographs of the Saeftinghe tidal marsh (Westerschelde estuary, SW Netherlands) (Photos: Stichting het Zeeuwse Landschap). (c) Tidal channel in a vegetated tidal marsh. (d) Tidal channel in a unvegetated tidal flat.

Apart from above described morphodynamic models, relatively few empirical field data exist on the initial formation and temporal evolution of tidal channel networks. This is probably because most of the tidal channel networks observed in the field are already in an equilibrium state. Hence the equilibrium geometric properties of tidal channel networks have been studied in detail (e.g., Fagherazzi et al., 1999; Rinaldo et al., 1999a; Rinaldo et al., 1999b; Marani et al., 2003; Novakowski et al., 2004; Shi et al., 1995a), but empirical data on the initial formation and temporal evolution of channel networks is scarce. Therefore, the initial formation of tidal channel

networks may be best studied after restoration or creation of new intertidal areas, since here the formation of tidal channel networks mostly must start from a non-channeled landscape state (D'Alpaos et al., 2007a; Wallace et al., 2005; Williams et al., 2002). With regard to the long-term evolution of tidal channel networks, no field data exist that relate changes in flow hydrodynamics (induced by vegetation establishment and reduced tidal prism) to the evolution of tidal channel networks. Typically, modeling studies assume that tidal prisms flood and drain from the intertidal platform entirely through the channel network, and hence predict that channel dimensions (width, depth) become smaller as the surrounding platform accretes higher in the tidal frame. However, field studies have shown that a large part of the tidal prism (~50 %) may flood and drain from intertidal platforms as sheet flow rather than as concentrated flow through the channels (French and Stoddart, 1992; Temmerman et al., 2005a).

1.3 Vegetation

Once a tidal flat becomes vegetated, we may assume that some important changes in flow hydrodynamics occur, affecting the sedimentation and erosion processes in the intertidal zone. At an initial stage, a tidal flat is typically colonized by vegetation patches of pioneer species. Experimental studies on the scale of individual vegetation patches (a few meters in diameter) of the pioneer species *Spartina anglica* (typical colonizer in estuaries and coastal areas in NW Europe), have shown that the tidal flow concentrates and accelerates around the vegetation patches, as a consequence of the friction exerted by the vegetation, and that this flow concentration may eventually cause erosion (e.g., Bouma et al., 2009; van Wesenbeeck et al., 2008). On the landscape scale, it has been shown by modeling (Temmerman et al., 2007) that, when the patches expand in size, the flow is increasingly concentrated in between the expanding vegetation patches which may lead there to channel erosion. Once the intertidal platform becomes entirely vegetated (i.e., the tidal marsh), the vegetation canopy strongly reduces platform flow velocities, and at the same time concentrates the flow in the tidal channels (Temmerman et al., 2005b).

The vegetation patches that colonize a tidal flat are dynamic in time. To what extent these changes in patch size and inter-patch distance affect the flow hydrodynamics, and how this may play a role in the channel formation on the intertidal platform is unknown so far. Moreover, no field data exist on the effect of vegetation establishment on the longer-term evolution (~10-100 years) of tidal channel networks.

1.4 The Scheldt estuary

After the major inundations along the Flemish part of the Scheldt estuary in 1976, the Belgian government launched the so-called Sigmaplan in 1977 to protect the estuary from flood disasters, by proposing (1) the heightening and strengthening of the dykes, (2) the building of a storm surge barrier, and (3) the construction of so-called flood control areas (FCA's) on formerly embanked land. However, continued mean high water level (MHWL) rise and increased human activity led respectively to a MHWL rise in the estuary of up to 1.5 m over the last century (Temmerman et al., 2004b) and a relative decrease in intertidal surface of about 20% (Meire et al., 2005). As a consequence, a revision of the Sigmaplan was necessary and it was decided to no longer build a storm surge barrier, but to extend the number of FCA's instead, and to foresee that an important part of these FCA's would be installed as FCA's with a controlled reduced tide (CRT) (i.e. that only a part of the tide in the estuary is introduced into the FCA-CRT areas). In this way, the protection against storm surges is combined with the restoration of tidal marsh ecosystem functions (**Chapter 5**; Cox et al., 2006; Maris et al., 2007). These FCA-CRT areas are constructed in such a way that they are connected with the estuary via a culvert or sluice system through the dyke, and are surrounded by a ring dyke to protect the surrounding land against flooding. The function is dual: (1) protection against storm surge flooding by the temporary storage of water during extremely high water levels, and (2) restoring tidal marshes by introducing the reduced tidal regime.

Whether or not these constructed tidal marsh areas will attain their objectives is largely dependent on the morphological evolution. First, the formation of a tidal channel network can be considered as necessary to successfully introduce the ecosystem functions of tidal areas. Secondly, changes in platform elevation are wanted for the colonization and evolution of tidal marsh ecosystems, however without endangering the preconceived water storage capacity and safety function. To evaluate the success of de-embankment, it is crucial to compare the de-embankment sites with natural intertidal areas. This inter-comparison enables to assess at what rate de-embankment sites evolve and at what time an equilibrium state is reached (e.g., for the channel drainage density, the platform elevation compared to MHWL), or in more general terms to assess when de-embankment sites are able to provide the ecosystems functions of the natural intertidal areas.

1.5 This study

As described in this chapter (**Chapter 1**), most studies on the morphogenesis and evolution of tidal channel networks are based on modeling work. A first objective of this thesis is to provide new insights on the channel properties and flow hydrodynamics in the intertidal landscape, based upon field and empirical data. Special attention goes out to the role of vegetation, both during the initial evolution of an unvegetated tidal flat towards a vegetated tidal marsh, as during the more long-term evolution of a low elevated tidal marsh towards a high elevated tidal marsh. The second objective focuses on the morphological evolution of a de-embankment site and the implications towards the safety and restoration functions of these areas. Essential questions hereby are: (1) how fast does a channel network develop and reaches an equilibrium state, and (2) how does the elevation of the platform change in the long-term and what is the effect of sea-level rise on elevation changes.

The thesis can be subdivided into two large parts. Part 1 (Chapters 2, 3 and 4) focuses on the natural tidal environment and studies the role of vegetation in the morphogenesis and evolution of tidal channel networks (objective 1). This part of the thesis can be considered as fundamental research on tidal channel networks. **Chapter 2** hereby explores the flow hydrodynamics around dynamic vegetation patches in a large-scale flow facility, and discusses the implications for the evolution of the intertidal landscape. **Chapter 3** relates the long term evolution of tidal channels to the observed changes on the intertidal platform, i.e., establishment of vegetation and the reduction of tidal prism. And **Chapter 4** compares the flow hydrodynamics of an unvegetated tidal flat with the flow hydrodynamics of a vegetated tidal marsh, and assesses the effect of vegetation on the observed tidal channel properties. Part 2 (Chapters 5 and 6) handles the morphodynamic evolution of a de-embankment site (objective 2), and incorporates fundamental research on tidal channel networks (Part 1) within a perspective of tidal marsh restoration. First, **Chapter 5** focuses on the observed platform elevation changes after introducing a daily tidal regime in the de-embankment site, models the more long-term (75 years) elevation changes under different scenarios of sea-level rise, and discusses the implications towards the safety and restoration objectives. Secondly **Chapter 6** studies the channel initiation and channel development after introducing the tidal regime, and assesses the rate of network evolution by comparing the tidal channel properties of the de-embankment site with the channel properties of a mature natural tidal marsh. **Chapter 7** is the synthesis of this PhD work and summarizes the most important findings on channel formation in the natural tidal environment, and reviews tidal channel initiation and platform evolution in a de-embankment site.

Chapter 2:

Flow interaction with dynamic vegetation patches: implications for biogeomorphic evolution of a tidal landscape

W. Vandenbruwaene, S. Temmerman, T. J. Bouma, P. C. Klaassen, M. B. De Vries, D. P. Callaghan, P. van Steeg, F. Dekker, L. A. van Duren, E. Martini, T. Balke, G. Biermans, J. Schoelynck, and P. Meire

Journal of Geophysical Research., 116, F01008, doi:10.1029/2010JF001788 (2011)

Abstract

Feedbacks between vegetation growth, water flow and landform are important for the bio-geomorphic evolution of many landscapes, such as tidal marshes, alluvial rivers and hill slopes. While experimental studies often focused on flow reduction within static homogeneous vegetation, we concentrate on flow acceleration around and between dynamically growing vegetation patches that colonize an initially bare landscape, with specific application to Spartina anglica, a pioneer of intertidal flats. Spartina patches were placed in a large-scale flow facility of 16x26 m, simulating the growth of two vegetation patches by increasing the patch diameter (D=1-3 m) and decreasing the inter-patch distance (d=2.3-0 m). We quantified that the amount of flow acceleration next to vegetation patches, and the distance from the patch where maximum flow acceleration occurs, increase with increasing patch size. In between the patches, the accelerated flow pattern started to interact as soon as $D/d \geq 0.43$-0.67. As the patches grew further, the flow acceleration increased until $D/d \geq 6.67$-10, from which the flow acceleration between the patches was suppressed, and the two patches started to act as one. These findings are in accordance with theory on flow around and between non-permeable structures, however the threshold D/d values found here for permeable vegetation patches are higher than for non-permeable structures. The reported flow interactions with dynamic vegetation patches will be essential to further understand the larger-scale bio-geomorphic evolution of landscapes formed by flowing water, such as tidal flats, floodplain rivers and hill slopes.

2.1 Introduction

Recent studies emphasize that two-way interactions between biological and physical processes, so called *bio-geomorphic* feedbacks, play a key role in the formation and evolution of many landscapes (see Corenblit et al., 2008; Murray et al., 2008 for a recent review). For example, the establishment of vegetation in an initially bare landscape modifies the patterns of water and air flow and of sedimentation and erosion, while the modified flow and sedimentation-erosion patterns influence the spatial patterns of vegetation establishment and die-back. These kinds of biological-physical feedbacks seem to determine the formation of both vegetation and landform patterns as landscapes evolve from a bare state to a vegetated state, or vice versa. This has been recently demonstrated for a number of landscape types, such as intertidal landscapes (e.g., D'Alpaos et al., 2007b; Kirwan and Murray, 2007; Marani et al., 2007; Temmerman et al., 2007), alluvial river channels and floodplains (e.g., Murray and Paola, 2003; Tal and Paola, 2007), dune landscapes (e.g., Baas and Nield, 2007) and hillslopes (e.g., Collins et al., 2004; Istanbulluoglu and Bras, 2005).

Most of the studies mentioned above are based on simulation modeling, while limited empirical data exist on the plant-flow feedbacks that occur when an initially bare landscape is colonized by patchy vegetation that dynamically grows in time. Flow hydrodynamics have been traditionally studied within homogeneous, static vegetation in flumes (e.g., Nepf and Vivoni, 2000; Shi et al., 1995b; Shi et al., 1996) and in the field (e.g., Leonard and Luther, 1995; Leonard and Croft, 2006; Neumeier and Amos, 2006). Such studies support the classical view that vegetation reduces flow velocities and hence reduces erosion and promotes sedimentation. However, in the case of patchy vegetation, recent flume and field studies have shown that more complex, so-called scale-dependent feedbacks occur (Bouma et al., 2009; Temmerman et al., 2007; van Wesenbeeck et al., 2008): at a small scale, within the vegetation patches, flow velocities and erosion are indeed reduced, and it has been experimentally demonstrated that this results in improved plant growth (positive feedback) (Van Wesenbeeck et al., 2008); but at a larger scale, the water is partly forced to flow around the vegetation patches, leading there to increased flow velocities, to erosion (Bouma et al., 2007), and to inhibition of plant growth just next to the vegetation patch (negative feedback) (Van Wesenbeeck et al., 2008) (Figure 2.1a).

Although scale-dependent feedbacks around static vegetation patches have been empirically demonstrated (Bouma et al., 2009; van Wesenbeeck et al., 2008), it is not known yet how dynamic vegetation patches, which grow in size and consequently come closer to each other, affect the *strength* of the scale-dependent feedbacks. In other words, the effect of patch size and inter-patch distance on the flow acceleration around vegetation patches is not yet understood.

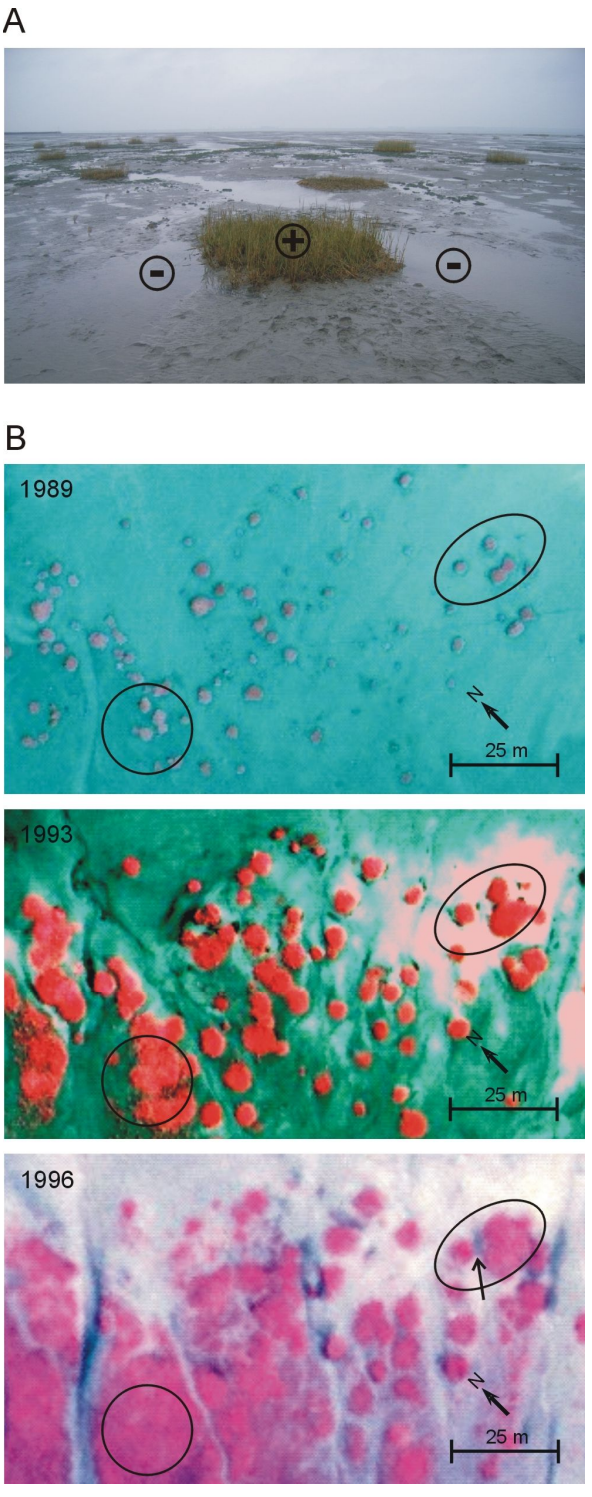

Figure 2.1 (a) Scale-dependent feedbacks around a vegetation patch in an intertidal landscape (*Spartina anglica* patches, SW Netherlands). The positive feedback (+) within the vegetation patch leads to flow reduction, sediment accretion, and improved plant growth. The negative feedback (-) around the patch results in flow acceleration and erosion, which negatively affects the plant growth conditions. (b) Aerial photographs showing the evolution of an intertidal landscape in time (SW Netherlands). The lateral expansion of patches results in an increase of patch size, and a decrease of inter-patch distance (cf. 1989 and 1993, patches within ellipse). In between the growing patches erosion may occur, resulting in channel initiation, and a stop in the lateral patch expansion (cf. 1993 and 1996, patches within ellipse, arrow points towards a pool, initiated by erosion in between the patches). The circle shows the growth of neighboring patches that merge into a closed vegetation field.

It has been shown that scale-dependent feedbacks between organisms and their environment result in the self-organization of regular spatial patterns in a broad range of ecosystems (see Rietkerk and Van de Koppel, 2008 for an overview). Recently there are strong indications that scale-dependent feedbacks are also crucial for the formation of landscapes that are affected by flowing water and that are colonized by patchy dynamic vegetation. For example, aerial photographs and modeling of an intertidal landscape suggests that colonization of a bare mudflat by laterally expanding vegetation patches results in sediment accretion within the vegetation patches and at the same time channel erosion in between the growing vegetation patches (Figure 2.1b, ellipse). The model suggests that, through this mechanism, an initially bare mudflat with few or no channels evolves into a vegetated marsh platform dissected by a regular pattern of channels (Temmerman et al., 2007). Similarly, a scaled flume study demonstrated that an unvegetated river floodplain with a braiding pattern of multiple shallow channels may develop by plant colonization into a vegetated floodplain with a single deep river channel (Tal and Paola, 2007). Here we stress that flow reduction within vegetation patches together with flow acceleration in between laterally growing vegetation patches is the key mechanism that is responsible for the shift between an unvegetated and vegetated landscape state. Therefore, it is crucial to quantify the amount of flow acceleration around and between growing vegetation patches, as a function of patch size and inter-distance. After all, the amount of flow acceleration will determine whether channels start to erode around the patches or not, and whether further lateral patch growth will be inhibited or not.

Scouring by flow acceleration around non-permeable flow-blocking structures, like piles, piers and abutments, has been extensively studied for a wide range of pile group arrangements (e.g., Ataie-Ashtiani and Beheshti, 2006; Melville, 1997; Melville and Chiew, 1999; Oliveto and Hager, 2002). When piles are placed close to each other, the surrounding accelerated flow patterns start to interact in between adjacent piles. It has been demonstrated that this interaction initiates when the ratio between pile diameter (D) and pile inter-distance (d) becomes larger than a critical value ($D/d > 0.25$-0.5) (Ataie-Ashtiani and Beheshti, 2006). This study further showed that piles act as a single pile (i.e. flow acceleration in between the piles is suppressed) as soon as a second, larger critical value of D/d is exceeded ($D/d > 4$).

In accordance with this general theory on flow around non-permeable structures (piles), we hypothesize that flow acceleration around vegetation patches increases with increasing patch size. Furthermore we expect that the accelerated flow starts to interact between two adjacent, laterally expanding vegetation patches, as soon as a first critical value of D/d is exceeded. As the vegetation patches further grow, and D/d further increases, we hypothesize that the two vegetation

patches start to act as one, as a second, larger critical D/d value is exceeded. Although this theory has been supported by experimental data for non-permeable structures (Ataie-Ashtiani and Beheshti, 2006), there are no experimental data yet on vegetation patches. We presume that the critical D/d values for vegetation patches will be larger than for non-permeable structures, due to the permeability of the vegetation patches.

In this study we focus on vegetation patches that colonize an intertidal landscape. *Spartina* species are very common colonizers (*Spartina anglica* in NW Europe; *Spartina alterniflora* in North America and Asia). After initial establishment of *Spartina* seedlings, the plants form circular patches due to lateral clonal growth (Callaway and Josselyn, 1992; Hubbard, 1965; Sanchez et al., 2001). This means that during the colonization process, the size of patches increases and at the same time the inter-patch distance decreases. Aerial photographs indicate that at some locations between expanding vegetation patches, channels may start to erode and further lateral growth of the vegetation patches may stop (Figure 2.1b, ellipse), while at other locations patches may merge together and form bigger *Spartina* fields (Figure 2.1b, circle) (Temmerman et al., 2007). The latter suggests that the flow acceleration around expanding vegetation patches may be suppressed if the patches get close enough to each other, something what has not been tested yet.

Here we present the results of a large-scale flume study, in which field-scale *Spartina anglica* patches (1-3 m diameter) were placed in a large-scale flow facility (16 x 26 meters). The aim of this study was to quantify the effects of increasing patch size and decreasing inter-patch distance on the amount of flow acceleration next to and in between the patches. The experimental results are interpreted in terms of implications for the bio-geomorphic evolution of an intertidal landscape that is colonized by patchy *Spartina* vegetation.

2.2 Methods

2.2.1 The flow facility

The experimental facility was developed at Deltares (www.deltares.nl, Delft, the Netherlands), within the so-called Vinjé basin. The facility consisted of an experimental basin of 16 meters wide, 26 meters long, and 0.5 meters deep, in which a uniform, uni-directional flow was generated (Figures 2.2a and 2.2b). Six pumps, with a total maximum discharge of 1.44 $m^3 s^{-1}$, were used for circulation of the water. In order to break down the turbulence generated by the pumps and to achieve a steady, homogeneous flow in the experimental basin, several flow-guiding and turbulence-damping structures were placed in between the pumps and the upstream edge of the

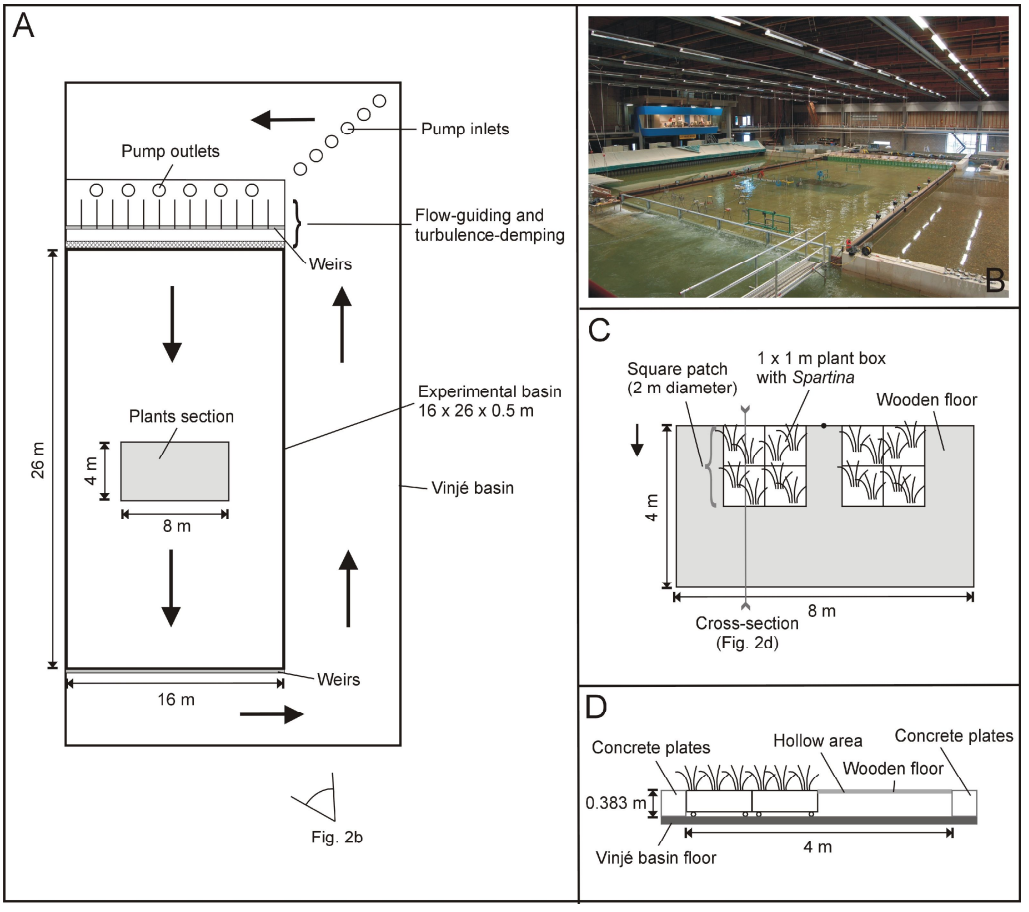

Figure 2.2 (a) Top view of the design of the flow facility. (b) Overview picture of the flow facility. (c) Top view of the central area of the flow facility, used for construction of different patch configurations. (d) Cross-section of the central area (see Figure 2c), showing in which way patch configurations were created.

experimental basin (Figure 2.2a). The water depth and flow velocity in the experimental basin were controlled by changing the height of the 16 weirs at the upstream and the 5 weirs at the downstream edge of the basin, and by changing the discharge of the pumps. For all experiments, water depth and flow velocity in the experimental basin were respectively kept at 0.3 m and 0.3 m/s, a representative flow velocity value for maximal tidal currents as observed on the intertidal flats in the Westerschelde estuary (Netherlands) (Bouma et al., 2005; Temmerman et al., 2005b). To cover the whole range of intertidal flow velocities, additional experiments were done at 0.1 and 0.2 m/s. The floor of the experimental basin consisted of flat concrete, with the exception of a central hollow area of 8 by 4 m that was used for placement of plant boxes or that could be covered by wooden plates (see Figures 2.2c and 2.2d).

2.2.2 Plants

Spartina anglica plants were grown in boxes with a surface area of 1 by 1 m and a depth of 0.2 m. The boxes were first filled to the top with sediment, consisting of silty sand. In open air and with irrigation of salt water, the Spartina anglica plants were subsequently grown from the seeds. Just before the start of each experiment, the plant boxes were moved to the flow basin and sunk into the floor of basin, by partial removal of the wooden floor in the center of the basin. In this way the top of the sediment surface in the plant boxes was always at the same level as the surrounding floor of the basin (Figures 2.2c and 2.2d). By moving and combining more or less plant boxes, *Spartina* patches with different sizes and different inter-distances were formed.

After the experiments the *Spartina anglica* vegetation of four plant boxes was harvested to determine plant characteristics. The vegetation was emergent and had a mean stem height of 0.59 ± 0.18 m, a shoot density of 658 ± 8 stems/m^2, and a standing biomass of 580 ± 49 g/m^2. These values are representative of field conditions (Van Hulzen et al., 2007). The mean shoot diameter at the base was 0.043 ± 0.012 m and halfway up was 0.03 ± 0.011 m.

2.2.3 Different patch configurations

In all experiments two *Spartina* patches were placed next to each other along a cross-section perpendicular to the incoming flow direction (see Figure 2.2c). Three series of experiments were carried out (see Table 2.1 for an overview). The first series mimics the lateral growth of *Spartina* patches as it occurs in the field when patches colonize a tidal flat, by a combination of increasing patch diameter and at the same time decreasing inter-patch distance (Figures 2.3a, 2.3b and 2.3c). In order to separate the effect of patch size and inter-distance, a second series of experiments was performed with a constant inter-patch distance and varying patch size (Figures 2.3d, 2.3e and 2.3c), and a third series with constant patch size and varying inter-patch distance (Figures 2.3f, 2.3b, 2.3e and 2.3g).

2.2.4 Patch shape and incoming flow velocity

The patches in our experiments were square to allow the quick building and breaking down of different patch configurations. However, in the field, individual patches have circular shapes. To determine the effect of patch shape on our results, we compared a square versus a circular patch (Figures 2.3h and 2.3i, and Table 2.1). During the experiments, the incoming flow velocity was always 0.3 m/s, except for one patch configuration where additional runs were done at 0.1 and 0.2 m/s (Figure 2.3f and Table 2.1).

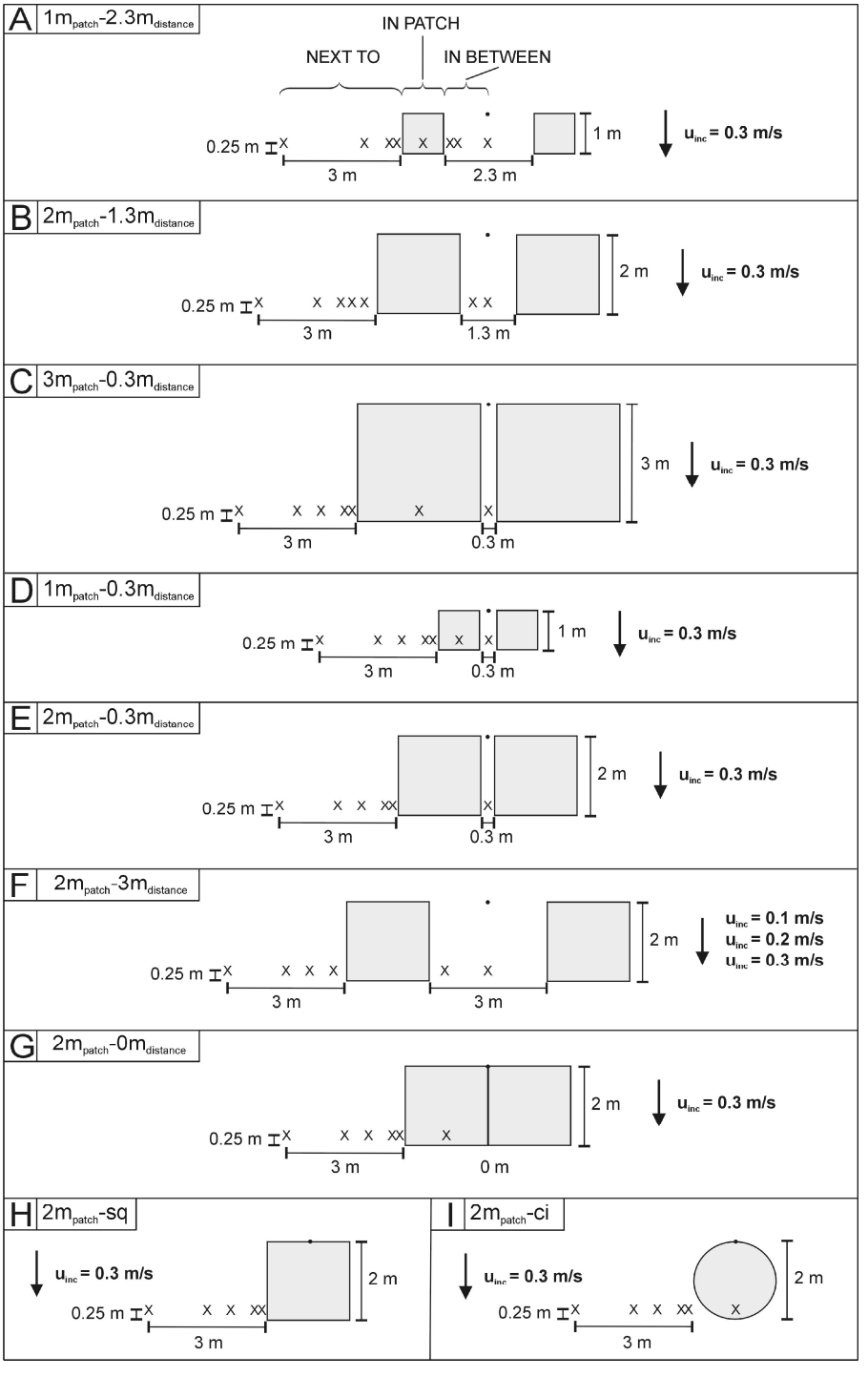

Figure 2.3 (a-i) Overview of all patch configurations used in the experiments with indication of the patch size and inter-patch distance, the flow meter positions (crosses), and the incoming flow velocity.

Table 2.1 Each patch configuration is part of one or two experimental series. In total there were 3 experimental series: (1) effect of increasing patch diameter and decreasing inter-patch distance, (2) effect of varying patch size and constant inter-distance and (3) effect of constant patch size and varying inter-distance. Two additional experiments were carried out to test the effect of patch shape (shape) and different incoming flow velocity (flow). The numbers in the notation of the experimental configurations (first column) refer to the corresponding patch diameter (see third column) and the corresponding inter-patch distance (see fourth column).

Experimental configuration	Number of patches	Patch diameter (m)	Inter-patch distance (m)	Incoming flow velocity (m/s)	Experimental series
$1m_{patch}$-$2.3m_{distance}$	2	1	2.3	0.3	1
$2m_{patch}$-$1.3m_{distance}$	2	2	1.3	0.3	1, 3
$3m_{patch}$-$0.3m_{distance}$	2	3	0.3	0.3	1, 2
$1m_{patch}$-$0.3m_{distance}$	2	1	0.3	0.3	2
$2m_{patch}$-$0.3m_{distance}$	2	2	0.3	0.3	2, 3
$2m_{patch}$-$3m_{distance}$	2	2	3	0.1, 0.2, 0.3	3, flow
$2m_{patch}$-$0m_{distance}$	2	2	0	0.3	3
$2m_{patch}$-sq	1	2	-	0.3	shape
$2m_{patch}$-ci	1	2	-	0.3	shape

2.2.5 Measuring flow velocities

For all experimental runs, flow velocities and directions were measured with 10 electromagnetic flow meters (EMFs) (manufactured by Deltares, frequency 25 Hz) and 1 Acoustic Doppler Velocimeter (ADV) (Nortek Vector, frequency 25 Hz). Two flow meters measured the incoming flow velocity at 5 m in front of the patches, while the other flow meters were placed along a cross-section next to, in the patch, and in between the patches (Figure 2.3a). As the patch configurations were changed, the positions of the flow meters relative to the vegetation edges were kept constant (Figure 2.3). At all locations, flow velocity was measured 0.12 m above the bottom surface. Test runs, in which vertical flow velocity profiles were measured, revealed that the flow velocity measurement at 0.12 m above the bottom is representative of the depth-averaged flow velocity. All flow velocities presented in the results section are time-averaged data over a period of about 12 minutes, with the error bars indicating the standard deviations about the mean.

2.2.6 Dimensionless analyses

To combine the data from different patch configurations, and in this way interpret our results in a more general way, several dimensionless parameters were introduced. First the effect

of patch diameter (D) on the maximum flow velocity (u_{max}) next to a vegetation patch was studied by plotting the D/h ratio (h = the water depth) against the dimensionless maximum flow velocity u_{max}/u_{inc} (u_{inc} = the incoming flow velocity). Secondly the distance from the vegetation edge d_{ve} was written in a dimensionless form (a) by dividing d_{ve} with the patch diameter (d_{ve}/D) for measuring locations next to vegetation patches, and (b) by dividing d_{ve} with the inter-patch distance (d_{ve}/d) for measuring locations in between vegetation patches. The spatial variations in measured flow velocities (u) were analyzed then by plotting d_{ve}/D and d_{ve}/d against the dimensionless measured flow velocity u/u_{max}. Finally, we wanted to assess the effect of patch growth on the degree of flow interaction in between the patches. Therefore as a measure for patch growth the ratio of patch diameter and inter-patch distance (D/d) was plotted against a measure for flow interaction, defined here as the difference in flow velocity next to the patches (u_n) and in between the patches (u_b), both measured at the same distance from the vegetation edge, written in dimensionless form as $(u_b-u_n)/u_{inc}$. We thus speak of flow interaction in between patches when the spatial flow patterns next to and in between the patches become asymmetrical.

2.3 Results

2.3.1 Combination of increasing patch size and decreasing inter-distance (Figure 2.4a)

For the smallest patch size (1 m diameter) with largest inter-patch distance (2.3m), there is a strong reduction of flow velocity (up to 35 % of the incoming flow velocity) within the vegetation patch (Figure 2.4a). Next to and in between the patches, there is also a small decrease in flow velocity close to the vegetation edges (at 0.15 m), but an increase up to 113 % further away from the edges. The increase remains constant over the rest of the cross-section. The flow patterns next to and in between the patches are the same, demonstrating that the two patches are still far away from each other and do not have an interactive effect yet on the flow between the patches.

After the patch size had grown to 2 m, and the inter-patch distance decreased accordingly to 1.3 m, the flow is increasingly accelerated next to and between the patches (up to 154 %) (Figure 2.4a). This increase in flow velocity is larger than for the previous configuration with smaller patches. Next to the patches, close to the vegetation edge, there is first a reduction in flow velocity (less than 50 % at 0.3 m), while only further away from the vegetation edge the flow velocity increases to a maximum value of 152 % at 0.9 m. In between the patches, however there is no reduction in flow velocity at 0.3 m away from the vegetation edge. Instead the flow velocity is directly increased to a maximum value of 154 %, which is comparable with the maximum value next to the patch. Hence the flow patterns next to and in between the patches are not symmetrical

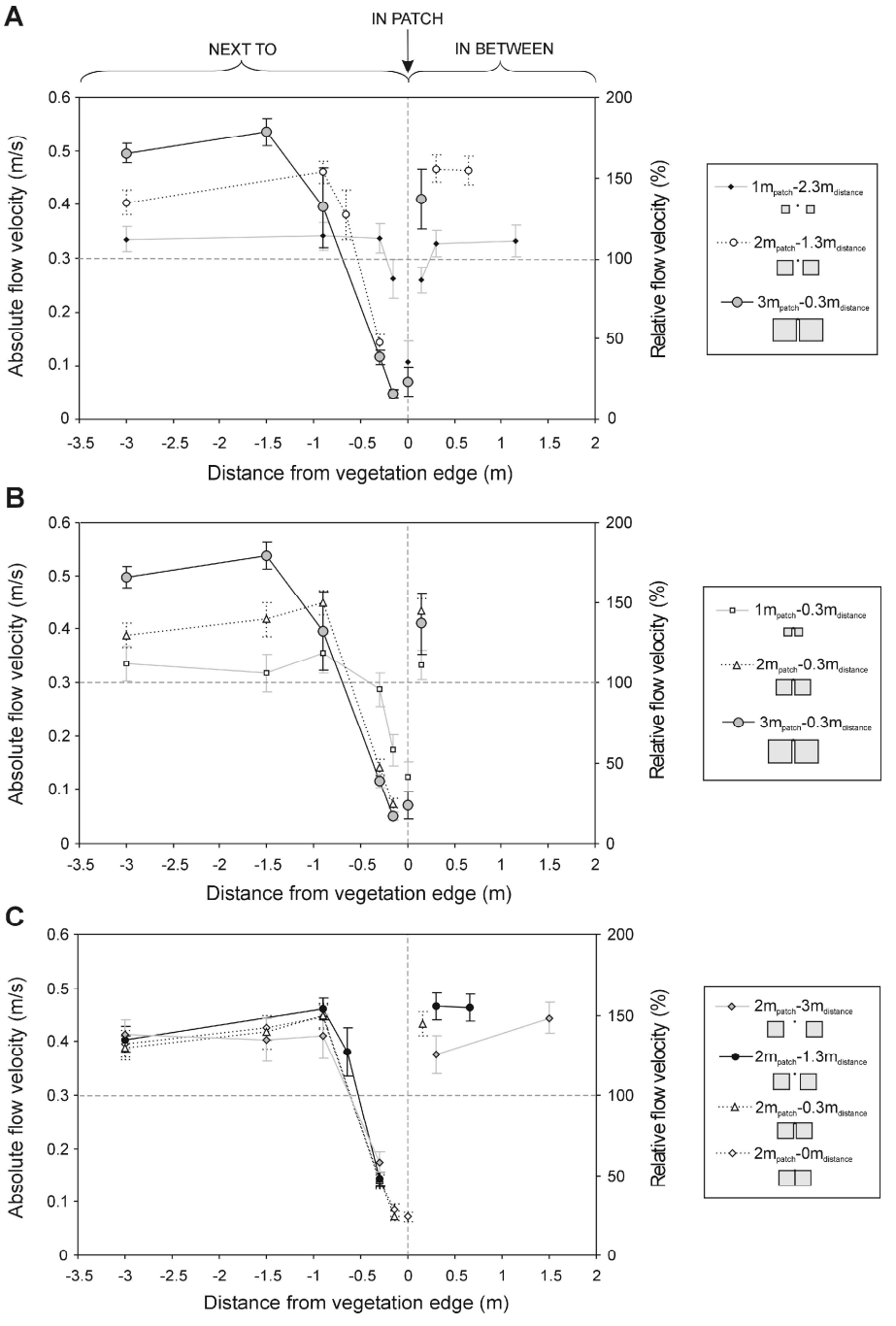

Figure 2.4 Time-averaged flow velocities with standard deviations (error bars), measured on locations (symbols) next to, in between and in the patches for the three experimental series. Flow velocities (in m/s on left Y-axis; in % of incoming flow velocity on right Y-axis) are plotted against the distance from the vegetation edges (m), with the 0-value representing the entire patch width. The incoming flow velocity was 0.3 m/s and is represented by the horizontal dashed line. Flow velocities in the patches are plotted on the vertical dashed line. (a) Combination of increasing patch size and decreasing inter-distance. (b) Increasing patch size, constant inter-distance. (c) Decreasing inter-patch distance, constant patch size.

anymore, demonstrating that the two patches have come so close now that an interactive effect occurs resulting in strong flow concentration in between the patches.

For the configuration with the largest patch size (3 m) and smallest inter-patch distance (0.3m), the maximum flow velocity next to the patches was increased even more up to 181 % (Figure 2.4a). Next to the patches, close to the vegetation edge (at 0.15 and 0.3 m), flow velocities are reduced, while further away from the edge (at 1.5 and 3 m), the flow velocity is increased towards the largest values (respectively 167 and 181 %). The increase in flow velocity in between the patches (up to 138 %) is much lower now than the maximum flow velocity next to the patch (181 %). This is even better illustrated when plotting the maximum flow velocities next to and in between the patches as a function of the patch growth (Figure 2.5a). Next to the patches the

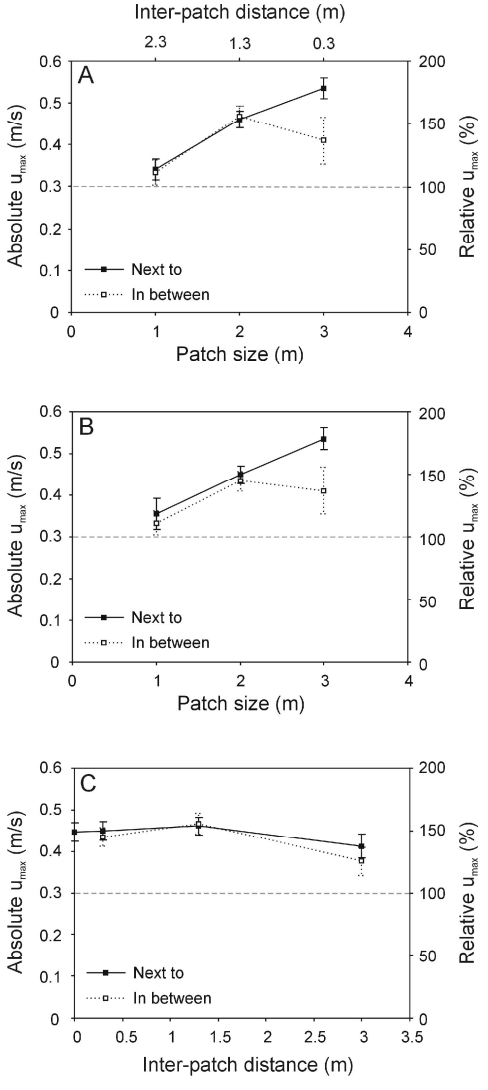

Figure 2.5 Comparison of the maximum flow velocity (m/s and %) next to and in between the patches for the 3 experimental series. (a) Effect of increasing patch size and decreasing inter-distance. (b) Effect of increasing patch size, constant inter-distance. (c) Effect of decreasing inter-patch distance, constant patch size.

maximum flow velocity increases with increasing patch size and decreasing inter-distance. In between the patches the same relationship is found when the patches grow from 1 to 2 m diameter, but when the patches further grow bigger and closer to each other, the flow velocity between the patches again decreases. The latter demonstrates that the two patches interact now in such a way that they start to act as one obstacle that the water is forced to flow around.

2.3.2 Increasing patch size, constant inter-distance (Figure 2.4b)

To distinguish the effect of patch size from the effect of inter-patch distance, a second series of experiments was carried out in which we varied patch size while maintaining a constant inter-distance. To avoid potentially artificial flow concentration caused by a nearby flow facility wall (especially the case for the largest patch size), a small inter-distance of 0.3 m was chosen. Similar to the previous experiment, we observe a reduction in flow velocity next to the patches, close to the vegetation edge, and an increase in flow velocity further away from the edge (Figure 2.4b). As in the previous experiment, the maximum flow velocity next to the patches increases with the patch size (Figure 2.5b, cf. Figure 2.5b and 5a). In between the patches, there is never flow reduction close to the vegetation edge but only flow acceleration (Figure 2.4b). Hence the flow patterns next to and in between the patches are asymmetrical, because the patches are always close to each other (0.3 m inter-distance). The maximum flow velocity next to and in between the patches is similar for the 1 and 2 m patch sizes (Figure 2.5b), but for the 3 m patch size the velocity is smaller in between than next to the patches, demonstrating that the two patches start to act as one object as they become bigger than 3 m in size

2.3.3 Decreasing inter-patch distance, constant patch size (Figure 2.4c)

To assess the effect of inter-patch distance, a third series of experiments was performed with a constant patch size of 2 m and varying inter-distance. Regardless of the inter-patch distance, the flow patterns next to the patches are not significantly different (Figure 2.4c). As observed for the previous experiments, there is always a reduction of flow velocity close to the vegetation edge, while further away from the edge, the flow velocity increased, in this series towards a maximum of about 154 % at 0.9 m. In between the patches the flow is accelerated to a maximum of 156 % and there is no flow reduction close to the vegetation edges as it occurs next to the patches. The maximum flow velocities vary little with changing inter-patch distance, and are comparable between and next to the patches (Figure 2.5c).

2.3.4 Effect of patch size on the maximum flow velocity

We observed that the maximum flow velocity next to the patches is related to the patch size (Figures 2.5a and 2.5b). By plotting all maximum flow velocities, written in a dimensionless form as $u_{max,n}/u_{inc}$, against the dimensionless patch diameter D/h (Figure 2.6), the following relationship was found:

$$\frac{u_{\max,n}}{u_{inc}} = \exp(a\frac{D}{h}) \quad (1)$$

where $u_{max,n}$ = the maximum flow velocity next to the patch (m/s); u_{inc} = the incoming flow velocity (m/s); D = the patch diameter (m); h = the water depth (m), and a is a regression coefficient. In this case, next to a square *Spartina anglica* patch, $a = 0.058$ ($R^2 = 0.94$; $p < 0.0001$) (Figure 2.6, solid line). In between the patches this relationship is valid for $D/h = 3.33$ and $D/h = 6.67$, however for $D/h = 10$ the corresponding $u_{max,n}/u_{inc}$ value clearly plots below the trend line (Figure 2.6).

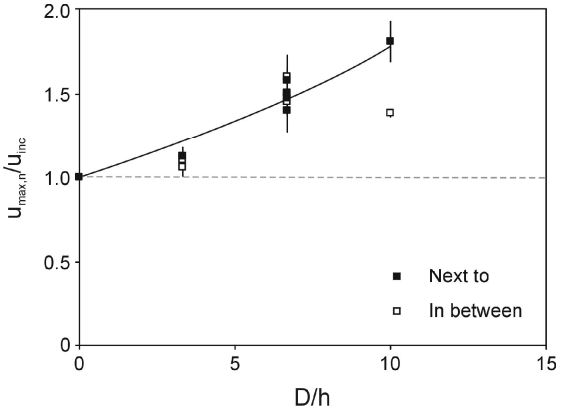

Figure 2.6 Dimensionless representation of the effect of patch size on the maximum flow velocity, including the case D/h = 0.

2.3.5 Quantifying scale-dependent feedbacks

Our observations showed that next to vegetation patches a typical flow patterning occurs: close to the vegetation edge there is a decrease in flow velocity, further away there is an increase (Figure 2.4). Secondly, the flow patterns are clearly affected by patch size (Figures 2.4a and 2.4b), while little effect is observed for the inter-patch distance (Figure 2.4c). To quantify the effect of patch size on the spatial variation in flow velocity next to the patch, a dimensionless analysis was performed, including all data points next to the patches (Figure 2.7a). For values of the dimensionless distance from the patch $d_{ve}/D \leq 0.45$ (left of the dashed line, Figure 2.7a), the

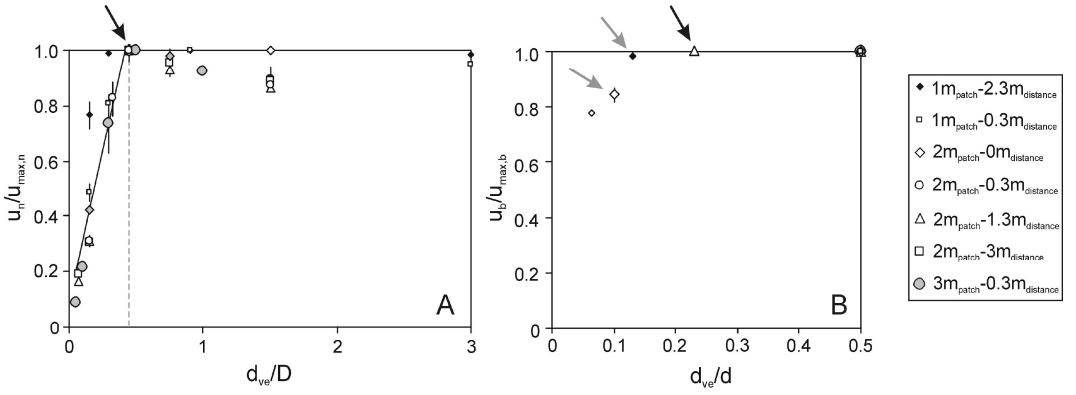

Figure 2.7 The spatial variation in flow velocity presented in a dimensionless way. (a) The effect of patch size on the spatial variation in flow velocity next to the patches. (b) The effect of inter-patch distance on the spatial variation in flow velocity in between the patches.

measured flow velocity increases with d_{ve}/D, until the maximum flow velocity is reached at d_{ve}/D = 0.45 (four of the seven configurations plot at this point, see black arrow Figure 2.7a). The following relationship is then observed for $d_{ve}/D \leq 0.45$ (solid line, Figure 2.7a):

$$\frac{u_n}{u_{\max,n}} = b\left(\frac{d_{ve}}{D}\right)^c + d \quad (2)$$

where u_n = the measured flow velocity at distance d_{ve}/D next to the patch (m/s); $u_{max,n}$ = the maximum measured flow velocity next to the patch (m/s); d_{ve} = the distance from the vegetation edge (m); and b, c and d are regression coefficients. In this case, next to a square *Spartina anglica* patch, b = 2.201 c = 1 and d = 0.074 (R^2 = 0.86; $p < 0.0001$). Equation (1) which describes the effect of patch size on the maximum flow velocity can be rewritten as:

$$u_{\max,n} = \exp(a\frac{D}{h})u_{inc} \quad (3)$$

by substituting $u_{max,n}$ in Equation (2) with Equation (3), the following relationship is found:

$$u_n = \exp(a\frac{D}{h})(b\left(\frac{d_{ve}}{D}\right)^c + d)u_{inc} \quad (4)$$

In this way the flow velocity next to the patch (u_n), at a given distance from the vegetation edge (d_{ve}), can be predicted solely based on the incoming flow velocity (u_{inc}) and the patch diameter (D), taking into account that Equation (4) is only valid if $d_{ve}/D \leq 0.45$.

For $d_{ve}/D > 0.45$, data points plot in a different way (right of the dashed line, Figure 2.7a). There maximum flow velocities may occur up to $d_{ve}/D = 1.5$ (only for one configuration) and in general $u_n/u_{max,n} \geq 0.85$ for all data points. At a certain distance from the vegetation edge there will no longer be patch-flow interaction, there $u_n = u_{inc}$. We did not observe this threshold distance in our experiments (at $d_{ve} = 0.3$ m, $u_n > u_{inc}$ for all patch configurations, see Figure 2.4).

Similar to the above-described dimensionless analysis of the flow patterns *next to* the patches, we performed a dimensionless analysis including all data points *in between* the patches, in order to quantify the effect of inter-patch distance (d) on the spatial flow pattern in between patches (Figure 2.7b). Here the maximum flow velocity is reached at $d_{ve}/d = 0.23$ (black arrow, Figure 2.7b). A significant decrease in measured flow velocities is observed for a d_{ve}/d value between 0.13 and 0.1 (grey arrows, Figure 2.7b). If we consider e.g. 2 m patches at an inter-distance of 1 m, the maximum flow velocity in between the patches occurs at 0.23 m from the vegetation edge ($d_{ve}/d = 0.23$) and the flow velocity significantly decreases only close to the vegetation edge at 0.10 m ($d_{ve}/d = 0.1$). Next to the patches the maximum flow velocity is reached at $d_{ve}/D = 0.45$ (black arrow, Figure 2.7a), and thus for a 2 m patch at a distance of 0.9 m from the vegetation edge. For $d_{ve}/D < 0.45$ the flow velocity next to the patch immediately decreases according to Equation (2) (see solid black line in Figure 2.7a), and reaches much lower u/u_{max} values than in between the patches. This example illustrates that in between interacting patches, the flow becomes concentrated. As opposed to the model next to the patches, we could not construct a significant model in between the patches.

2.3.6 Flow interaction in between patches

Except for the 1 m patches at 2.3 m inter-distance, all patch configurations have an asymmetrical flow pattern, by which we mean that the spatial flow pattern in between the patches differs from the spatial flow pattern next to the patches (Figure 2.4). We consider that there is flow interaction in between two adjacent patches, when the flow patterns next to and in between the patches are asymmetrical. The degree of flow interaction is quantified here as the difference in flow velocities next to and in between the patches, measured at a same distance from the vegetation edge. This dimensionless measure for the degree of flow interaction, $(u_b\text{-}u_n)/u_{inc}$, was related than to a dimensionless measure for lateral patch growth, D/d (Figure 2.8). For the 1 m patches at 2.3 m inter-distance ($D/d = 0.43$, grey arrow, Figure 2.8), $(u_b\text{-}u_n)/u_{inc}$ values are close to

zero (both at 0.15 and 0.3 m), indicating that flow interaction in between patches is absent. Indeed for this configuration, the observed flow patterns next to and between the patches were symmetrical (Figure 2.4a, $1m_{patch}$-$2.3m_{distance}$). However with increasing lateral patch growth (i.e. increasing values of D/d), the degree of flow interaction increases (i.e. $(u_b-u_n)/u_{inc}$ values increase), whereby the strongest increase occurs at 0.3 m from the vegetation edge (cf. both trend lines, Figure 2.8). Considering the measurements at 0.15, 0.65 and 1.5 m, one patch configuration does not follow the observed trend (i.e. $3m_{patch}$-$0.3m_{distance}$, see black arrow, Figure 2.8). There the flow interaction is lower as expected, caused by the suppressing of the flow velocity (see in between, Figure 2.6). We infer that from a given D/d value between 6.67 and 10, patch growth suppresses the increase in flow velocity in between patches.

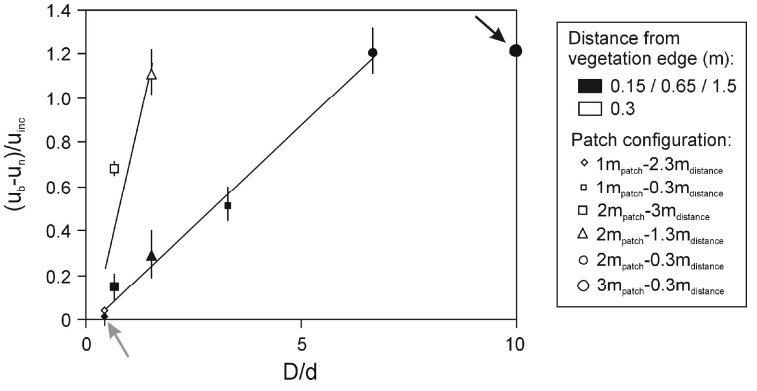

Figure 2.8 The degree of flow interaction $(u_b-u_n)/u_{inc}$ in function of the lateral patch growth D/d.

2.3.7 Comparing square and circular patch shape

The flow patterns next to a square patch and a circular patch were very comparable (Figure 2.9). There is no significant difference in flow velocity for all measuring locations, except

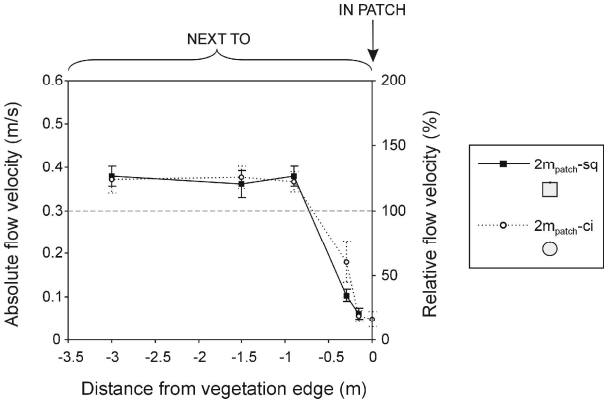

Figure 2.9 Effect of patch shape: comparison of flow velocities (m/s and %) next to a square patch and a circular patch.

at 0.3 m from the vegetation edge where the flow velocity for a circular patch is higher. This may imply that the increase in flow velocity next to circular patches occurs closer to the vegetation edge, and secondly that flow interaction in between circular patches occurs at smaller inter-patch distances. Nevertheless the flow patterns for both shapes were very similar and we may conclude that our experiments with square patches are also representative for circular patches, as observed more commonly in the field.

2.3.8 Effect of varying incoming flow velocity

By using a single patch configuration, the effect of different incoming flow velocities was tested. The relative increase and decrease of flow velocities around the patches was not significantly different for all 3 incoming flow velocities. However, the initiation of erosion, and the limitation of plant growth is determined by the absolute flow velocities. It is clear that the absolute increase in flow velocity increases with greater incoming flow velocity (Figure 2.10).

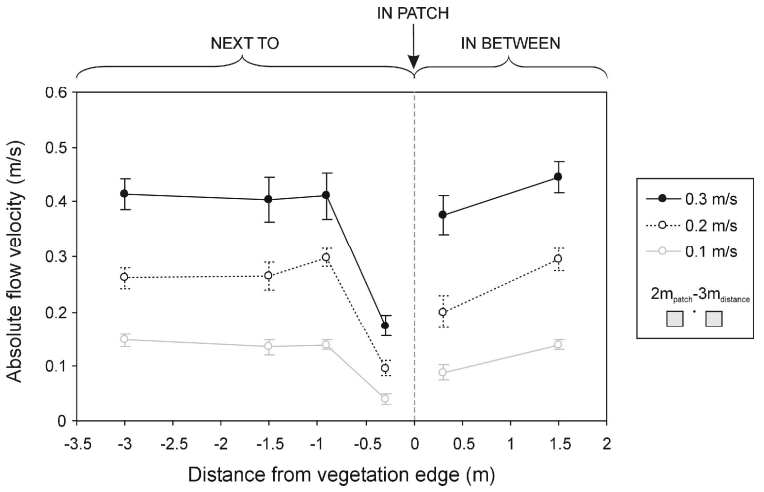

Figure 2.10 Effect of incoming flow velocity. Absolute flow velocities (m/s) plotted against the distance from the vegetation edge (m) for the 3 incoming flow velocities.

2.4 Discussion

The importance of bio-geomorphic feedbacks between vegetation, flow and landform changes is increasingly recognized for many landscape types (Corenblit et al., 2008; Murray et al., 2008). While most bio-geomorphic studies so far are based on models in which vegetation is considered to reduce flow velocities and reduce erosion (e.g., D'Alpaos et al., 2007b; Istanbulluoglu and Bras, 2005), we showed empirically that flow reduction is only a local effect

within and close to vegetation patches, while flow acceleration dominates next to and between the patches. In the field, it has been demonstrated that this flow acceleration next to *Spartina anglica* patches may initiate at some point the erosion of channels (Bouma et al., 2007; Van Hulzen et al., 2007) and thereby limit the further lateral growth of the vegetation (van Wesenbeeck et al., 2008). As the patch size D in our experiments became larger and the inter-distance d smaller, the patches started to interact ($D/d \geq$ 0.43-0.67) and ultimately, when patch size and inter-distance passed a second critical threshold ($D/d \geq$ 6.67-10), the flow acceleration in between the patches again decreased (Figure 2.6). This implies that, once this second critical threshold is passed, the merging of two growing adjacent patches is not hindered anymore by flow acceleration. For the outside, next to the patches, we found a positive relationship between the amount of flow acceleration and the patch size (Figure 2.6), suggesting that channel formation is more likely around larger patches. This is supported by field data, showing that deeper channels occur next to larger *Spartina anglica* patches (van Wesenbeeck et al., 2008). The formation of deeper channels next to laterally growing patches may limit at some point the further expansion of the patch. In the field, experiments with *Spartina anglica* transplants showed that the survival and growth of the transplants was strongly suppressed in the channels (van Wesenbeeck et al., 2008).

Our results on flow interaction between nearby vegetation patches qualitatively agree with general theory on flow around cylindrical, non-permeable flow-blocking structures (e.g. bridge piles or abutments). For such structures, flow interaction was reported at $D/d >$ 0.25-0.5 (D = pile diameter, d = pile inter-distance), depending on the pile-group arrangement (Ataie-Ashtiani and Beheshti, 2006). For *Spartina anglica* vegetation patches, we found that flow interaction occurs when $D/d \geq$ 0.43-0.67 (Figure 2.8). For piles with a side-by-side arrangement (as in our experiments), the piles were found to act as a single pile at $D/d >$ 4 (Ataie-Ashtiani and Beheshti, 2006), while we observed decreased flow interaction between *Spartina anglica* patches for $D/d \geq$ 6.67-10 (Figure 2.8). The critical threshold values that we report are higher for vegetation patches than for piles, likely because piles are non-permeable structures while vegetation patches may be regarded as a porous structure. This effect of porosity is important for vegetation patches with different vegetation densities (e.g. caused by different plant species morphology or different stem densities): with increasing vegetation density, we expect that more water is forced to flow around the vegetation patches, resulting in flow interaction between adjacent patches starting for lower D/d values. As a consequence, vegetation patches with higher vegetation densities will have stronger effects on bio-geomorphic landscape evolution (e.g., stronger flow concentration and channel erosion in between growing vegetation patches) (Temmerman et al., 2007).

In between interacting *Spartina anglica* patches we always observed flow acceleration and flow concentration (Figure 2.7b). But what determines now if growing patches can merge together or not? The answer for this probably lies in the larger scale landscape process. Our experiments demonstrate that for a range of incoming flow velocities, the relative flow acceleration will always remain the same. However, the absolute flow velocity next to and in between the patches depends on the absolute value of the incoming flow (Figure 2.10). So for patches that occur at more sheltered sites, where the incoming flow velocities are lower (e.g. by a high density of surrounding patches), the accelerated flow around the patches remains in absolute terms too low to initiate scouring, which has been shown to be velocity dependent (van Wesenbeeck et al., 2008). Moreover, for single*Spartina* patches in the field, it has been demonstrated that larger patches are characterized by higher growth rates (Balke, 2009). Flow acceleration is thus not only too low to initiate scouring, but also has no effect on the growth patches, despite the increase in flow acceleration around larger patches (Figure 2.6).At these sites, *Spartina* patches can easily merge together and eventually form closed *Spartina* fields. However, if patches are more exposed, incoming flow velocities are higher, and as a consequence the absolute flow acceleration around the patches will be also higher. At this point further lateral patch growth may lead to several evolutionary scenarios. If the ratio between the patch size D and the inter-distance d of expanding vegetation patches exceeds a critical threshold value ($D/d \geq 6.67$-10 for *Spartina anglica* patches, see Figure 2.8), the flow acceleration in between the patches becomes suppressed and patches may merge together. However, if patch growth continues, and the critical threshold value is not exceeded, the increasing flow acceleration will become sufficiently large to initiate channel formation and will limit the further lateral patch growth. The newly formed channels may develop further and evolve towards the larger tidal channels that typically dissect intertidal marsh vegetation (Temmerman et al., 2007). This explanation is supported by time series of aerial photographs, indicating that at some locations the lateral growth of *Spartina* patches is limited by increasing flow-induced erosion next to the patches, while at other locations this limitation does not occur and patches grow together (Figure 2.1b). Furthermore, for the high incoming flow velocities, flow-induced erosion may even lead to erosion of the vegetation patch itself. Reported erosion rates of *Spartina* patches reach values up to 0.1 m/yr, and are not affected by the size of the vegetation patch (Balke, 2009).

In our flume study we always used two square patches that were placed next to each other relative to the incoming flow direction. In the field, more complex situations may occur: the patches are mostly circular in shape (but this had no significant effect on our results, see Figure

2.9), more complex configurations of more than two patches may occur, and the direction of the incoming flow velocity may be variable.

Our study focused on the intertidal landscape, however our results may also have implications for other landscape types. Some similar effects on flow concentration and channel formation have been reported for other landscapes that are affected by flowing water and by the colonization of patchy vegetation. For example, Coulthard (2005) mentioned the formation of erosion gullies next to vegetation patches in a scaled flume study on alluvial channel braiding. In a more extended flume experiment, it has been demonstrated that plant colonization on the floodplain of a braiding river may concentrate the flow to a single river channel (Gran and Paola, 2001; Tal and Paola, 2007). In addition, flow deviation around vegetation patches was also reported for other landscape types, such as hill slopes (e.g., Bochet et al., 2000), high dynamic rivers with emergent vegetation (e.g., Schnauder and Moggridge, 2009), and more low dynamic rivers with submerged vegetation (e.g., Cotton et al., 2006). In the latter, an extensive study of the bed morphology showed channel formation in between vegetation patches.

2.5 Conclusions

Our study quantified the amount and spatial patterns of flow acceleration next to and between dynamically growing vegetation patches of *Spartina anglica* (Figures 2.6 to 2.8, Equations (1) to (4)). We quantified that the flow acceleration next to vegetation patches, and the distance from the vegetation patch where maximum flow acceleration occurs, increase with increasing patch size (respectively Figure 2.6 and Equation (1); Figure 2.7 and Equation (2)). We found that flow interaction in between two patches started as soon as $D/d \geq 0.43$-0.67 (D = patch size; d = inter-patch distance). Further patch growth (increasing D/d) resulted in increasing flow acceleration in between the patches, until a second critical condition was reached, at $D/d \geq 6.67$-10, where flow acceleration was suppressed, and the two patches started to act as one. These findings are in accordance with general theory on flow around and between non-permeable structures, like bridge piles and abutments, however the threshold D/d values reported here for flow interaction and flow suppression are higher than for non-permeable structures, due to the permeability of the vegetation patches. The reported interactions between flow hydrodynamics and dynamic vegetation patches will be essential to further understand the larger-scale bio-geomorphic evolution of tidal landscapes, and other landscapes affected by flowing water and colonized by patchy vegetation, such as river floodplains, river beds, and hill slopes. Our study provides clear empirical evidence that such scale-dependent bio-geomorphic feedbacks should be included in models describing the formation and evolution of landscapes.

Chapter 3:

Intertidal channel evolution: crucial impact of vegetation establishment and minor role of tidal prism change

W. Vandenbruwaene, T. J. Bouma, P. Meire and S. Temmerman

Abstract

The long-term evolution (10-100 years) of tidal channel networks is generally considered to interact with the morphodynamic and ecological evolution of the surrounding intertidal platform. During this evolution, the most important changes on the intertidal platform are: (1) the establishment of vegetation when a bare tidal flat evolves towards a vegetated tidal marsh, and (2) a reduction in tidal prism caused by continued sediment accretion. In this study we assessed the relative role of vegetation establishment and reduction in tidal prism by comparing channel networks of three different stages in the intertidal landscape evolution: (1) a tidal flat, (2) a low elevated tidal marsh, and (3) a high elevated tidal marsh. By use of aerial photographs, we derived for each stage several geometric channel network properties (drainage density, channel width and watershed area), and we compared the changes in geometric relationships during the intertidal landscape evolution. We found that when a tidal flat becomes vegetated there is a strong increase in drainage density. Once the intertidal platform is vegetated no further changes are observed in drainage density as the marsh platform accretes higher in the tidal frame and as the tidal prism decreases. Moreover, the relationship between watershed area and channel width does not change during the evolution of a low elevated marsh towards a high elevated marsh. This is explained by partitioning of the tidal prism between concentrated channel flow versus platform sheet flow. The volumes of water transported as sheet flow are larger for a low elevated marsh (lower position in tidal frame) than for a high elevated tidal marsh, while the volumes of water transported as concentrated channel flow are comparable for both systems. In conclusion this study demonstrates the strong impact of intertidal vegetation on the evolution of channel network dimensions, while the role of tidal prism changes is of minor importance.

3.1 Introduction

Tidal channel networks are a typical feature of intertidal flats and marsh landscapes. They form the main transport paths for water, sediments, nutrients, etc., and hence play a crucial role in the geomorphic and ecological functioning of intertidal landscapes. Predicting the response of tidal channel networks to environmental and human forcing factors, such as sea level rise, is therefore a key issue for understanding the response of intertidal ecosystems.

The formation and evolution of tidal channel networks is generally considered to interact with the morphodynamic and ecological evolution of the surrounding intertidal platform (e.g., Kirwan and Murray, 2007; D'Alpaos 2007). On the long-term (10-100 yr), an intertidal platform may evolve by sediment accretion from an initially unvegetated tidal flat, low in the tidal frame, towards a higher elevation, where colonization by marsh vegetation takes place. Once the vegetated stage is reached, continued mineral and organic sediment accumulation direct the marsh platform towards a high equilibrium position in the tidal frame (e.g., Allen, 1990; Allen, 2000; Pethick, 1981; Temmerman et al., 2003a). During this process the increase in platform elevation thus results in (1) vegetation establishment at a certain point in time, and (2) a gradual decrease in flooding frequency and tidal prism, (which is the volume of water that floods and drains from the intertidal basin). In this study we focus on the effect of vegetation establishment and temporal decrease of tidal prism on the long-term (~10-100 years) evolution of intertidal channel networks.

Firstly, it may be expected that vegetation establishment on an initially bare tidal flat has an important impact on changes in channel network properties. At an initial stage, a tidal flat is typically colonized by vegetation patches of pioneer species. Experimental studies on the scale of individual vegetation patches (a few meters in diameter) of the pioneer species *Spartina anglica*, have shown that the tidal flow concentrates and accelerates around the vegetation patches, as a consequence of the friction exerted by the vegetation, and that this flow concentration may eventually cause erosion (e.g., **Chapter 2**; Bouma et al., 2009; van Wesenbeeck et al., 2008). On the landscape scale, it has been shown by modeling (Temmerman et al., 2007) that, when the patches expand in size, the flow is increasingly concentrated in between the expanding vegetation patches which may lead there to channel erosion. Although this process has been demonstrated to be important during the initial stages of plant colonization taking place on the rather short-term of about one decade (Temmerman et al., 2007), it has not been documented yet whether vegetation establishment has also a more longer-term (~10-100 years) effect on tidal channel network evolution. Here we hypothesize that vegetation establishment results in a long-lasting extension of intertidal channel networks, through the formation of concentrated flow and channel erosion in between vegetated areas.

Secondly, tidal prism is widely considered as the main factor that determines the geometric properties of tidal channels, in which a larger tidal prism implies that larger volumes of water need to be transported to and from the tidal basin through the tidal channels, resulting in larger channel cross-sectional area. Empirical relations between tidal prism and channel cross-sectional area have been demonstrated for tidal inlets (e.g., O'Brien, 1931; O'Brien, 1969; Myrick and Leopold, 1963; Jarrett, 1976), and have recently been used to describe the spatial variations in channel cross-sectional area through an intertidal marsh landscape (D'Alpaos et al., 2010). However the long-term temporal evolution of channel networks, in relation to intertidal platform accretion and resulting decrease of tidal prism, has been studied rather poorly. Long-term (~10-100 years) field observations (e.g., Gardner and Bohn, 1980; Shi et al., 1995a; Steel and Pye, 1997) generally did not cover the entire evolution of a low bare tidal flat towards a high vegetated tidal marsh, and moreover did not relate changes in geometric channel properties to temporal changes in tidal prism. Apart from these empirical studies, mainly simulation models have been used to study the temporal evolution of intertidal channel networks (e.g., D'Alpaos et al., 2005; D'Alpaos et al., 2006; D'Alpaos et al., 2007b; Fagherazzi and Furbish, 2001; Fagherazzi and Sun, 2004; Kirwan and Murray 2007). These models typically assume that tidal prisms flood and drain from the intertidal platform entirely through the channel network, and hence predict that channel dimensions (width, depth) become smaller as the surrounding platform accretes higher in the tidal frame. However, field studies have shown that a large part of the tidal prism (~50 %) floods and drains from intertidal platforms as sheet flow rather than as concentrated flow through the channels (French and Stoddart, 1992; Temmerman et al., 2005a). Temmerman et al. (2005) further demonstrated that the percentage of platform sheet flow (as opposed to concentrated channel flow) increases with inundation depth of the marsh platform. Up to know it has never been studied to what extent intertidal channel dimensions are determined by this partitioning of the tidal prism into platform sheet flow and concentrated channel flow. Based on hydrodynamic field studies of this flow partitioning (Temmerman et al., 2005a), we hypothesize that vertical accretion from a low to a high tidal marsh, and the consequent decrease in tidal prism, would not lead to major changes in channel geometric properties, as the part of the tidal prism that is conveyed through the channels does not change significantly.

In this paper we study the long-term (10-100 years) evolution of tidal channel networks by time-series analyses of aerial photographs. For identical locations, we determined channel geometric properties (drainage densities, mainstream lengths, channel widths, watershed areas, tidal prisms and tidal discharges) during 3 stages of the intertidal landscape evolution, i.e. (1) a low bare tidal flat that evolved into (2) a low-elevated, vegetated marsh, and finally (3) a high-

elevated marsh. We expect that vegetation establishment promotes channel formation and leads to a strong increase in channel drainage density. We further hypothesize that during the evolution from a low to high marsh, i.e. as the tidal prism decreases, only very minor changes occur in the channel network properties.

3.2 Study area

The Scheldt estuary is located in the northwest of Belgium and the southwest of the Netherlands (Figure 3.1a). The estuary is characterized by a semi-diurnal meso- to macrotidal regime, with at the mouth a mean tidal range of 4.46 and 2.97 m during spring and neap tides respectively. Further upstream, the mean tidal range increases towards respectively 5.93 and 4.49 m near Temse, and then progressively decreases to 2.24 and 1.84 m near Ghent (Claessens and Meyvis, 1994). Due to the salinity gradient along the estuary, the tidal marshes can be subdivided into salt, brackish and freshwater marshes (Figure 3.1b). For more detailed information about the Scheldt estuary, we refer to Meire et al. (2005).

The Saeftinghe study area is a 3000 ha intertidal area located in the brackish zone of the estuary with a local mean tidal range of 4.88 m. (Figure 3.1b). Nowadays large parts of Saeftinghe consist of high tidal marsh (elevation above mean high water level) with a marsh platform (with levee-basin topography) that is dissected by a well-developed intertidal channel network. The highest elevated zones are located in the south and northeast, the lowest elevated zones in the northwest. Three major channels (around 800 m wide) drain and irrigate almost the entire intertidal area (Figure 3.1c). The evolution of Saeftinghe can be considered as rapidly. Nearly 80 years ago, the average surface elevation was 0.5-1 m lower and only 25% of the area consisted of vegetated tidal marsh while the remaining area consisted of bare intertidal flats and channels. Nowadays about 70% of the Saeftinghe area is vegetated marsh. In this study we focus on the nowadays high elevated northeastern part of Saeftinghe (Figures 3.1c and 3.1d). The marsh vegetation is dominated there by *Elymus athericus*, a grass-like species that forms a dense vegetation cover, with canopy heights up to 0.9 m. At some lower sites *Aster tripolium* and *Scirpus maritimus* are dominant, while at the highest elevations in the most eastern part a climax vegetation of *Phragmites australis* is already present.

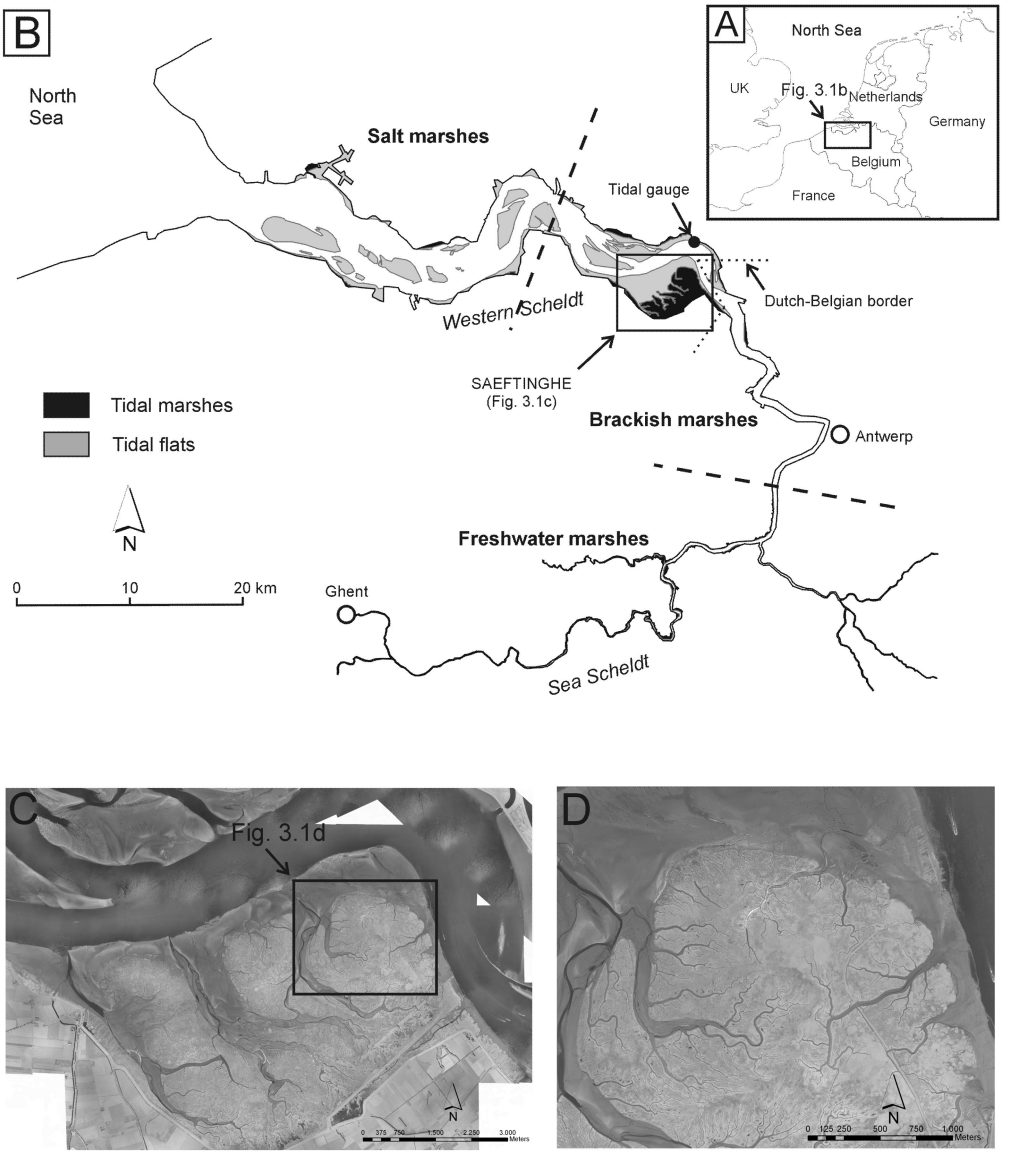

Figure 3.1 The Scheldt estuary. (a) Location within Western Europe. (b) Location of the salt, brackish and freshwater tidal marshes (separated by dashes lines), location of the Saeftinghe study area. (c) False color aerial photograph (represented in black and white) of Saeftinghe. (d) False color aerial photograph (represented in black and white) of the Saeftinghe study area.

3.3 Methods

3.3.1 Site and time step selection – tidal flat, low tidal marsh and high tidal marsh

Many data are available for the Scheldt estuary (e.g. aerial photographs, intertidal elevation maps, tidal data) and this over a period of almost one century. We selected data for the northeastern part of Saeftinghe for three time steps, depending on the availability of both aerial

pictures and elevation maps for these time steps, and in order to cover all stages of landscape evolution from bare intertidal flats, over low-elevated vegetated marshes, up to high marshes. For the first two time steps (1935 and 1957) black and white aerial photographs were digitized (with 0.5 m resolution) and georeferenced. For the third time step (2004) false color infrared aerial photographs were digitized (with 0.5 m resolution) and georeferenced by the RIKZ (Rijksinstituut voor Kust en Zee). Furthermore we collected elevation data from topographic surveys which were performed as close as possible to the years of our aerial photographs. Topographic surveys were performed in 1931 and 1951, and for both campaigns Digital Elevation Models (DEMs; with 20 x 20 m resolution) were available. For the recent aerial photographs (2004) a LiDAR survey was performed in the same year, and a DEM with a 2 x 2 m resolution was available. All DEMs were provided by the RIKZ. Finally tidal data were available for the years of interest, from a tidal gauge station at Bath (close to Saeftinghe; see Figure 3.1b).

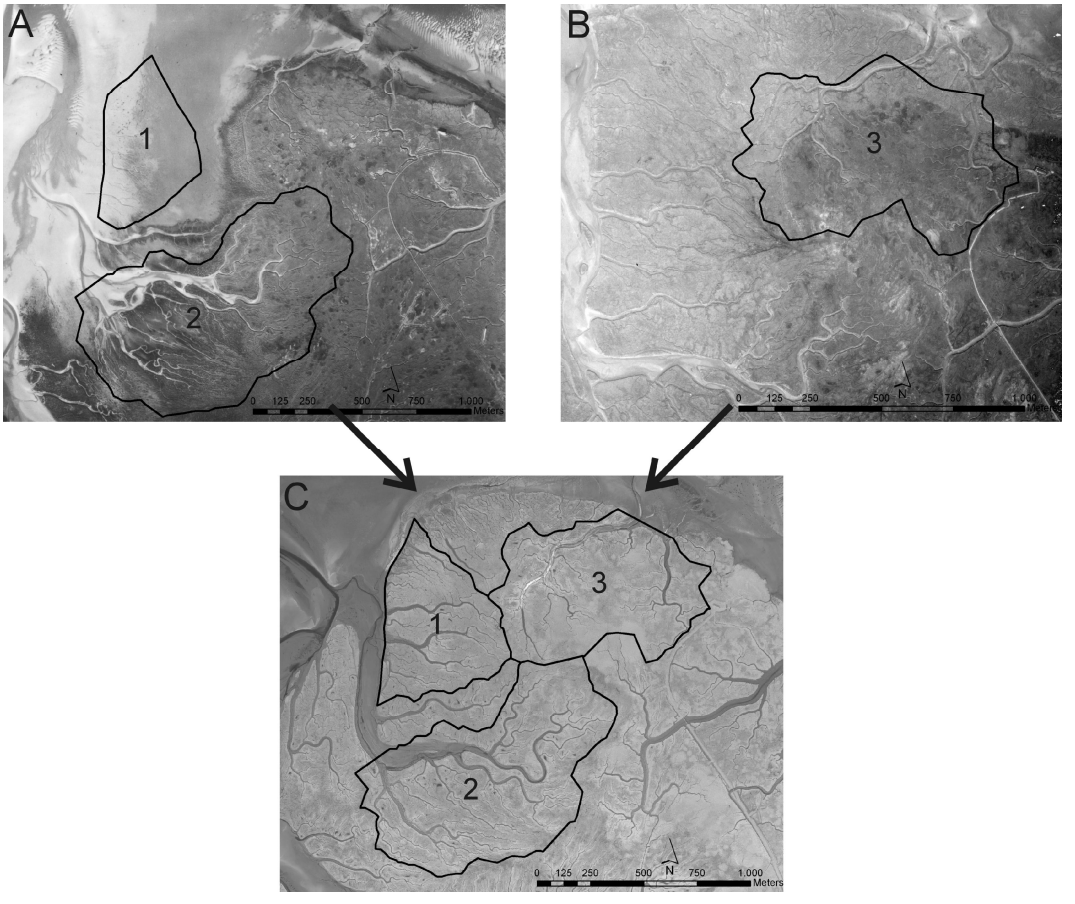

Figure 3.2 Aerial photographs of the Saeftinghe study area in 1935 (a), in 1957 (b) and in 2004 (c), with indication of the three sub-areas (sites). The photographs for 1935 and 1957 are black and white aerial photographs, the 2004 photograph is a false color aerial photograph represented as black and white.

Within the study area, three sub-areas (sites) were selected to cover the different stages during evolution of an intertidal landscape: site 1 is an area that evolved from bare tidal flat (in 1935) to high-elevated vegetated marsh (2004) (Figure 3.2a and 3.2c); site 2 evolved from low-elevated marsh (1935) into high-elevated marsh (2004) (Figure 3.2a and 3.2c); and site 3 was a high-elevated marsh (1957) that remained a high-elevated marsh (2004) (Figure 3.2b and 3.2c). The delineation of the sites was based on the watershed areas of the channel networks. The average and standard deviations of platform elevation, the mean high water level (MHWL), and the position of the platform elevation to MHWL are summarized for the three sites and time steps in Table 3.1.

Table 3.1 Overview of the average and standard deviations of the platform elevation, the MHWL, and the position of the platform elevation to MHWL for the different sites and time steps.

	Site 1		Site 2		Site 3	
	1935	2004	1935	2004	1957	2004
Elevation (mNAP)	1.7 ± 0.35	2.82 ± 0.18	1.97 ± 0.33	3 ± 0.18	2.52 ± 0.15	3.08 ± 0.24
MHWL (mNAP)	2.45	2.73	2.45	2.73	2.46	2.73
aMHWL (m)	-0.75	0.09	-0.48	0.27	0.06	0.35

3.3.2 Extracting tidal channel networks from aerial photographs

Two different methods were necessary to extract tidal channel networks, one for the black and white aerial photographs (1935 and 1957), and one for the false color infrared photographs (2004). Vegetation on false color images has typically a red color (reflection of infrared) and the corresponding pixel values in the red band are high, while tidal channels have no red color and are characterized by low pixel values in the red band. Based on a threshold pixel value in the red band, values above the threshold were reclassified as 1 (=channel), values below the threshold were reclassified as 0 (=marsh platform) (using ArcGIS 9.2). The best value for the threshold pixel value was determined by comparing different extracted networks with the visually observed networks. Although the extracted networks met quite well the observed networks, some of the channel pixels were classified as marsh pixels or vice versa. This resulted for example in loss of channel connectivity for the smallest channels (typical around channel widths of 2 pixels = 1m) or the presence of channel isles in the marsh. For isolated misclassified pixels these errors were solved by using a neighboring filter and reclassifying the pixels correctly. However for clusters of misclassified pixels, situations were more complex and errors could not be solved in a fully automatic manner. As a next step, the extracted raster networks were converted to line features, where lines were created at the boundaries between 0 and 1 pixels, so that the lines represented the channel edges of the networks. Erroneous channel edges were edited manually by visual

comparison with the aerial photographs. The three most important manual steps were: (1) editing some of the line features of the extracted channel edges, (2) deleting unnecessary lines in the marsh or in the channels, and (3) extending channel edges where channel connectivity was lost. By applying this third step, channels were delineated to about channel widths of 0.5 m (= the cell size of the aerial photograph). Some similar semi-automatic approaches have been applied for channel networks extracted from LiDAR data (e.g., Mason et al, 2006).

Although the tidal channels are clearly visible on the black and white aerial photographs, no (semi-)automatic classification could be applied to extract the channel networks. Here the channel networks were delineated manually by constructing line features along the channel edges, based on visual interpretation. Despite the comparable cell sizes of the false color and the black and white photographs, edge detection was more difficult with black and white tones, and channels could be detected up to channel widths of about 1.5 m.

In order to make the channel networks from both types of photographs comparable, we cut off the networks once the channel width is less than 2 m over a distance along the channel of more than 10 m. This approach excludes inconsistencies in the visual interpretation once the channel width approaches the resolution of the aerial photographs.

3.3.3 Quantifying geometric channel properties

3.3.3.1 Building the network skeleton

The network skeleton is the pattern that connects all loci of the channel centerlines (Fagherazzi et al., 1999). Every point along the skeleton was located at the half of the channel width. This was done by construction of Thiessen polygons, based on the line features of the channel edges. As a next step, point features were built every meter along the skeleton. For each of these points we calculated values for the considered geometric parameters explained below (i.e. watershed area, mainstream length and channel width).

3.3.3.2 Watershed area A, mainstream length L and channel width w

In terrestrial river networks watershed areas are exclusively delineated by elevation gradients, however, for tidal channel networks elevation differences are very limited and water flow is mainly determined by energy gradients (Rinaldo et al., 1999a; Marani et al., 2003). Based on earlier modeling work on marsh flow hydrodynamics (D'Alpaos et al., 2005; Marani et al., 2003; Rinaldo et al., 1999a; Temmerman et al., 2005b) the following assumptions were made to determine watershed areas in the Saeftinghe tidal marsh: (1) water over a platform always flows perpendicular away from the nearest stream thread (during flood tide) or perpendicular towards the

nearest stream thread (during ebb tide) at flow velocities that are spatially homogeneous above the platform; (2) the contributing watershed area increases along channels with increasing distance from channel heads, measured along the channel network. The watershed areas were calculated using the hydrology tools in the ArcGIS 9.2 software (Spatial Analyst extension). This algorithm is designed for terrestrial networks and requires as input a Digital Elevation Model. Based on the above described assumption (1), we first created a raster file representing the shortest distance between every platform raster cell and the nearest stream thread. For assumption (2), the distance from the mouth (measured along the network) was spatially represented by an allocation raster file. By summing both raster files, a virtual Digital Elevation Model (DEM) was made, incorporating our postulated assumptions, which was used as input for the hydrology algorithm. As output a flow accumulation raster file was created returning the watershed surface areas along the network skeleton.

The upstream mainstream length L was determined, for every skeleton data point, by attributing the length of the longest upstream channel within the corresponding sub-watershed. By plotting the watershed area against the mainstream lengths, Hack's law (Hack, 1957) was evaluated.

For the channel width w, first a distance raster (Euclidean distance) was created using the channel edges as the target. At the skeleton data points the raster values represented half the channel width, and by attributing and multiplying the raster values with a factor two, the channel width w was found. Channel widths were plotted against watershed area, tidal prism and tidal discharge. Due to absence of vegetation on the tidal flat, edge detection was not possible for site 1 (Figure 3.2a) and channel widths could not be calculated.

3.3.3.3 Mean overmarsh tidal prism and flood discharges

The cross-sectional dimensions of tidal channels (width, depth, cross-sectional area) have traditionally been related to the spring tidal prism, which is the water volume that is stored during spring tides in the corresponding watershed area and that is considered as the maximum water volume that is discharged through the channel cross-section (D'Alpaos et al., 2010; Jarrett, 1976; O'Brien, 1969; Myrick and Leopold, 1963). For tidal marsh channels, especially overmarsh tides (overtop the marsh platform level) are relevant because maximum channel flow velocities typically occur when the surrounding platform is flooded and drained (e.g., Bayliss-Smith et al., 1979; French and Stoddart, 1992; Pethick, 1980; Temmerman et al., 2005b). Here we relate channel dimensions to the mean overmarsh tidal prism, which is the mean tidal prism of all high tides that overtop and thus flood the marsh platform. We calculated tidal prisms for a low elevated

tidal marsh (site 2) in 1935 and the corresponding high elevated site in 2004 (elevations site 2, see Table 1). As a first step, we constructed the flooding frequency distribution in 2004 based on the high water levels between 2000 and 2009 at a station close to Saeftinghe (Figure 3.1b, tidal gauge) (tidal data provided by RIKZ). In 2004, site 2 (platform elevation 3 m NAP) was flooded during 29 % of all high waters, which corresponds with a mean overmarsh high water level of 3.25 m NAP (Figure 3.3a). For the period of 1935 only yearly MHWL and MLWL were available. We constructed the 1935 frequency distribution of high water levels by subtracting the frequency distribution of 2004 with the difference in MHWL between 2004 and 1935 (i.e. 0.28 m, Table 1; frequency distribution 1935, Figure 3.3a). In 1935, site 2 (platform elevation 1.97 m NAP) was flooded during 85% of all high waters which corresponds with a mean overmarsh high water level of 2.59 m NAP (Figure 3.3a). By multiplying the watershed areas with the difference between mean overmarsh high water level and marsh elevation (i.e. water depth, equal to 0.62 m in 1935 and 0.25 m in 2004), the mean overmarsh tidal prisms for 1935 and 2004 were calculated. The same algorithm was used to calculate tidal prisms for the evolution of a high elevated marsh (site 3, see Figure 3.2b and 3.2c and Table 1).

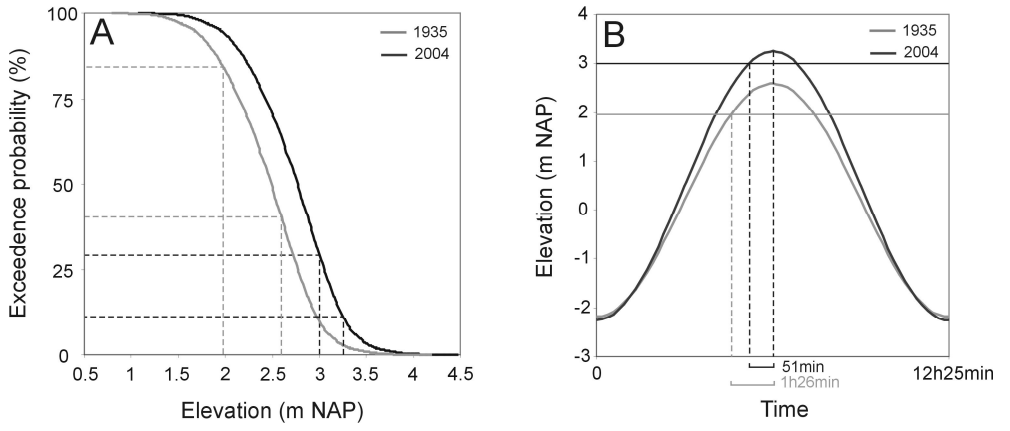

Figure 3.3 (a) High water frequency distributions for the tidal gauge station near Saeftinghe (Figure 3.1b) in 2004 (based on observations from 2000 till 2009) and in 1935 (based on difference in MHWL between 2004 and 1935), with indication of the mean platform elevations and the corresponding mean overmarsh high water levels. (b) 1935 and 2004 mean overmarsh tidal curves, used to determine the halve hydroperiods for site 2. Horizontal lines represent the mean platform elevations.

When intertidal platforms grow higher within the tidal frame, because of sediment accretion, not only the mean overmarsh tidal prism decreases but also the mean time period during which the marsh platform is flooded (i.e., mean overmarsh hydroperiod). Hence intertidal channel dimensions must be ultimately determined by changes in the tidal discharge, which is the tidal prism divided by the hydroperiod. In the case of flood or ebb discharges this is thus halve the

hydroperiod (assuming symmetric tide). The mean overmarsh hydroperiods were calculated then for the two sites (sites 2 and 3, each two time steps), by considering a sinusoidal water level fluctuation with a semi-diurnal tidal period of 12h25min and with the mean overmarsh tidal amplitudes observed for every time step, and accounting for the observed platform elevations for every time step and for every site (Figure 3.3b).

3.3.3.4 Unchanneled flow length and channel drainage density

To evaluate the drainage density of tidal channel networks, previous studies have used the frequency distribution of so-called flow lengths on the marsh platform (e.g., Marani et al., 2003; D'Alpaos et al., 2005; D'Alpaos et al., 2007b). The flow lengths are calculated here as the shortest distance from any platform point to the nearest channel edge. The frequency distribution of flow lengths is then a measure for the channel drainage density: the shorter the flow lengths, the higher the drainage density. Additionally, the channel drainage density was evaluated in the classical way: the total channel length in a sub-watershed was divided by the corresponding sub-watershed area. This analysis was performed for every location along the stream threads.

3.4 Results

3.4.1 Evolution of channel drainage density

During the evolution from a bare low-elevated tidal flat (site 1 in 1935) to a vegetated high-elevated tidal marsh (site 1 in 2004) (Figure 3.2a and 3.2c), a large increase in drainage density is observed (Figure 3.4a). The probability to have larger unchanneled flow lengths is much smaller for the tidal marsh than for the tidal flat. Moreover, the maximum unchanneled flow length is nearly 5 times smaller in the tidal marsh than in the tidal flat (respectively 80 m versus 365 m). Between 1935 and 2004 there is an increase in mainstream length, whereby the largest increase is observed for the largest watershed areas, with about 3.5 times longer mainstream lengths in the tidal marsh than in the tidal flat (550 m versus 160 m, Figure 3.4b). Continued channel tributary formation results in higher channel drainage densities in 2004 (0.01-0.02 m/m²) compared to the initial tidal flat channel drainage densities (< 0.01 m/m²). This channel tributary formation was especially important for the larger watershed areas (> 10000 m², Figure 3.4c). However, for the smaller tidal flat watershed areas, some important channel tributary formation already occurred (Figure 3.4c).

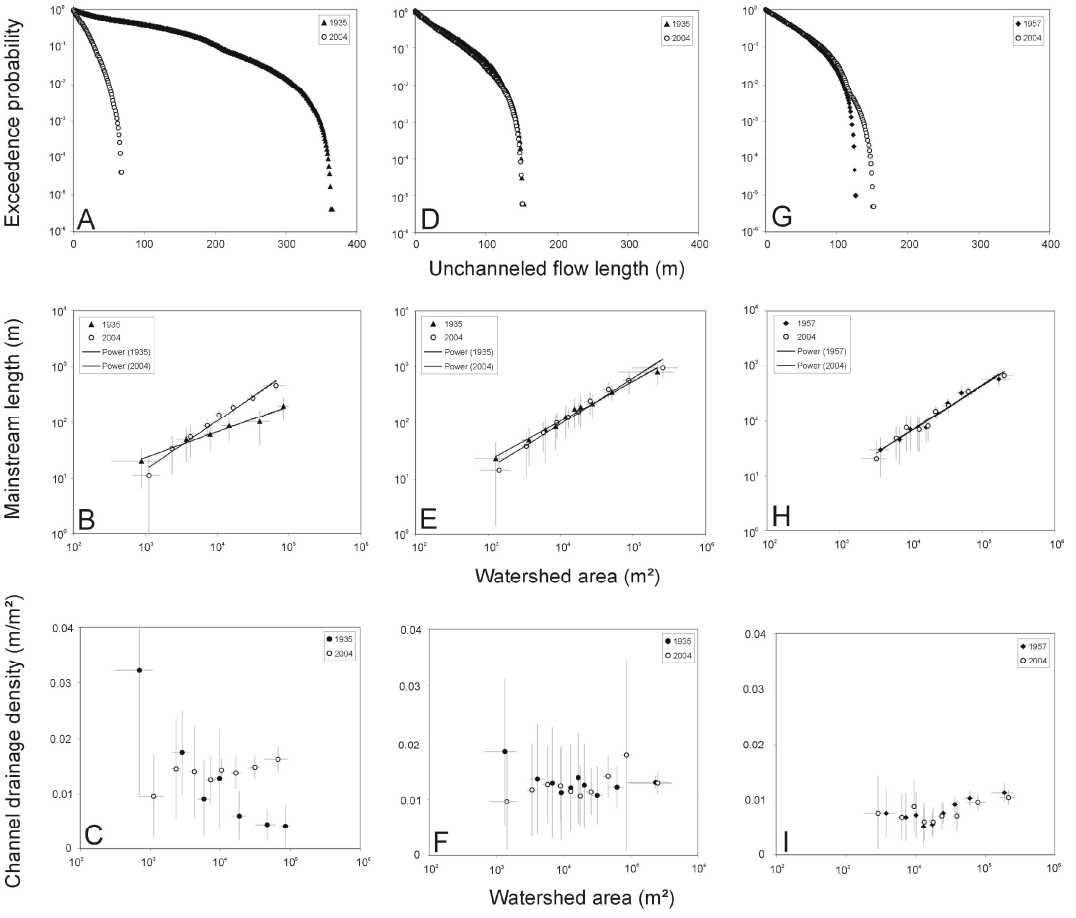

Figure 3.4 Overview of the changes in unchanneled flow length, in watershed area-mainstream length relationship and in channel drainage density, for the evolution of a tidal flat towards a low elevated tidal marsh (a-c), a low elevated tidal marsh towards a high elevated tidal marsh (d-f), and a high elevated tidal marsh towards a high elevated tidal marsh (g-i).

When a low elevated tidal marsh (site 2 in 1935) evolves towards a high elevated tidal marsh (site 2 in 2004) (Figure 3.2a and 3.2c), no important changes in drainage density are observed (Figure 3.4d, 3.4e and 3.4f). The exceedence probability distribution is very similar and the maximum unchanneled flow length is about 150 m for both systems. The relationship between watershed area and mainstream length is nearly equal for the low and high elevated tidal marsh, and the channel drainage densities range between 0.01 and 0.02 m/m².

During the evolution of a high elevated marsh (site 3 in 1957 and 2004, Figure 3.2b and 3.2c) the drainage density does not change much (Figure 3.4g, 3.4h and 3.4i). The exceedence probability of the unchanneled flow lengths is comparable in 1957 and 2004, with the maximum unchanneled flow lengths ranging from 127 m (1957) to 152 m (2004). The mainstream lengths remain equal, and the channel drainage densities vary around 0.01 m/m².

3.4.2 Evolution of channel widths

For all considered time steps and all considered sites (sites 2 and 3), a positive relationship is found between the channel width and the corresponding watershed area, tidal prism and flood discharge (Figure 3.5a-3.5f). For site 1 no such analysis were performed because

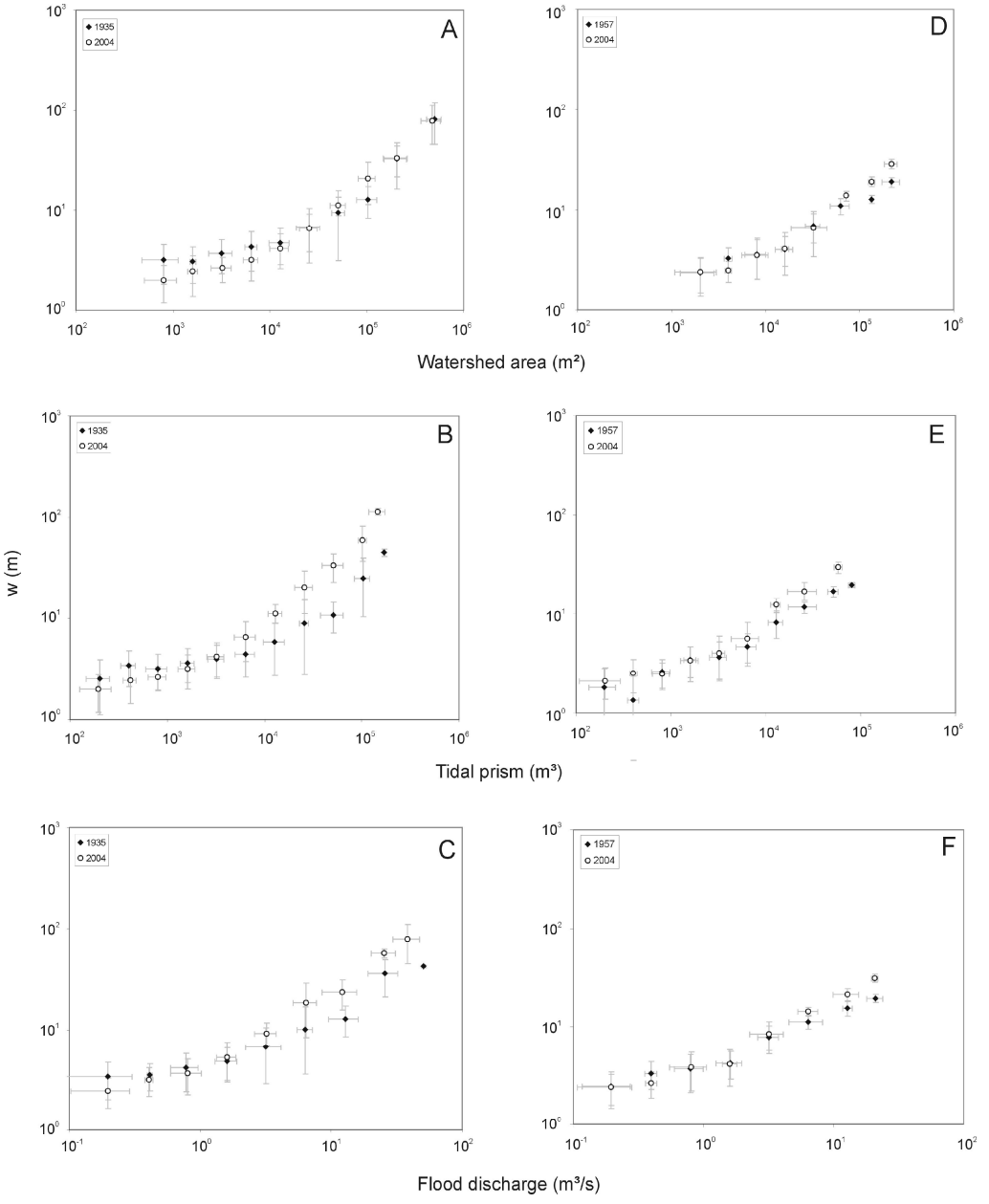

Figure 3.5 Overview of the relationships channel width versus watershed area, tidal prism and flood discharge for the evolution of a low elevated tidal marsh towards a high elevated marsh (a-c) and a high elevated tidal marsh towards a high elevated tidal marsh (d-f).

channel edges could not be detected on the aerial photographs of the tidal flat, and consequently channel widths were not derived. During the evolution of a low elevated marsh (site 2 in 1935) towards a high elevated marsh (site 2 in 2004), the watershed area-channel width relationship shows no significant changes. However, when plotting channel widths against tidal prisms, we observe that the tidal prism-channel width relationships for 1935 and 2004 become strongly deviant with increasing tidal prism (Figure 3.5b). The same is observed for the flood discharge relationship (Figure 3.5c). As a next step in the tidal marsh evolution, a high elevated tidal marsh (site 3 in 1957) evolves further towards a higher position in the tidal frame (site 3 in 2004). The relationship between watershed area and channel width is again comparable for a large range in watershed area, but becomes deviant for the largest watershed areas (Figure 3.4d). A similar deviation is observed for the relationship between tidal prism and channel width (Figure 3.4e), and the relationship between flood discharge and channel width (Figure 3.4f).

3.5 Discussion

Although quite some modeling work has been done recently on the long-term (~10-100 years) morphodynamics of intertidal landscapes (e.g., D'Alpaos et al., 2005; D'Alpaos et al., 2006; Fagherazzi and Furbish, 2001; Fagherazzi and Sun, 2004; Kirwan and Murray 2007; D'Alpaos et al. 2007; Temmerman et al., 2007), comparably little empirical knowledge is available on long-term tidal channel network evolution in response to changes in intertidal vegetation, platform elevation, and tidal prism. Here we demonstrated that vegetation establishment has a particularly strong impact on increased channel drainage density, while subsequent increase in intertidal platform elevation and decrease in tidal prism have no considerable effect on the drainage density and width of channels.

By comparing aerial photographs we found that vegetation establishment on an initially bare intertidal platform leads to a drastic increase of channel drainage density through channel network extension, as demonstrated by the decrease in unchanneled flow length (Figure 3.4a), the increase in mainstream length (Figure 3.4b) and the increase in channel length per square meter (Figure 3.4c). An explanation for this is found in the way by which a tidal flat becomes vegetated. The tidal flat is at a first stage typically colonized by vegetation patches of pioneer species, which is in our study area especially *Spartina anglica*. Within and around these patches, so-called scale-dependent feedbacks occur between the vegetation, the water flow and the sediment transport (**Chapter 2**; Bouma et al., 2009; Temmerman et al., 2007; van Wesenbeeck et al., 2008): at a small-scale, within the vegetation patches, flow velocities are reduced because of the friction exerted by the vegetation on the flow; but at a larger scale, this vegetation friction causes the water

to flow partly around the vegetation patches, leading there to increased flow velocities and eventually to erosion. The latter effect has been empirically demonstrated for *Spartina anglica* patches that colonize tidal flats in the field (van Wesenbeeck et al., 2008) and in flumes (**Chapter 2**; Bouma et al., 2009). Furthermore, vegetation patches are dynamic in time, and an increase in patch size and decrease in distance between the patches results in an increase in the flow concentration in between the patches (**Chapter 2**). The shift from a bare tidal flat, mainly characterized by sheet flow, towards a patchy vegetated intertidal landscape consequently leads to more concentrated flow patterns and an increase in channel formation. In between the formed channels, the vegetation patches further colonize the platform and start to merge, whereas in the channels plant growth has been shown to be inhibited (van Wesenbeeck et al., 2008). Finally a young marsh is formed where closed vegetation fields are dissected by unvegetated tidal channels (e.g., Temmerman et al., 2007). From this point on, the vegetated channel banks become more resistant against erosion due to the soil binding with extensive root systems (Garofalo, 1980), and consequently we observed no important changes in drainage density (Figures 3.4d-3.4i). Also other studies confirm this, and report that after vegetation has established the further planimetric network evolution is mainly characterized by tidal meandering (e.g., Marani et al., 2002).

Although the largest difference in drainage density is observed between a bare tidal flat and a vegetated tidal marsh (Figure 3.4a), some smaller differences in drainage density are present within the vegetated tidal marsh (cf. 2004 in Figure 3.4a and 3.4g). These spatial variations in drainage density may be a consequence of differences in tidal flat colonization by vegetation patches. As demonstrated in **Chapter 2** flow acceleration around vegetation patches, and as a consequence channel initiation, is dependent on the patch size and the distance between the patches. As a tidal flat becomes colonized by different patch configurations, one can expect variable scale-dependent feedbacks around patches, and hence a different evolution of tidal channel networks. Moreover, during the colonization with patchy vegetation, other parameters like elevation affect the evolution of vegetation patches: *Spartina* patches at higher elevations are larger compared to lower elevations (Castellanos et al., 1994), and patches at higher elevations are characterized by higher growth rates (Van Hulzen et al., 2007). However, this does not exclude the presence of large vegetation patches at low elevated sites. As demonstrated in our experiments (**Chapter 2**), flow acceleration between vegetation patches becomes suppressed from a critical threshold ratio between patch size D and inter-distance d ($D/d \geq 6.67$-10 for *Spartina anglica* patches, see Figure 2.8), and patches may start to merge. The spatial variability in drainage density in this study is also observed for other tidal marshes (Marani et al., 2003).

During the evolution of a low elevated vegetated marsh towards a high elevated marsh, there is a large decrease in overmarsh tidal prism due to the much faster increase in platform elevation compared to the rise of mean high water level (MHWL) (Table 1, site 2). In accordance with existing insights and models on tidal channel morphodynamics (e.g., D'Alpaos et al. 2005; D'Alpaos et al.2007; D'Alpaos et al.2010; Kirwan and Murray 2007), one could consider that overmarsh tidal prisms and corresponding tidal discharges flow entirely through the channel network. One would expect then that for equal tidal prisms and discharges, channel widths would be similar on the low marsh (1935) and high marsh (2004), or in other words, the channel widths would have adapted to the increase in marsh elevation and corresponding decrease in overmarsh tidal prisms. However for the larger tidal prism (>10000 m^3) and discharges (>3 m^3/s) we observed a different relationship between channel width and tidal prism in 2004 and 1935 (Figures 3.5b and 3.5c). Although this could be explained by a delay between tidal prism change and adaptation of the channel widths, it is not very likely because channel dimensions adapt rather quickly (in the order of years) to an imposed tidal prism (e.g., **Chapter 6**; Byrne et al., 1975; Wallace et al., 2005; Williams et al., 2002). A much more plausible explanation is found when the tidal prism is considered not to flow entirely as concentrated flow through the channels, but as observed in several studies, is partly considered to flow as sheet flow over the intertidal platform (e.g., French and Stoddart, 1992; Temmerman et al., 2005a). Indeed, by neglecting the sheet flow, the calculated tidal prisms overestimate the real volumes of water that flow through the channels. As demonstrated by field measurements by Temmerman et al. (2005), concentrated channel flow only occurs when the surrounding vegetated platform is flooded by less than 0.2 m of water height above the channel banks, while during higher flooding sheet flow occurs. Because site 2 was on a lower position in the tidal frame in 1935, the tidal prism is a larger overestimation of the channel discharges for 1935 than for 2004. This explains why the channel width-tidal discharge relationship is different for the low marsh (1935) and high marsh (2004) (Figure 3.5c). In reality more water is thus transported as sheet flow in 1935 than in 2004, whereas the amount of concentrated flow through the channels is comparable for both periods. Hence, the relationship between the channel width and the watershed area does not significantly change as the intertidal platform accretes higher in the tidal frame and as the overmarsh tidal prism decreases (Figure 3.5a). This suggests that for equal watershed areas in 1935 and 2004, the same volumes of water flow through the channels, resulting in comparable channel widths. The factor that hereby determines these same volumes of water is most likely the vegetation cover. Due to the large friction difference between the vegetated platform and the unvegetated tidal channels, flow becomes concentrated towards the channels (e.g., Temmerman et al., 2005b). Because the canopy

characteristics (i.e. vegetation height and density) are very comparable for the low marsh in 1935 and the high marsh in 2004, it can be assumed that the volume of water that becomes concentrated in the channels is comparable for both years. Once the vegetation becomes inundated by water levels higher than the canopy height, the above-canopy tidal prism is mainly transported as sheet flow via the marsh edge (Temmerman et al. 2005a; 2005b).

During the evolution of a high elevated tidal marsh (site 3), the decrease in overmarsh tidal prism is much smaller as during the evolution of a low marsh towards a high marsh (cf. site 2 and 3, Table 1). This results in a smaller overestimation of tidal prism and tidal discharge for site 3 compared to site 2 (cf. Figure 3.5e and 3.5b, and 3.5f and 3.5c). However, the changing relationship between tidal prism and channel width is in the case of site 3 also affected by changes in channel width. Indeed, as opposed to site 2 where the relationship between watershed area and channel width is constant in time (Figure 3.5a), an increase in channel width is observed for the larger watershed areas of site 3 (Figure 3.5d). This may be a consequence of changes in sediment supply, caused by dredging activities in the estuary: as the larger channels of site 3 are in direct connection with the estuary (not the case for site 2, see Figure 3.2c), an increase in sediment supply induces channel infilling and thus a decrease in cross-sectional area. This decrease in cross-sectional area is then counterbalanced by an increase in channel width.

This study provides new insights on the evolution of intertidal channel networks that should form the basis for improvement of existing models of intertidal morphodynamics. Most existing models (D'Alpaos et al. 2005; D'Alpaos et al. 2007; Kirwan and Murray 2007) assume that the whole tidal prism floods and drains the intertidal platform through the channel network. Hence these models consider that changes in the tidal prism govern the evolution of channel networks, for example in response to sea level rise. Here we demonstrated empirically that tidal prism changes are not such a good predictor of changes in tidal channel dimensions, and we explained this as the tidal prism is not completely transported as concentrated flow through the channel network, but also partly as sheet flow over the intertidal platform. Furthermore, we demonstrated that vegetation establishment causes important extension of the channel network and leads to increased channel drainage density, which is explained as the vegetation concentrates the flood and ebb tidal exchange towards the channels. The latter effect of vegetation is shown here to be so important that it should be explicitly considered in simulation models of intertidal morphodynamics (e.g., Temmerman et al. 2007), while changes in tidal prism only play a minor role.

3.6 Conclusions

When a tidal flat becomes vegetated there is a strong increase in drainage density. The probability to have larger unchanneled flow lengths is much smaller in the vegetated tidal marsh than in a tidal flat, and the maximum unchanneled flow length is nearly 5 times smaller in a tidal marsh. This is explained as the vegetation friction leads to concentrated flow patterns and channel erosion, while on a bare tidal flat sheet flow dominates. During the evolution of a low elevated tidal marsh towards a high elevated tidal marsh no important changes in drainage density are observed. This is explained by partitioning of the tidal prism between concentrated channel flow versus platform sheet flow. The volumes of water transported as sheet flow are larger for a low elevated marsh (lower position in tidal frame) than for a high elevated tidal marsh, while the volumes of water transported as concentrated channel flow are comparable for both systems. Hence the relationship between watershed area and channel width does not change as the marsh platform accretes higher in the tidal frame and as the tidal prism decreases. In conclusion this study demonstrated the strong impact of intertidal vegetation on the evolution of channel network dimensions, while the role of tidal prism changes is of minor importance.

Chapter 4:

Effects of vegetation on large-scale flow patterns and landforms on intertidal floodplains

W. Vandenbruwaene, T. J. Bouma, P. Meire and S. Temmerman

Abstract

Vegetation exerts an important control on the large-scale flow patterns and landforms in the intertidal landscape. Studies on this effect of vegetation are however scarce and present insights are exclusively based on modeling work. In this research we measured large-scale flow patterns and landforms in the field, both in a vegetated tidal marsh as in an unvegetated tidal flat. Flow patterns were determined by measuring water levels, flow velocities and flow directions. We found that during the flood and ebb phase flow patterns in a vegetated tidal marsh are clearly routed through the tidal channel network, whereas on an unvegetated tidal flat the platform floods and drains more like a sheet flow. In the tidal marsh there is a strong reduction of flow on the vegetated platform and a concentration of flow in the channels, whereas on the tidal flat the channel and platform flow velocities are intermediate and very comparable. These hydrodynamic processes are clearly reflected in the landform differences between vegetated marshes and bare tidal flats: (1) for comparable watershed areas the channel widths and channel depths are distinctively larger in a tidal marsh than in a tidal flat (due to the flow concentration towards channels in a tidal marsh), and (2) vegetated marsh platforms are typified by the presence of a levee-basin topography (due to platform flooding from the channels), while a levee-basin topography is typically absent on bare tidal flats (due to platform flooding as sheet flow).

4.1 Introduction

It is increasingly recognized that landscape formation and evolution is governed by mutual interactions between biological and physical components of landscapes, so-called *bio-geomorphic* interactions (Corenblit et al., 2008; Murray et al., 2008; Reinhardt et al., 2010). For intertidal floodplains (i.e. tidal flats and tidal marshes), recent studies have highlighted that vegetation plays a key role in the routing of water flow and sediment transport (e.g., Temmerman et al. 2005), and therefore must have a determinant effect on landforms (e.g., D'Alpaos et al. 2007; Kirwan and Murray 2007; Marani et al. 2007; Temmerman et al. 2007). This interaction between intertidal vegetation, water flow, and landforms seems determinant for the bio-geomorphic response of tidal marshes, such as their response to sea-level rise by sediment trapping (e.g., Kirwan et al. 2010) and their mitigating effect on storm surge flood propagation (e.g., Wamsley et al. 2010). While all of the above-mentioned studies are based on numerical landscape-scale modeling, which inevitably involves assumptions and simplifications of reality, few or no empirical field studies exist that quantified the impact of intertidal vegetation on large landscape-scale flow patterns and landforms.

An intertidal floodplain typically consists of a rather flat platform, which is either vegetated (i.e. tidal marsh) or unvegetated (i.e. tidal flat), and which is dissected by a network of bare tidal channels. Flow velocity patterns have been studied traditionally on specific isolated locations, either on the platform within and above the vegetation canopy (e.g., Leonard and Croft, 2006; Neumeier and Amos, 2006) or on locations in the channels (e.g., Baylis-Smith et al., 1979). Other studies additionally compared total channel discharges with water volumes above corresponding watershed areas (during high water), demonstrating a partitioning of the tidal prism into concentrated channel flow versus sheet flow (French and Stoddart, 1992; Temmerman et al., 2005a). However, in these cases water volume calculations were based on the classical insights on watershed delineation (e.g., Rinaldo et al, 1999), and no direct measurements of two-dimensional flow patterns, both on the landscape scale or on the smaller scale, were performed. Nevertheless, more recent field work demonstrated that there is an exchange of water between two distinct first-order channels (small-scale), indicating that the classical view on watershed delineation should deserve more care (Torres and Styles, 2007). Moreover, there are to our knowledge no studies that focus on the larger landscape-scale flow patterns, including the interaction between channel and platform flow.

Modeling work demonstrated that vegetation plays a crucial role in the reduction of flow velocities on the intertidal platform, consequently leading to flow concentration in the tidal channels. Hence, flood propagation in the unvegetated channels goes faster as on the vegetated

platform, and consequently water flows from the channel network towards the platform (Temmerman et al., 2005b). Moreover, the model simulations demonstrate that if all vegetation is removed from the platform, flood propagation through the channels and over the platform becomes similar (small difference in flow velocities), and platform flooding rather occurs as sheet flow. However, no empirical data on landscape-scale flow patterns exist that compare the effect of a vegetated platform versus an unvegetated platform. We assume that in the field flow reduction on a vegetated platform (tidal marsh) leads to higher water levels and flow velocities in the channels, and flow directions more or less perpendicular to the channel edges, whereas on an unvegetated platform (tidal flat) water levels and flow velocities are comparable on the platform and in the channels, and the flow rather occurs as a sheet flow.

Concerning the geomorphology of tidal marshes and tidal flats, we expect that these differences in flow patterns will result in different landform features. In general, tidal marshes and tidal flats are characterized by a relatively flat platform, dissected by a network of tidal channels. For the vegetated tidal marshes, a lot of research has been done on the tidal channel properties (e.g., Fagherazzi et al., 1999; Rinaldo et al., 1999; Marani et al., 2003) and on the microtopography of the platform (e.g., Temmerman et al., 2004a). However, not much attention has been paid to the landform features of an unvegetated tidal flat and consequently the comparison of these features with a vegetated tidal marsh is lacking. Firstly, we hypothesize that due to the presence of vegetation on a marsh platform, flow becomes concentrated in the unvegetated tidal channels, leading to larger channel widths and channel depths compared to the channels of an unvegetated tidal flat (i.e. for comparable watershed areas). Secondly, we expect that the presence of vegetation causes flow routing through the channels, followed by flow routing from the channels towards the platform. This leads to a decrease in flow velocity over the platform and results in the formation of levees along the channel edges. On the unvegetated tidal flat, flow rather occurs as sheet flow and no levees are formed along the channel edges.

In this research we focused on the larger landscape-scale flow patterns and the landform features of a vegetated tidal marsh and an unvegetated tidal flat. We therefore collected an extensive field dataset on flow hydrodynamics (water levels, flow directons and flow velocities), and on channel and platform morphology.

4.2 Study area

This study is performed on a vegetated tidal marsh (Saeftinghe) and unvegetated tidal flat (Paulina) within the Scheldt estuary (Belgium, SW Netherlands) (Figure 4.1a). The estuary is characterized by a semi-diurnal meso- to macrotidal regime, with at the mouth a mean tidal range

of 4.46 and 2.97 m respectively during spring and neap tides. Further upstream, the mean tidal range increases towards respectively 5.93 and 4.49 m near Temse, and then progressively decreases to 2.24 and 1.84 m near Ghent (Claessens and Meyvis, 1994). Due to the salinity gradient along the estuary, the tidal marshes bordering the stream channel can be subdivided into salt, brackish and freshwater tidal marshes (Figure 4.1b) (for more detailed information about the Scheldt estuary, see e.g. Meire et al., 2005).

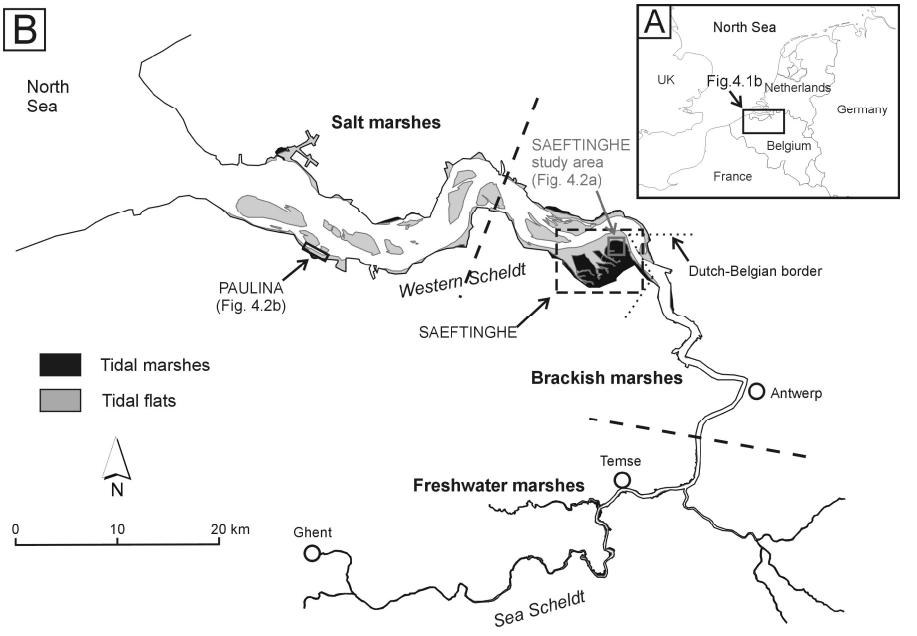

Figure 4.1 The Scheldt estuary. (a) Location within Western Europe. (b) Location of the salt, brackish and freshwater tidal marshes (separated by dashes lines), location of the Saeftinghe and Paulina study area.

The vegetated Saeftinghe tidal marsh is located in the brackish part of the estuary and has an intertidal area of about 3000 ha (Figure 4.1b). Saeftinghe is a typical high tidal marsh (elevation above mean high water level) with a marsh platform that is characterized by a levee-basin microtopography and that is dissected by a well-developed channel network. In this study we focus on a marsh area of 650 by 450 meters in the high elevated northeastern part of Saeftinghe (Figure 4.1b and 4.2a). There the mean marsh platform elevation is 2.9 m NAP (i.e. the Dutch ordnance level = local mean sea level), which is 0.17 m above MHWL (mean high water level), with a standard deviation of 0.19 m. This means that the marsh platform is only flooded by spring tides. The marsh vegetation is dominated by *Elymus athericus*, a species that forms a dense vegetation cover and that during summer has a mean canopy heigth of 0.43 m with a standard deviation of 0.1 m. At some sites *Aster tripolium* and *Scirpus maritimus* are observed, and for the highest elevations in the most eastern part *Phragmites australis* is present.

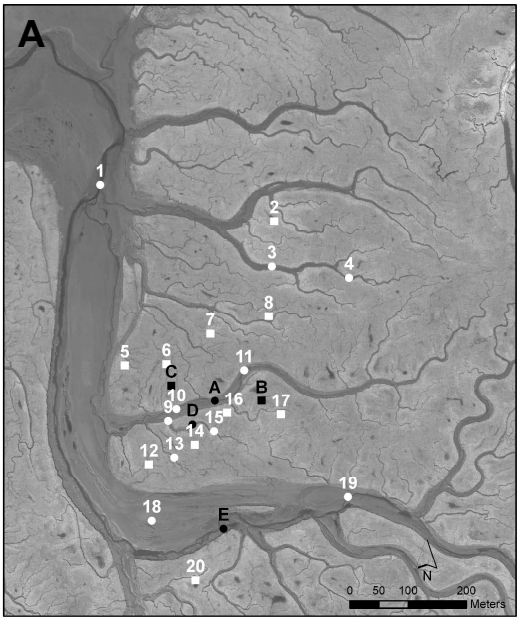

Figure 4.2 Aerial photographs of the Saeftinghe (a) and Paulina (b) study areas. White symbols represent the locations of the water level (divers) measurements, black symbols the locations of the flow measurements. Square symbols indicate the platforms measurements, circles indicate the channel measurements.

The unvegetated Paulina tidal flat is located along the saltwater part of the Scheldt estuary (Figure 4.1b). Between the embankment and the tidal flat, a small salt marsh borders the tidal flat area (Figure 4.2b). The maximum width of the Paulina tidal flat (i.e. shortest distance from marsh edge to the low water line) is nearly 550 m, and the length of the considered study area is 900 m. The elevation of the tidal flat decreases towards the low water line, under a mean slope of 0.18 % (i.e. an elevation decrease of 0.18 m over a distance of 100 m) for the largest part of the tidal flat, and a more steep slope (> 0.3 %) for the area closer to the low water line (boundary between two zones represented by black line, Figure 4.2b). The mean elevation of the tidal flat platform is 0.18 m NAP, which is 2.18 m below MHWL, with a standard deviation of 0.3 m. This means that the tidal flat is inundated by every semi-diurnal tide, even during neap tides. Several channel networks can be distinguished in the tidal flat area, with their network locations largely located in the zone more close to the low water line (Figure 4.2b). One network (most western) has a larger extent and is connected with the tidal marsh channel network.

4.3 Methods

4.3.1 Water levels

In the tidal marsh water levels were measured at 10 locations in the channel network and at 10 locations on the vegetated marsh platform, with a denser grid of locations in the southern part of the study site (locations 12-16, Figure 4.2a). Water levels were measured by use of a diver (Schlumberger, type DIVER). This device contains a water pressure sensor that records the water surface level with an accuracy of 1 cm. To accurately cover the tidal movement, the measuring frequency was set at 2 minutes. At every location, the divers were attached to wooden poles which were hammered into the ground. The x and y coordinates (in Dutch coordinate system) of the divers were determined by use of a DGPS (Thales z-max, accuracy 1-2 cm). The elevations (z coordinates; in m NAP) of the divers' pressure sensors were measured by use of a total station (Sokkia SET510k, accuracy 1-3 mm). Hence the water levels measured relative to the divers' pressure sensors were recalculated to absolute water levels in m NAP. We consider a maximum error on the absolute water levels of ± 1.5 cm (combined error on diver and total station). Divers were attached to the wooden poles about 5 centimeters above the sediment bed surface. On the tidal flat water levels were measured at 6 locations in the channel network and at 10 locations on the tidal flat platform (Figure 4.2b). Installation of the divers and determination of the diver elevations was performed in the same manner as for the tidal marsh. Water levels were measured

on the tidal marsh from the 19th of August till the 25th of August 2009 (spring tides), and on the tidal flat from 27th of August till the 2nd of September 2009 (mean tides).

First, differences in water levels between the channel and platform locations were evaluated by calculating for every time step (every 2 min) the mean and standard deviation of the channel water levels and of the platform water levels. For the tidal marsh we made a distinction between the highest tides (0.43-0.58 meters above the marsh platform) and medium high tides (0-0.43 meters above the platform). The highest tides completely overtop the marsh platform and submerge the vegetation canopy on most locations, whereas the medium high tides overtop most parts of the platform but do not submerge the vegetation canopy. For the tidal flat all observed inundation events completely flooded the platform, and therefore only one group of platform-overtopping tides was considered.

Secondly, spatio-temporal changes in water levels were analyzed by calculating two-dimensional water surfaces in different time steps during the flood phase (starting from the time that all divers become flooded), and during the ebb phase (ending at the time just before the first diver falls dry). Two-dimensional water surface maps were calculated in ArcGis 9.2 by use of spatial interpolation (topo to raster tool in ArcGis 9.2). To improve hydrological correctness of the tidal marsh water surfaces, additional "observation" points were added along the channel network. Water level values were then interpolated to these points based on linear interpolation of the measured channel water levels, following the stream threads. Water surfaces maps were calculated then using all points as input (measured channel and platform water levels, and interpolated channel water levels).

4.3.2 Flow velocities and flow directions

At 5 locations in the tidal marsh (3 in the channels, 2 on the platform) and at 6 locations in the tidal flat (2 in the channels, 4 on the platform) flow velocities and flow directions were measured (see respectively Figures 2a and 2b for locations). Flow measurements were performed with two Nortek Aquadopp Current Profilers (ADCPs) and one high resolution Nortek Aquadopp Current Profiler (HR ADCP). The two ADCPs were equipped with an acoustic frequency of 2 MHz, and were set to a cell size of 0.1 m and a maximum profiling range of 4 m. The HR ADCP was also equipped with an acoustic frequency of 2 MHz, but was set to its minimum cell size of 1 cm, corresponding with a maximum profiling range of 1.28 m. The accuracy of the (HR) ADCP devices is 1% of the measured value ± 0.5 cm/s. The flow velocities in the north-, east-, and z-directions were averaged over time periods of 2 minutes (to obtain the same time intervals as for the water level measurements). Flow measurements were performed during the same periods for

which water levels were measured (see § 4.3.1). In the tidal marsh, the flow was measured first at locations A and B (Figure 4.2a) during 6 tides between the 19th and the 22nd of August. During the subsequent 6 tides from the 22nd till the 25th of August, the ADCP's were moved to locations C, D, E. The HR ADCP was each time placed at a platform location (locations B and C). On the tidal flat, first 6 tides were measured from the 27th till the 30th of August at locations A, B and C (Figure 4.2b). Then all flow devices were relocated to locations D, E and F, and the subsequent 5 tides were measured from the 30th of August till the 2nd of September. The HR ADCP was each time placed at the location with the highest elevation, and thus the lowest inundation heights (locations C and E, Figure 4.2b).

Flow velocities in tidal marshes and flats are known to vary during a tidal cycle, and therefore are best analyzed in relation to the changing water level. In intertidal landscapes there is typically a positive linear relationship between the maximum water level and the maximum flow velocity during a tidal cycle (e.g., Bouma et al., 2005). Therefore the flow velocity patterns were analyzed here for the different locations, by plotting the maximum depth-averaged flood flow velocity against the maximum inundation height at high tide. We investigated this relationship spatially, by including data from all measuring locations, and temporarily, for all observed tides. We compared the relationship between 4 groups of locations: (1) the channel and (2) platform locations on the bare tidal flat; (3) the channel and (4) platform locations on the vegetated marsh. For the tidal flat we excluded the flow measurements at locations C and E because they are located far from the in-channel measurements (locations B and F, Figure 4.2b). Furthermore we expect flow to behave differently at these locations due to the local morphology (i.e. local gentle slope of the platform), and their position relatively close to the vegetated marsh edge. The flow directions were analyzed together with the two-dimensional water surface maps, showing the spatio-temporal changes in water surface slopes and associated flow directions during a tidal inundation cycle (see § 4.3.1).

4.3.3 Channel and platform morphology

On the tidal flat and in the tidal marsh the channel morphology was investigated by topographic surveying using a total station (Sokkia SET510k, accuracy 1-3 mm). For parts of the channel networks, stream thread points were measured about every 2-10 m, together with two accompanying channel edge points (on both sides one). Using this method, the entire range of channel widths was covered in the tidal flat. For the tidal marsh, the same was done for the channels with comparable channel widths, and for a few locations with larger channel widths. For each cross-section (one stream thread point, two edge points), the channel width and channel depth

were determined as respectively the planimetric distance between the two edge points, and the difference in elevation between the mean elevation of the two edge points and the elevation of the stream thread point. Differences between tidal flat and tidal marsh channel morphology were evaluated by plotting the channel width against the channel depth.

Next the relationship between channel width and corresponding watershed area (as a proxy for channel forming discharge; see e.g. Rinaldo et al. 1999a; Marani et al. 2003) was investigated through the channel networks, and this relationship was compared between the vegetated marsh and bare tidal flat. In terrestrial river networks watershed areas are exclusively delineated by elevation gradients, however, for tidal channel networks elevation differences are very limited and water flow is mainly determined by energy gradients (Rinaldo et al., 1999a; Marani et al., 2003). To determine virtual watershed areas in the Saeftinghe tidal marsh and the Paulina tidal flat the following assumptions were made: (1) water over a platform is considered to flow perpendicular away from the nearest stream thread (during flood tide) or perpendicular towards the nearest stream thread (during ebb tide) at flow velocities that are spatially homogeneous above the platform; (2) the contributing watershed area increases along channels with increasing distance from channel heads, measured along the channel network. The watershed areas were calculated using the hydrology tools in the ArcGIS 9.2 software (Spatial Analyst extension). This algorithm is designed for terrestrial networks and requires as input a Digital Elevation Model. Based on the above described assumption (1), we first created a raster file representing the shortest distance between every platform raster cell and the nearest stream thread. For assumption (2), the distance from the mouth (measured along the network) was spatially represented by an allocation raster file. By summing both raster files, a virtual Digital Elevation Model (DEM) was made, incorporating our postulated assumptions, which was used as input for the hydrology algorithm. As output a flow accumulation raster file was created returning the watershed surface areas along the stream threads. By plotting the watershed areas against the channel widths the differences in channel forming mechanisms between the tidal marsh and the tidal flat were assessed. For the tidal flat only smaller watershed areas and corresponding channel widths could be included because the largest network (with the larger watershed areas) (Figure 4.2b, most westward network) is connected with the Paulina tidal marsh network, thus partly draining the vegetated tidal marsh. This network was therefore excluded from our analysis in order to keep only the networks that have watershed areas falling entirely within the unvegetated tidal flat area.

Finally the presence of a levee-basin microtopography on the intertidal platform was investigated by quantification of changes in platform elevation (using Digital Elevation Models)

with distance to the channel edges. We compared the elevations close to the channel edges (≤ 4 m from the edge) with the elevations further away from the channels (> 20 m from the edge), both for the vegetated marsh platform and bare tidal flat platform.

4.4 Results

4.4.1 Water levels and flow directions

4.4.1.1 Mean water levels in the channel network and on the platform

In general terms the mean water level on the tidal marsh platform lags behind the mean water level in the channels during the flood tide, which means that the instantaneous water level is higher in the channels than on the adjacent platform (Figure 4.3a). This is explained by faster flood wave propagation through the bare channels than over the vegetated marsh platform. During the ebb tide the opposite pattern is observed. The mean water level on the platform lags behind the mean water level in the channels, which means that the instantaneous water level in the channels is lower than on the platform. This is explained by faster drainage of the channels than of the platform (Figure 4.3a).

When looking more in detail, the instantaneous water level gradients between the channels and the platform decrease with increasing water depth above the platform, both during the flood and ebb phase. Figure 4.3a illustrates this for two types of inundations with different maximum water depth. For the highest observed inundation events that entirely overtop the marsh platform and that submerge the vegetation canopy on most locations (Figure 4.3a, circles), the mean water level in the channels is up to 13 cm higher than on the marsh platform during the first 15 min of inundation of the platform divers. This water surface difference starts to decrease when the water level rises above the mean platform elevation plus one standard deviation (Figure 4.3a), and becomes negligible by the moment that the water level reaches the mean vegetation canopy height (Figure 4.3a). During the rest of the flood phase, when water levels exceed the mean vegetation height, the mean water levels are not significantly different between the channels and platform. During the ebb phase, this difference remains also insignificant until the water level drops again below the mean vegetation canopy height. As opposed to the flood phase, now the platform water level becomes higher than the water level in the channels. With decreasing water level, the water level gradient between platform and channels increases up to 30 cm at the moment that all except one platform diver fall dry (Figure 4.3a).

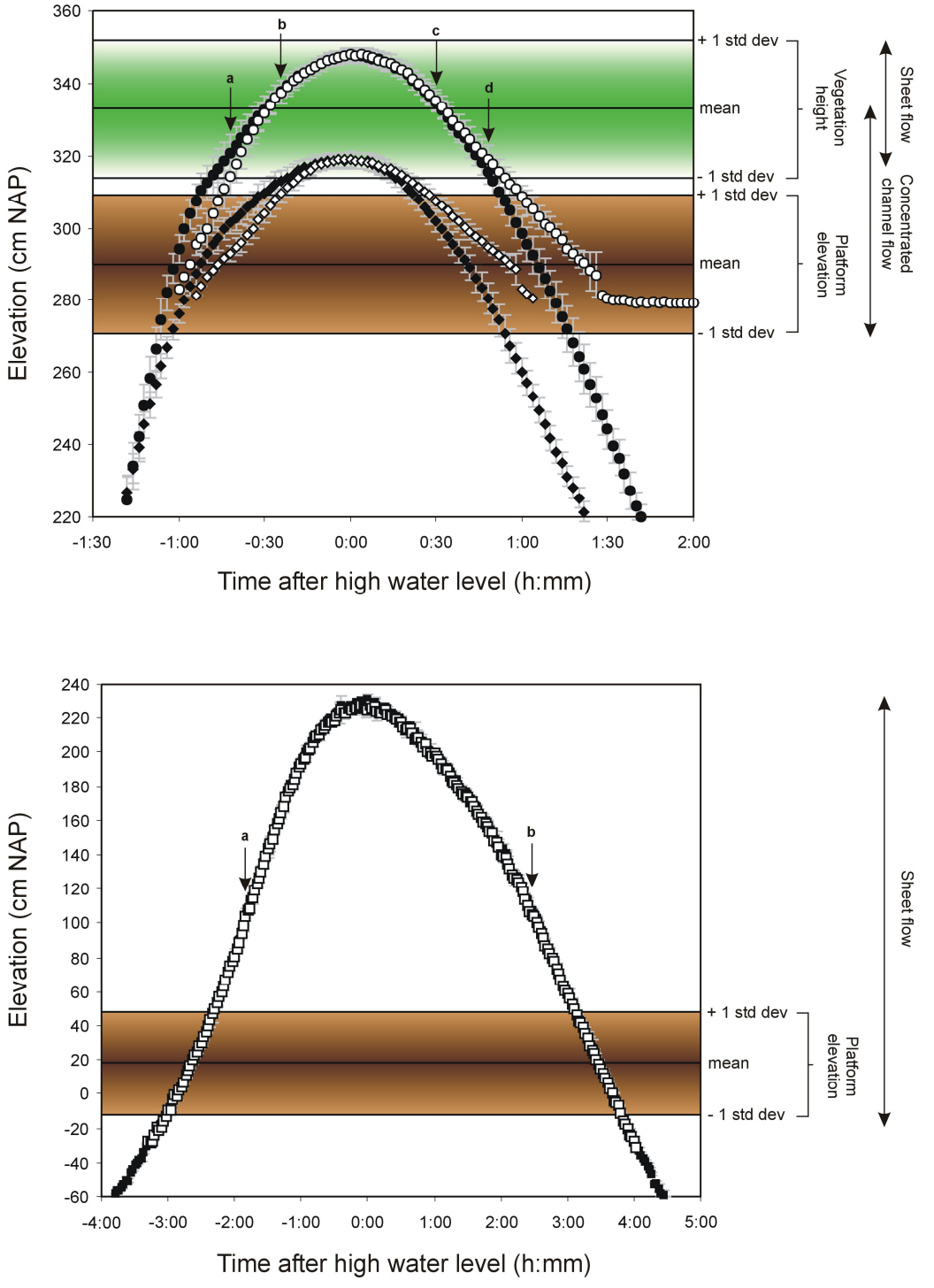

Figure 4.3 (a) Comparison between the instantaneous mean water level in the marsh channels (black markers) and on the marsh platform (white markers) for a high inundation event (circles) and a medium inundation event (diamonds). (b) Comparison between the instantaneous mean water level in the tidal flat channels (black markers) and on the tidal flat platform (white markers) for one inundation event. Arrows indicate the time steps of the instantaneous water surfaces presented in Figure 4 (arrows a-d) and 5 (arrows a-b).

For medium high inundation events that just overtop the marsh platform surface at most locations but that do not overtop the vegetation canopy (diamonds, Figure 4.3a), very similar patterns are observed as described above. The differences between the mean water level in the channel and on the platform remain for almost the whole of the flood and ebb phase, and disappear only very close to the moment of high tide. These medium high inundation events do not overtop the mean vegetation canopy height and thus no phases occur with negligible water level differences between the platform and channels (Figure 4.3a).

As opposed to the tidal marsh, on the unvegetated tidal flat there is no difference between the channel and the platform mean water level during the initial stages of platform flooding (cf. Figure 4.3a and 4.3b). The lack of difference between channel and platform water levels is observed for the entire period of tidal flat inundation (i.e. flood and ebb phase).

4.4.1.2 Spatio-temporal changes in water level and flow directions

Contour maps of instantaneous water surfaces are shown for the highest observed tide in the tidal marsh (see also Figure 4.3a, circles), for different time steps during the flood and ebb phase (Figure 4.4a-d, time steps indicated on Figure 4.3a by arrows a-d). During the flood phase at the time that all divers in the study area become flooded (arrow a, Figure 4.3a), we observe that at the mouth of the large channel (at diver location 1) the water level is higher as the water levels at the more upstream locations in the channel network (i.e., towards the channel heads) (Figure 4.4a). Within the wide main channel (between location 1 and 18 in Figure 4.4a) the water surface slope is 0.0069 %, while in the smaller tributary channels there is a steeper water surface slope of 0.023 % (between location 10 and 11) and 0.096 % (between location 9 and 15). In contrast to these rather gentle water surface slopes within the channel network, the water surface slopes between the channels and adjacent platform locations are considerably steeper, e.g. up to 0.27 % between location 10 and 14. Water levels during the flood phase are thus higher in the channels as on adjacent platform locations (see also Figure 4.3a). In general we may consider that water in shallow intertidal areas flows from the higher water levels to the lower water levels. Hence the contour maps demonstrate that during the flood phase the water flow is preferentially routed through the channel network, and is subsequently directed from the channels onto the marsh platform. This is not only observed on the large scale of the main channel, but also for the smaller tributary channels. In the channels, the flow directions derived from the water levels are confirmed by the flow directions measured with the ADCPs. At locations A, D and E the water flows towards the channel heads with the flow directions parallel to the channel axis (Figure 4.4a, black arrows). On the platform locations B and C water flows to the east according to the ADCPs, which is not

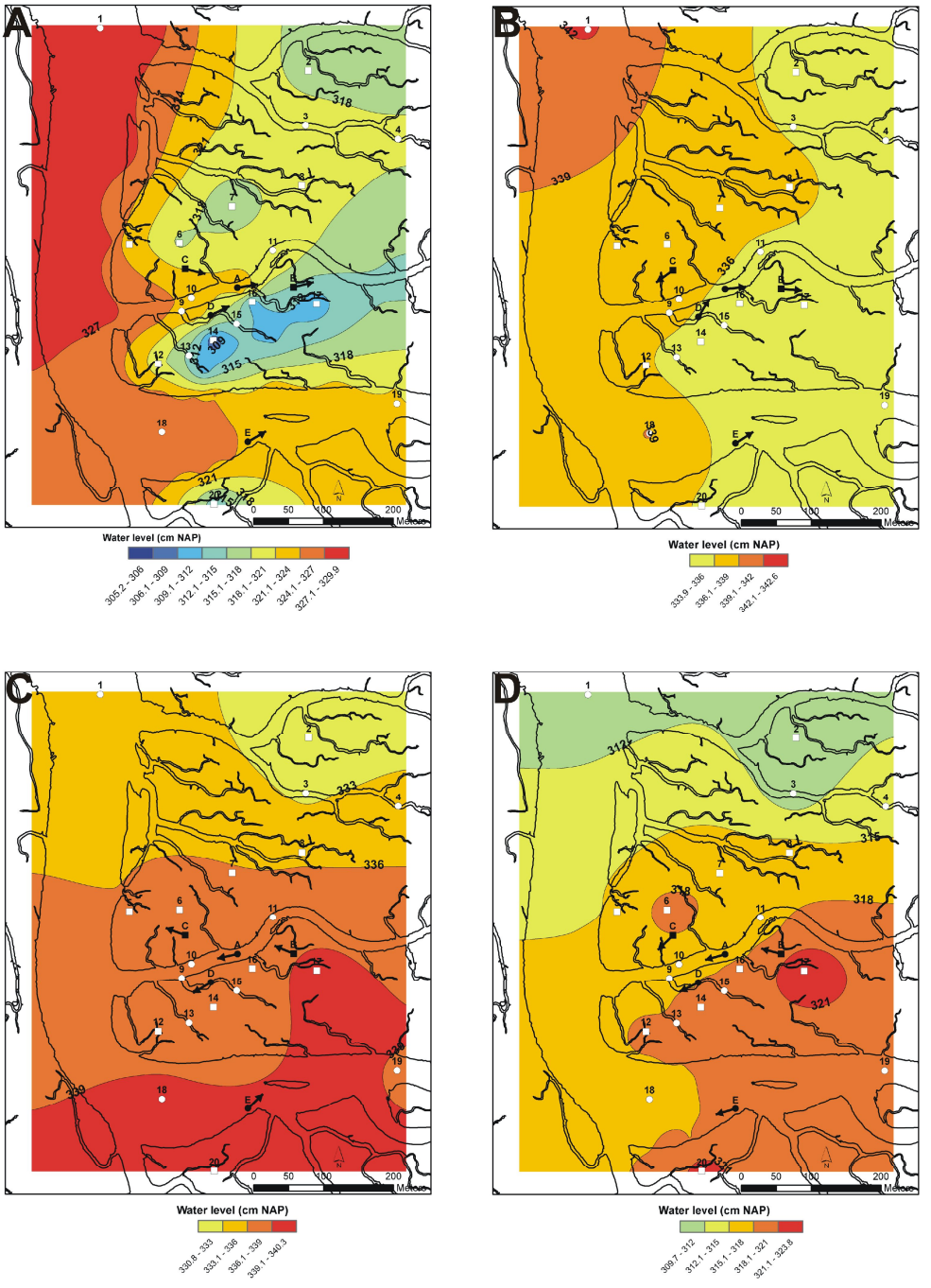

Figure 4.4 Contour maps of instantaneous water surfaces for the highest observed tide in the vegetated tidal marsh, for different time steps during the flood (a and b) and ebb phase (c and d). Different time steps are indicated on Figure 4.3a.

perfectly in line with the interpolated water surface slopes (Figure 4.4a). Once the greater part of the vegetation becomes overtopped (arrow b, Figure 4.3a), more large-scale sheet flow occurs, from the mouth of the main channel towards the rest of the area, and flow routing is no longer directed from the channel network onto the marsh platform (Figure 4.4b). During the ebb phase (when vegetation remains overtopped, arrow c, Figure 4.3a) similar sheet flow patterns occur, now with the flow routes more or less opposed to the incoming flow (cf. Figure 4.4c and 4.4b). Later during ebb, at the time just before the first diver falls dry (arrow d, Figure 4.3a), again the same flow patterns are observed as during the flood phase, but now the water levels on the marsh platform are higher as in the channels (Figure 4.3a), and the water in the channel network flows from the channel heads towards the mouth of the large channel (Figure 4.4d).

For the highest observed tide over the tidal flat, instantaneous water surface slopes are always less than 0.15 % and we do not observe any clear water surface gradients related to the channel network or any other, more large-scale gradients (see Figures 4.5a-4.5b). However, the flow directions measured with the ADCPs do show clear patterns. During flooding the water flows from the flat edge towards the marsh edge in a more or less southern direction (locations A-F, Figure 4.5a). During the ebb phase most of the flow directions are towards the mouth of the estuary or towards the flat edge (except location F, Figure 4.5b), and in general the observed ebb flow directions are opposite to the flood flow directions.

4.4.2 Flow velocities

In the tidal marsh there is a large difference between the observed flow velocity maxima in the channel network, and on the vegetated marsh platform (Figure 4.6). In the channels, the maximum flood flow velocities range from 0.3 m/s up to 1 m/s, while on the marsh platform all observed flow velocity maxima are below 0.07 m/s. In the channel network there is a clear positive linear relationship between the inundation height at high tide and the maximum flood flow velocity (R^2=0.89; $p<0.0001$). This means that for a given channel location the maximum flood flow velocity is higher for higher tides (temporal variation), but also that in wider, deeper channels (location E, Figure 4.4a) higher flow velocity maxima occur than in smaller, shallower channels (location D, Figure 4.4a) (spatial variation). On the vegetated platform there is also an increase in flow velocity with increasing inundation height (R^2=0.10; $p=0.36$), however the slope of this relationship is much lower for the vegetated platform (0.047) than for the channels (0.38). For the tidal flat, observed flow velocity maxima range from 0.1 m/s to 0.4 m/s and are intermediate between the flow velocity maxima observed on the tidal marsh platform and in the tidal marsh channels (Figure 4.6). Both in the channels and on the platform of the tidal flat there is clear

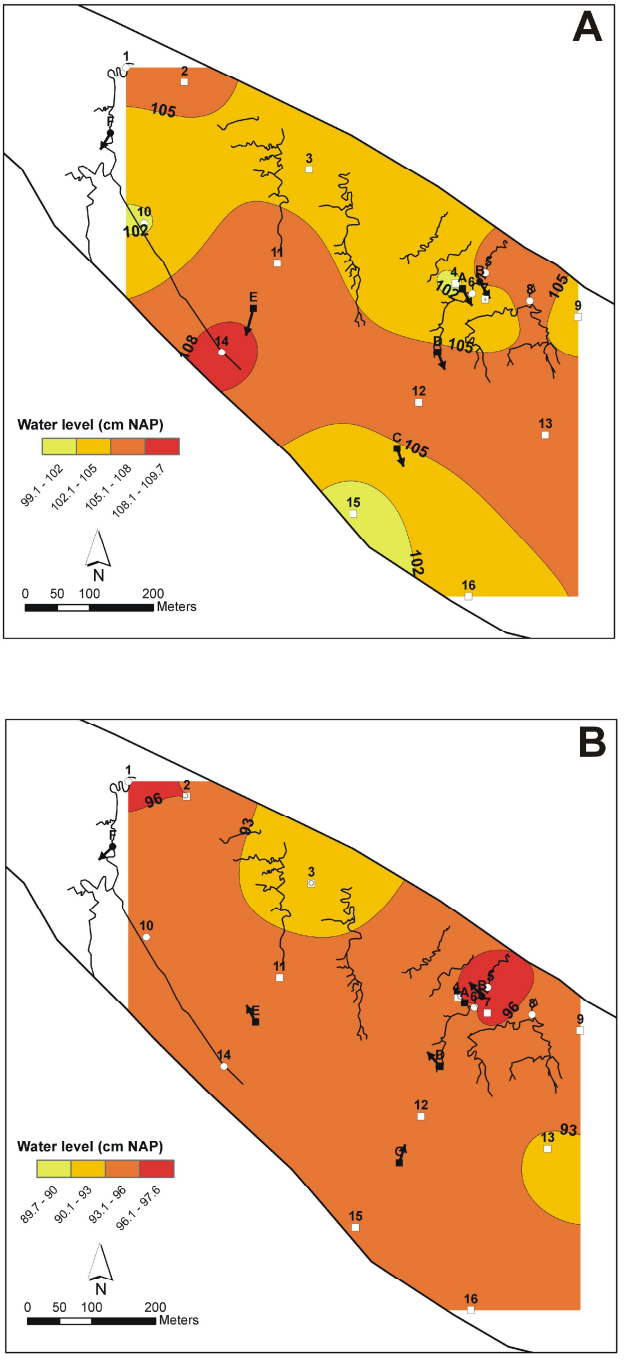

Figure 4.5 Contour maps of instantaneous water surfaces for the highest observed tide in the unvegetated tidal flat, for one time step during the flood phase (a) and one time step during the ebb phase (b). Time steps are indicated on Figure 4.3b.

positive linear relationship between the inundation height and the maximum flood flow velocity (R^2=0.65; p=0.003) for the channels; R^2=0.67; p=0.002 for the platform). The slope of this relationship is very comparable for the channels and platform locations on the tidal flat (0.21 and 0.16 respectively), and these slope values are intermediate between the slope values for the tidal marsh platform (0.047) and marsh channels (0.38). This means that for the same maximum inundation height, the maximum flood flow velocity would be smallest on the vegetated marsh platform and highest in the marsh channels, while intermediate and very comparable on the bare platform and in the channels of the tidal flat.

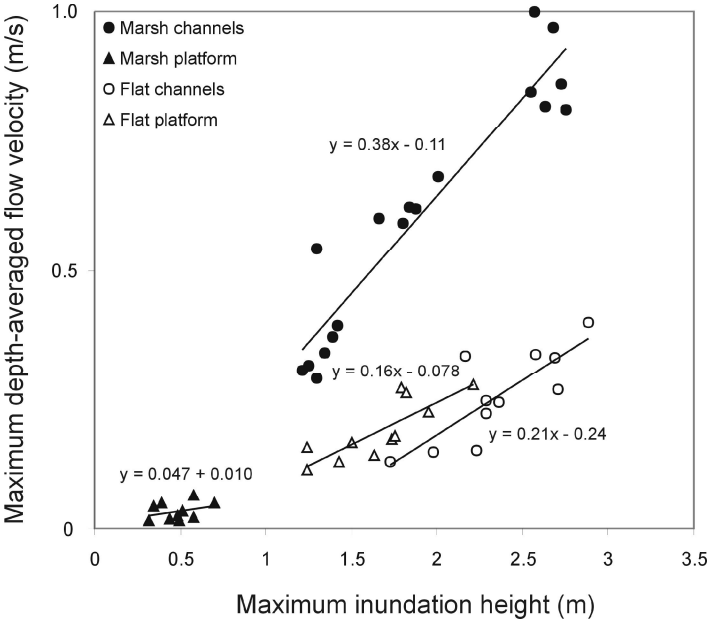

Figure 4.6 Relationship between the maximum inundation height and the maximum depth-averaged flow velocity for the channels and the platform of a tidal marsh and a tidal flat.

4.4.3 Morphology

4.4.3.1 Levee-basin topography on the platform

The tidal marsh platform is characterized by a typical levee-basin microtopography. Close to the channel edges (≤ 4 m) the levees have a median elevation that is 15 cm higher than the median basin elevation further away from the channel edges (> 20 m) (two sample t-test, p<0.0001) (Figure 4.7). On the tidal flat, the platform close to the channel edges (≤ 4 m) has a median elevation that is 14 cm lower than further away from the channels (> 20 m) (two sample t-test, p<0.0001) (Figure 4.7). Hence a levee-basin microtopography is clearly absent on the tidal flat platform.

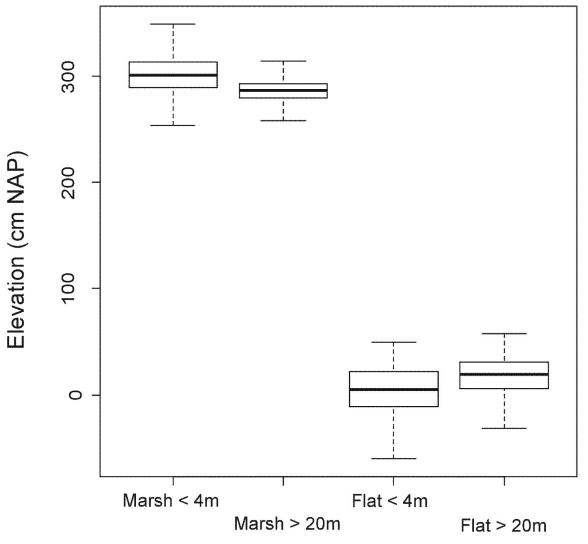

Figure 4.7 Boxplots of the tidal marsh and tidal flat platform elevation, close to the channel edges (≤ 4 m) and further away from the channel edges (> 20 m).

4.4.3.2 Channel width-to-depth ratios

For comparable channel widths, the channels in a tidal marsh are more deeply incised compared to the tidal flat channels (Figure 4.8). Only near the tidal marsh channel heads (i.e., the

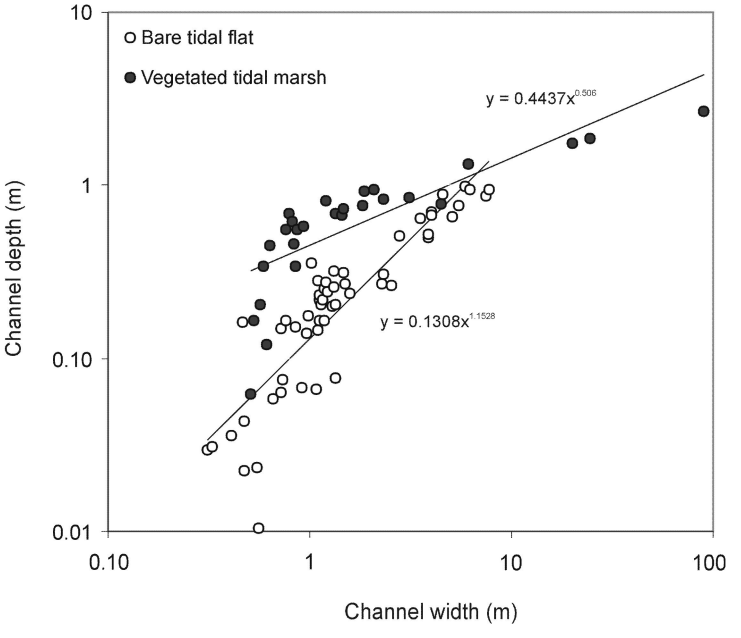

Figure 4.8 Relationship between channel width and channel depth for a bare tidal flat and a vegetated tidal marsh.

smallest channel widths) some of the cross-sections are not yet deeply incised. For both systems the channel depth increases with the channel width, however the slope of this relationship is considerably steeper for the tidal flat channels (1.15) than for the tidal marsh channels (0.51). This implies that with increasing channel width the difference in channel depth between both systems decreases (see trend lines, Figure 4.8). Moreover is the trend line for the tidal flat close to the 1:1 line, which means that with increasing channel width the width-to-depth ratio (=β) remains more or less constant. On the tidal flat the mean β value for the observed range in channel widths is 8.6. For the tidal marsh the slope of the trend line is considerably lower than the slope of the 1:1 line, which means that with increasing channel width the width-to-depth ratio increases. The mean β value for the same range of channel widths on the marsh as observed on the tidal flat is 2.7, however for the widest marsh channels β already attains a value of 34.

4.4.3.3 Watershed areas versus channel widths

The channels in a tidal marsh system are for comparable watershed areas wider (3-7 times) compared to the channels in a tidal flat system (Figure 4.9). This also implies that for comparable watershed areas tidal marsh channels are deeper (Figure 4.8 and 4.9), and hence have a larger cross-sectional area.

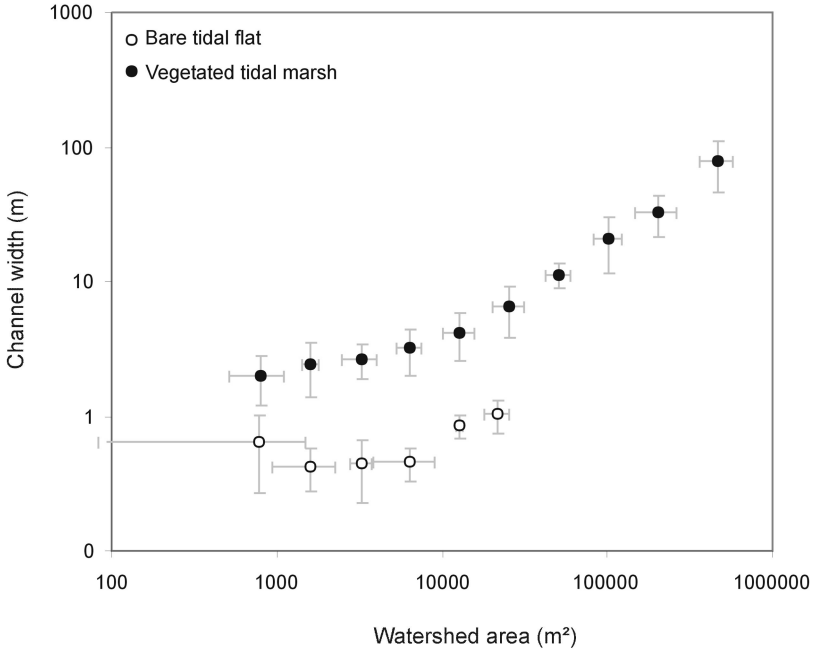

Figure 4.9 Relationship between watershed area and channel width for a bare tidal flat and a vegetated tidal marsh.

4.5 Discussion

Recent modeling studies have highlighted the role of intertidal vegetation in determining large-scale flow patterns (e.g., Temmerman et al. 2005) and landform formation and evolution (e.g., D'Alpaos et al., 2007b; Kirwan and Murray, 2007; Marani et al. 2007; Temmerman et al., 2007). Nevertheless no field studies exist that systematically describe and compare the large-scale flow patterns through the channel network and over the platform of unvegetated tidal flats and vegetated tidal marshes, and that relate these flow patterns to landform differences between flats and marshes. We found that during the flood and ebb phase flow patterns in a tidal marsh are clearly routed through the tidal channel network (Figures 4a and 4d), whereas on a tidal flat the platform floods and drains more like a sheet flow (Figures 5a and 5b). In the tidal marsh there is a strong reduction of flow on the vegetated platform and a concentration of flow in the channels, whereas on the tidal flat the channel and platform flow velocities are intermediate and very comparable (Figure 4.6). These hydrodynamic processes are clearly reflected in the landform differences between vegetated marshes and bare tidal flats: (1) for comparable watershed areas the channel widths and channel depths are distinctively larger in a tidal marsh than in a tidal flat (due to the flow concentration towards channels in a tidal marsh) (Figures 8 and 9), and (2) vegetated marsh platforms are typified by the presence of a levee-basin topography (due to platform flooding from the channels), while a levee-basin topography is typically absent on bare tidal flats (due to platform flooding as sheet flow) (Figure 4.7).

As suggested by earlier modeling studies, vegetation plays an important role in the flow hydrodynamics of tidal marshes (Temmerman et al., 2005b): hydrodynamic models have demonstrated that during flooding there is a strong reduction of flow on the vegetated platform, which causes flow concentration towards the unvegetated tidal channels. This leads to faster flood propagation and higher water levels in the channels than on the platform, and results in flood flow directions from the tidal channels towards the marsh platform, via flow paths more or less perpendicular to the channel edges (Temmerman et al., 2005b). Our field data proof that flow concentration towards tidal marsh channels indeed occurs, and is related to the reduction of flow on the vegetated marsh platform (Figure 4.6). Moreover, the higher water levels in the tidal marsh channels during the flood phase (Figure 4.3a) and the measured flow directions on the platform (Figure 4.4a, locations B and C) confirm earlier modeled flow patterns (Temmerman et al., 2005b). However, the higher water levels in the channels during flooding cannot only be attributed to friction exerted by the vegetation on the flow. In the tidal marsh the levee-basin topography is distinctively present (Figure 4.7), with 25% of the levee surface area below an elevation of 289 cm NAP, 50% below an elevation of 301 cm NAP, and 75% below an elevation of 313 cm NAP

(Figure 4.7). Within this interquartile range (289 till 313 cm NAP) the highest differences in channel water level and platform water level are observed (up to 13 cm, Figure 4.3a). This implies that during flooding of the platform, much of the flow is still confined within the channel network due to the levees, and that the flow towards to basins is not perpendicular to the channel edges but is rather routed through small channels with poorly developed levees that penetrate into the basins. Once that more than 75% of the levees becomes flooded (> 313 cm NAP), the water level differences decrease (< 6 cm, Figure 4.3a), and eventually disappear when almost all of the levees (> 97 %) are flooded (> 336 cm NAP). Hence it cannot be excluded that apart from the vegetation friction, also the micro-topography of levees controls the flow routing patterns. We may argue that once more than 75% of the levees becomes flooded (> 313 cm NAP), the effect of micro-topography probably becomes limited, and the observed water level differences may be increasingly caused by the friction exerted by the vegetation on the flow. As the water level rises towards 336 cm NAP, more vegetated area becomes entirely overtopped and moreover, within the non-overtopped areas the water rises into the less dense upper parts of the vegetation canopy. Consequently less friction is felt in the upper part of the water column and the differences in flood propagation and water level between the channels and marsh platform decrease. Eventually as the water level approaches high water, most of the vegetated area becomes entirely overtopped and the flow patterns are no longer concentrated to the channel network but are dominated by more large-scale sheet flow (Figure 4.4b). The occurrence of this sheet flow has already been suggested by previous studies (e.g., **Chapter 3**; French and Stoddart, 1992; Temmerman et al., 2005a), but has never been demonstrated by the direct measurement of two-dimensional water level surfaces (Figure 4.4b). During the ebb phase the flow patterns initially occur as more large-scale sheet flow (Figure 4.4c) and are then again concentrated to the tidal channel network (Figure 4.4d), now with lower water levels in the channels than on the platform (Figure 4.3a).

A tidal flat platform is characterized by the absence of vegetation and levees next to the channel edges (Figure 4.7). This implies that relatively few friction is exerted on the platform flow and that water is not concentrated to the channels when the platform becomes inundated or drained. As a result, the observed flow patterns during the flood and ebb phase are not routed through the tidal channel network, but rather occur as a sheet flow (Figure 4.5a and 4.5b). Moreover, there is no difference between the water levels in the channels and on the platform (Figure 4.3b), and the flow velocities in the channels are very comparable with the flow velocities on the platform (Figure 4.6). Several modeling studies assume that once an intertidal platform becomes flooded all water first has to flow through the channel network (e.g., D'Alpaos et al., 2005; D'Alpaos et al., 2006; D'Alpaos et al., 2007b; Fagherazzi and Furbish, 2001; Fagherazzi

and Sun, 2004; Kirwan and Murray 2007). This study however demonstrates that for a tidal flat, which is characterized by a lower position in the tidal frame and thus a higher tidal prism compared to a tidal marsh, a relatively small part of the tidal prism is forced to flow through the channel network.

These differences in flow hydrodynamics have their implications on the landforms of intertidal landscapes. For comparable watershed areas, the channels in a tidal marsh are wider compared to the tidal flat (Figure 4.9). Furthermore, if we compare equal channel widths, channels in a tidal marsh are deeper compared to the tidal flat, and hence the cross-sectional area of channels in a tidal marsh are for comparable watershed areas larger than in a tidal flat (Figures 4.8 and 4.9). Despite the lower position of a tidal flat in the tidal frame and the consequent longer inundation times, the part of the tidal prism that is forced to flow through the channels is determinative for the channel dimensions: on a tidal flat a smaller part of the tidal prism is forced to flow through the network and consequently channel dimensions are smaller.

This study provides empirical data on large-scale flow patterns in tidal flats and marshes, which should form the basis for improvement of existing models of intertidal hydrodynamics and morphodynamics. Most existing models (D'Alpaos et al., 2005; D'Alpaos et al., 2007b; Kirwan and Murray, 2007) assume for simplicity that the channel network immediately conveys all water that floods to, and drains from the intertidal platform. Here we demonstrated empirically that flow routing through the channel network is important for a vegetated high tidal marsh, as long as the flood depth of the platform does not exceed the vegetation canopy height. As soon as the vegetation is submerged more large-scale sheet flow occurs instead of concentrated flow through the channel network. Furthermore, for a bare tidal flat we demonstrated empirically that concentrated channel flow is very limited and that most of the flow occurs as sheet flow. By showing that these differences in flow patterns are related to landform differences between tidal flats and marshes, our study should stimulate the improvement of existing models on intertidal hydrodynamics and morphodynamics (e.g., D'Alpaos et al. 2007; Kirwan and Murray, 2007; Temmerman et al., 2007).

Chapter 5:

Sedimentation and response to sea-level rise of a restored marsh with reduced tidal exchange: comparison with a natural tidal marsh

W. Vandenbruwaene, T. Maris, T.J.S. Cox, D.R. Cahoon, P. Meire and S. Temmerman

Geomorphology, doi:10.1016/j.geomorph.2011.03.004 (2011)

Abstract

Along coasts and estuaries, formerly embanked land is increasingly restored into tidal marshes in order to re-establish valuable ecosystem services, such as buffering against flooding. Along the Scheldt estuary (Belgium), tidal marshes are restored on embanked land by allowing a controlled reduced tide (CRT) into a constructed basin, through a culvert in the embankment. In this way tidal water levels are significantly lowered (ca. 3 m) so that a CRT marsh can develop on formerly embanked land with a ca. 3 m lower elevation than the natural tidal marshes. In this study we compared the long-term change in elevation (ΔE) within a CRT marsh and adjacent natural tidal marsh. Over a period of 4 years, the observed spatio-temporal variations in ΔE rate were related to variations in inundation depth, and this relationship was not significantly different for the CRT marsh and natural tidal marsh. A model was developed to simulate the ΔE over the next century. (1) Under a scenario without mean high water level (MHWL) rise in the estuary, the model shows that the marsh elevation-ΔE feedback that is typical for a natural tidal marsh (i.e. rising marsh elevation results in decreasing inundation depth and therefore a decreasing increase in elevation) is absent in the basin of the CRT marsh. This is because tidal exchange of water volumes between the estuary and CRT marsh are independent from the CRT marsh elevation but dependent on the culvert dimensions. Thus the volume of water entering the CRT remains constant regardless of the marsh elevation. Consequently the CRT MHWL follows the increase in CRT surface elevation, resulting after 75 years in a 2-2.5 times larger elevation gain in the CRT marsh, and a faster reduction of spatial elevation differences. (2) Under a scenario of constant MHWL rise (historical rate of 1.5 cm a^{-1}), the equilibrium elevation (relative to MHWL) is 0.13 m lower in the CRT marsh and is reached almost 2 times faster. (3) Under a scenario of accelerated MHWL rise (acceleration of 0.02 cm a^{-1}), the CRT marsh is much less able to keep up with the MHWL rise; after 75 years the CRT elevation is already 0.21 m lower than for the natural marsh. In conclusion, this study demonstrates that although short-term (4 years) ΔE rates are similar in a

restored CRT marsh and natural tidal marsh, these ecosystems may evolve differently in response to sea-level rise in the longer term (10-100 years).

*5.*1 Introduction

Rise in sea-level and an increased storm intensity and frequency have become a severe threat to low elevated coastal zones and estuaries. In these areas, tidal marshes have an important function in dissipation of tidal energy and protection against storm surges (Mitsch and Gosselink, 2000). Besides their safety function, tidal marshes play an important role in the cycling of nutrients (e.g., Gribsholt et al., 2005; Jacobs et al., 2008; Struyf et al., 2006) and they are characterized by a high habitat diversity. Despite these valuable ecosystem functions, there has been a significant loss in tidal marsh area on a global scale in the last decades, mainly induced by human activities (e.g. embankment, harboring). Several countries have plans now to restore tidal marshes on formerly embanked land, or have executed such plans rather recently, in order to restore the valuable ecosystem functions of tidal marshes (Bakker et al., 2002; Cox et al., 2006; French, 2006; Maris et al., 2007; Pethick, 2002; Williams and Faber, 2001; Wolters et al., 2005). Whether or not de-embankment or managed retreat will be successful is largely dependent on the induced sedimentation and erosion processes. An increase in surface elevation will affect the water storage capacity of a de-embanked area and hence its buffering effect on flooding. On the other hand changes in elevation are crucial for the colonization and evolution of tidal marsh ecosystems.

In the Scheldt estuary (Figures 5.1a and 5.1b) the mean high water level (MHWL) increased much faster compared to the Belgian coastal zone (respectively 1.5 m and 0.3 m over the last 100 years) (Temmerman et al., 2004b). During the last century, the relative surface of intertidal areas decreased by about 20% (Meire et al., 2005). To cope with the problems of MHWL rise and the loss of intertidal area, formerly embanked areas along the Belgian part of the estuary were converted into flood control areas with a controlled reduced tide (CRT) (Cox et al., 2006; Maris et al., 2007). These areas are connected with the estuary via a culvert or sluice system through the dyke, and are surrounded by a ring dyke to protect the surrounding land against flooding. The function is dual: (1) protection against storm surges by the temporary storage of water, and (2) restoring tidal marshes by introducing the reduced tidal regime. Due to the low position of the formerly embanked land surface in the tidal frame, a complete de-embankment would solely lead to tidal flat development. A reduced tidal regime is therefore essential to attain the restoration objective. The reduced tidal regime (CRT) differs from the tidal regime on a natural tidal marsh in that the inundation depth is reduced and the duration of flooding is longer (longer stagnant phase) (Cox et al., 2006; Maris et al., 2007). After introduction of the reduced tide on the formerly embanked land, sedimentation and erosion processes will affect the surface topography. Since the resulting surface elevation changes will be determinant for the water storage capacity of

the flood control area and the ecological development of a marsh system, accurate knowledge of patterns in rates of elevation change is essential.

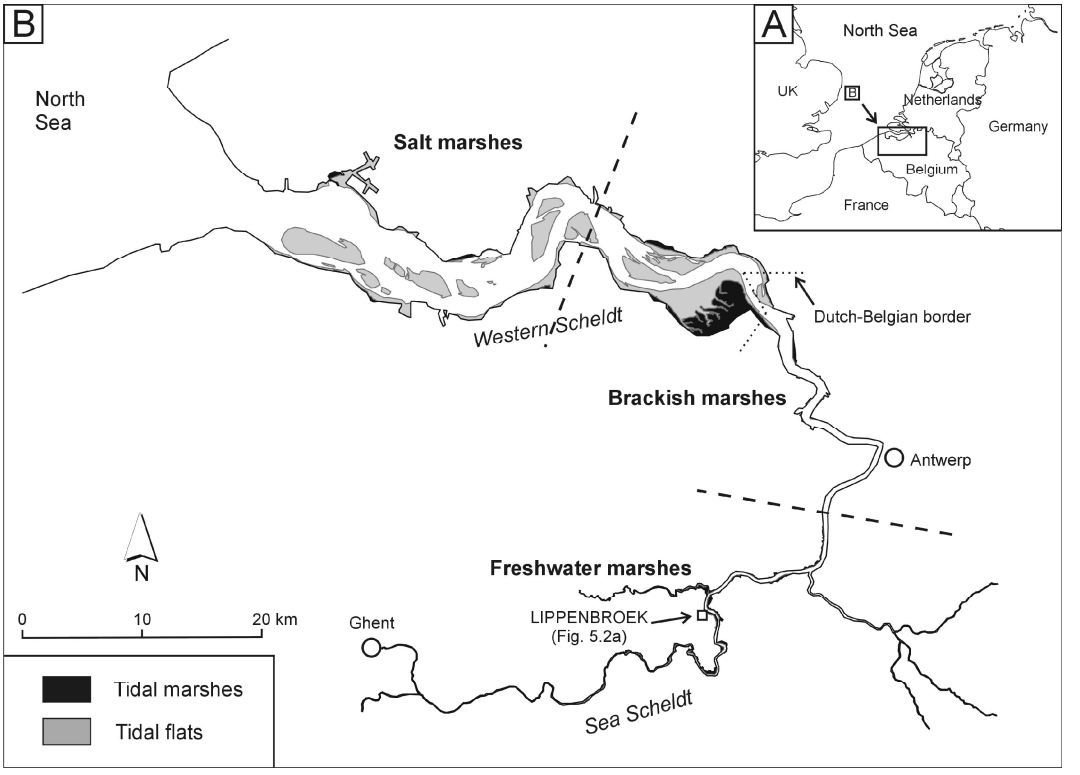

Figure 5.1 The Scheldt estuary. (a) Location within Western Europe. (b) Location of the salt, brackish and freshwater tidal marshes (separated by dashes lines), location of the Lippenbroek study area.

On natural tidal marshes, *spatial* variations in sedimentation rates are controlled by spatial variations in surface elevation and distance from tidal channels (e.g., Leonard, 1997; Temmerman et al., 2003b). The higher a marsh platform is located in the tidal frame, the less it is inundated and the smaller the increase in elevation is (e.g., Allen, 1999; Allen, 2000; Pethick, 1981; Temmerman et al., 2003a). Furthermore, with regard to the tidal channels, the sedimentation rate is typically highest close to channels and decreases with increasing distance from channels (i.e., increasing distance from sediment source) (e.g., French et al., 1995; Reed et al., 1999). *Temporal* variations in marsh sedimentation rates are related to variations in tidal inundation (frequency, height, duration) and seasonal variations in suspended sediment supply (Hutchinson et al., 1995; Leonard, 1997; Temmerman et al., 2003a). The combined effect of spatial and temporal variations in sedimentation rate results in a number of typical patterns for the long-term changes in marsh elevation and marsh vegetation. (1) Spatial elevation differences on a marsh platform decrease with time, as low platform locations increase faster in elevation than high platform

locations, leading to a reduction of spatial variation in flooding frequency, and hence a loss of habitat diversity. (2) Under a scenario of *constant* sea-level rise and sufficient sediment supply, the marsh platform rises progressively in the tidal frame, resulting in a decrease in flooding frequency and hence a decrease in the platform rise. Eventually the marsh platform reaches an equilibrium level (relative to mean sea-level), and the rate of platform rise becomes equal to the rate of sea-level rise (e.g., Allen, 1990; French, 1993; Kirwan and Temmerman, 2009; Temmerman et al., 2004b). This asymptotic rise of marsh elevation drives the succession of marsh vegetation from a low-marsh pioneer vegetation (with high inundation frequency) towards a high-marsh climax vegetation (with low inundation frequency) at equilibrium level. (3) Under a scenario of *accelerating* sea-level rise, the marsh platform is progressively more and more inundated. This is partly counterbalanced by an increase in the rate of platform rise and as a consequence marshes can maintain a (lower) equilibrium level. In this way, (lower-marsh) vegetation can still be sustained. However, if a critical threshold of high sea-level rise rate and low sediment supply is exceeded, the marsh vegetation dies off, leading to a bare mudflat or open water (e.g., Reed, 1995). It is clear that the precise nature of these three mechanisms described above, critically depend on the *strength* of the feedback between increase in elevation and inundation: the stronger this feedback, (1) the faster elevation differences will decrease and habitat diversity will be reduced; (2) the higher the equilibrium level relative to mean sea level; and (3) the higher the ability of marshes to keep up with accelerations in sea-level rise.

It may be expected that in a marsh system that develops under a controlled reduced tidal (CRT) regime, the above-described sediment deposition mechanisms and consequent changes in elevation will be different from a natural tidal marsh. For a CRT marsh the tidal curve is strongly deformed, with lower and longer inundations. A negative relationship between the spatial variations in elevation (flooding frequency) and the rate in surface elevation rise may also be expected in a CRT marsh, however, it is uncertain whether the strength of this relationship is comparable with a natural tidal marsh. Changes in marsh elevation are not only determined by sedimentation processes, but are also affected by organic matter accumulation and autocompaction (Nyman et al., 2006; Cahoon et al., 1995). In the natural tidal marsh, the tidal freshwater vegetation already reached a climax state, while on the CRT marsh pioneer vegetation prevails (Jacobs et al., 2009). These differences in vegetation structure not only lead to differences in organic matter accumulation, but also affect the flow hydrodynamics and hence sedimentation processes. Furthermore, the temporal feedback between increase in elevation and inundation, which is typical for a natural tidal marsh, may be expected to be absent in a CRT marsh. In the latter case, an increase in soil elevation does not necessarily lead to a decrease in tidal inundation

depth. For each tide, the same volume of water enters the area through the high inlet sluice, and consequently the high water levels in the CRT marsh follow the overall increase in soil elevation. Thus, it is unclear (1) how fast elevation differences and associated habitat diversity decrease in a CRT marsh, (2) how fast and at what level an equilibrium elevation is reached under a scenario of constant sea-level rise, and (3) it is unclear whether a CRT marsh is able to keep up with an accelerated sea-level rise.

In this study we quantified the spatial and temporal variations in elevation change (ΔE) in a CRT marsh and an adjacent natural tidal marsh, and compared the strength of the ΔE -inundation feedback for both systems. Based on our data we built a model to simulate the change in platform elevation in response to sea level rise for the next century. We compared the CRT marsh and the natural tidal marsh, under a scenario *without* sea-level rise, a scenario with *constant* sea-level rise, and a scenario with *accelerating* sea-level rise. We evaluated the results of our model in terms of: (1) the rate at which elevation differences decrease, (2) the rate and level at which an equilibrium elevation is attained under a constant sea-level rise, and (3) the ability to keep up with an accelerating sea-level rise.

5.2 Study area

The Scheldt estuary is located in the northwest of Belgium and the southwest of the Netherlands (Figure 5.1a), it has a reach of about 160 km (up to Ghent), and is characterized by a semi-diurnal meso- to macrotidal regime. Due to the salinity gradient along the estuary, the tidal marshes can be divided into salt, brackish and freshwater marshes (Figure 5.1b). Suspended sediment concentration (SSC) in the estuary strongly varies in time and space. Averaged SSC in the upper part of the water column (which floods the natural tidal marshes and enters the CRT area) range from 0.03 to 0.06 g l^{-1} between the mouth and the Dutch-Belgian border, up to 0.1-0.15 g l^{-1} between the border and the Lippenbroek. Further upstream, the SSC again slightly decreases to 0.05-0.1 g l^{-1}. (for more detailed information about the Scheldt estuary, see e.g. Meire et al., 2005).

The Lippenbroek CRT marsh serves as a case study for much larger CRT areas (~100s of ha), currently under construction along the Scheldt estuary. The Lippenbroek study area is located in the freshwater zone (Figure 5.1b). At the Lippenbroek the tidal range is nearly 6 m, which is the maximum range observed in the estuary. Before March 2006, the study area was a polder area with a low elevation (2.3-3.2 m TAW, TAW = the Belgian Ordnance Level), with the higher elevated zones more close to the river dyke, and two artificial ditches (Figure 5.2a). As opposed to the embanked polder, the adjacent natural tidal marshes increased in elevation with rising MHWL,

resulting nowadays in a marsh platform elevation around 5.7 m TAW. To create similar tidal conditions in the lower elevated polder (2.5 to 3.4 m lower), the principle of controlled reduced tide (CRT) was introduced (Cox et al., 2006; Maris et al., 2007).

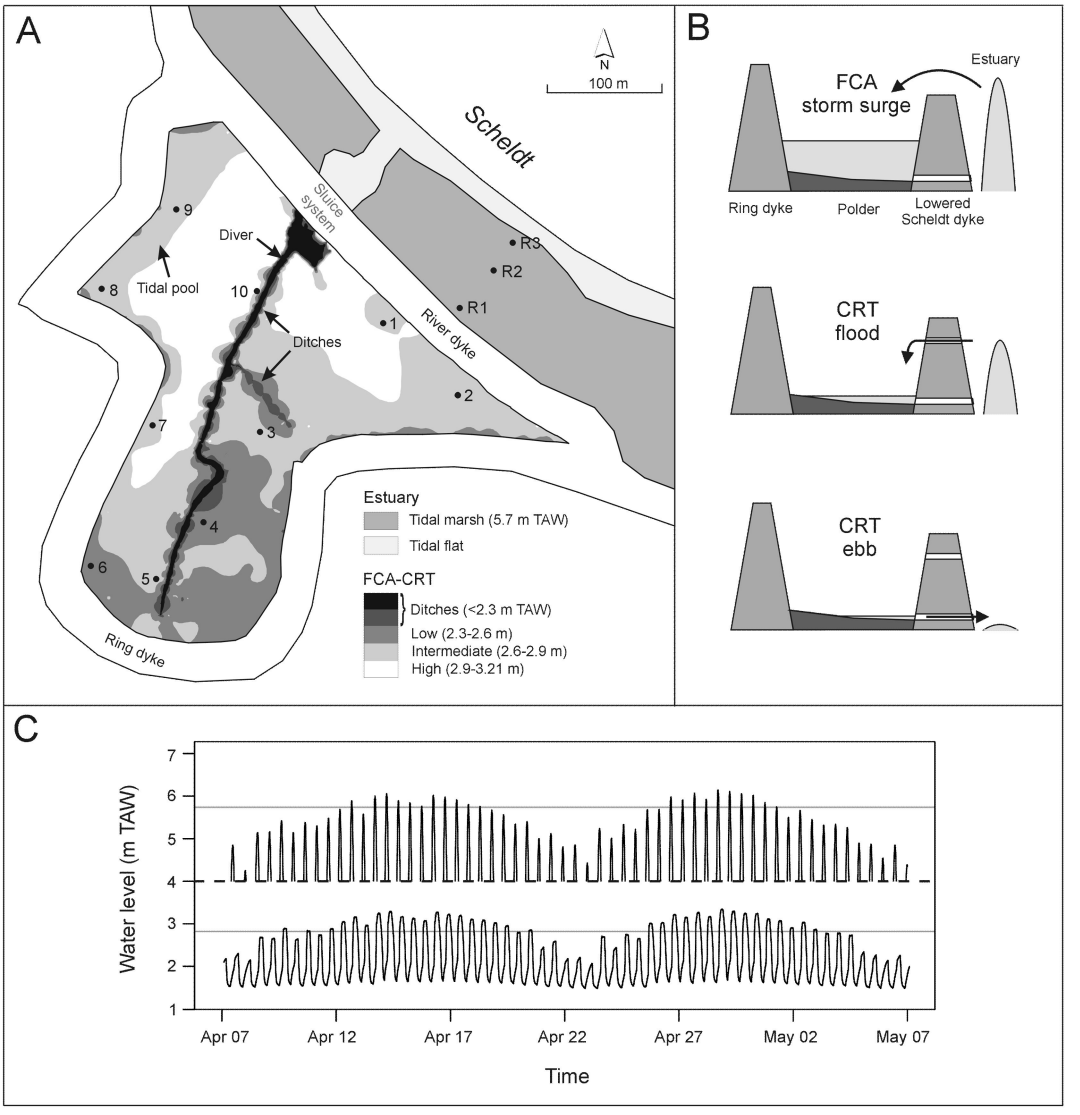

Figure 5.2 (a) The Lippenbroek flood control area (FCA) with controlled reduced tide (CRT), represented together with the former polder morphology and with indication of the surface elevation tables (SETs) in the CRT (1-10) and in the adjacent natural tidal marsh (R1-R3). (b) Working principle of the FCA-CRT, illustrated for a storm surge (at the top), and for a mean tide during flood (in the middle) and during ebb (at the bottom). (c) Water levels in the Lippenbroek CRT (at the bottom) and in the estuary nearby the Lippenbroek (at the top) for two spring-neap tide cycles. For the estuary, only the water levels above 4 m TAW are presented (above the heavy dashed line). The two grey lines indicate the mean elevation of the Lippenbroek (bottom line) and the adjacent natural tidal marshes (top line).

To construct the Lippenbroek flood control area (FCA) with a controlled reduced tide (CRT), 3 major adaptations were necessary: (1) building a ring dyke to protect the surrounding land from flooding (Figure 5.2a), (2) lowering the river dyke for temporary storage of storm surge water, and (3) constructing an inlet (high in the river dyke) and an outlet sluice (low in the river dyke) to introduce the daily tidal regime (Figure 5.2b). By using a high inlet and a low outlet, the spring-neap variations in tidal flooding frequency and height were successfully installed in the polder, however, with a clear longer stagnant phase than in the estuary (Figure 5.2c) (Cox et al., 2006; Maris et al., 2007). Secondly long-term CRT morphodynamics have an important effect on the CRT high water levels. In the CRT the supply of water only depends on the sluice dimensions and not on the surface elevation changes (or sediment volume changes). Consequently, an increase in surface elevation results in an increase in high water level. This is an important difference with natural tidal marshes where a rise in surface elevation has no effect on the high water levels, and where consequently the supply of water decreases.

The frequency distribution of elevations (relative to MHWL) strongly differs for the CRT area and the adjacent natural tidal marshes (Figure 5.3). In the natural marshes almost all locations

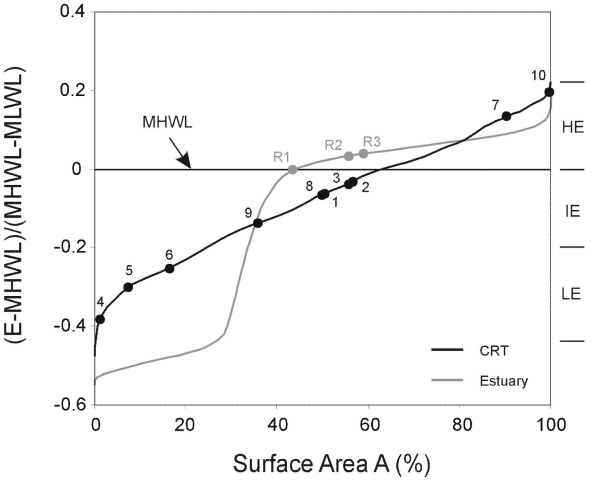

Figure 5.3 The frequency distribution of the CRT (former polder) elevations and the elevations in the natural intertidal zones along the estuary. Elevations (E) are represented by the relative positions in the tidal frame (MHWL-MLWL) compared to the MHWL (E-MHWL). The elevation is subdivided (right side) into high elevated (HE), intermediate elevated (IE) and low elevated (LE).

have reached a high equilibrium level (0 to 0.1 times the tidal frame above MHWL), while lower marsh locations (0 to 0.4 times the tidal frame below MHWL) are very scarce and mainly represented by steep slopes and cliffs between the tidal marsh and the tidal flat. These steep slopes and cliffs represent a large range in elevation, only covered by a small area of intertidal zone (about 10%, see Figure 5.3). Hence the frequency distribution of natural intertidal elevations is strongly bimodal. In contrast, in the CRT, there is a remarkably even distribution of elevations from -0.4 to +0.2 times the tidal frame. About 35% of the CRT area is located above MHWL,

where flooding frequencies are more or less comparable with the high natural tidal marshes. The other 65% of the CRT area is gradually distributed below MHWL and is characterized by low marsh conditions, a very scarce condition along the natural intertidal zone of the Scheldt estuary (Figure 5.3).

5.3 Methods

5.3.1 Field data

5.3.1.1 ΔE rates

At 10 sites in the Lippenbroek and 3 sites in the adjacent tidal marsh, rates of wetland vertical development (i.e., elevation change) were measured using Surface Elevation Tables (SETs) (Cahoon et al., 2002) (measuring locations, see Figure 5.2a). SET measurements incorporate all surface and subsurface process influences on marsh elevation that occur on the marsh surface and between the marsh surface and the base of the SET benchmark (see below). These processes include surface sediment deposition, surface erosion, soil organic matter accumulation (the net balance of root production and root decomposition), autocompaction processes, and shrink-swell from water storage (Cahoon et al., 1995). In this paper, the rate of wetland vertical development is described by the ΔE rate which is the rate in surface elevation change over a certain period in time. If ΔE is positive there is an increase in surface elevation, if ΔE is negative there is a decrease in surface elevation.

A SET consists of a vertical stainless steel rod which was hammered into the ground till a stable layer was reached (here 10 to 15 m deep). The upper part of the rod is about 0.5 m above the soil surface. This rod was used then as a fixed reference point from which accurate soil elevation measurements were performed. During the measurements, a horizontal bar was attached to the vertical rod. After putting the bar horizontally (by use of a leveling system), the vertical distance between the horizontal bar and the soil surface was measured by letting down 9 vertical pins and measuring the length of the pins sticking out above the horizontal bar. This procedure was repeated for 4 different directions, so 36 measurements were carried out for each site. Every 2 months the procedure was repeated measuring the same 36 points. In that way the elevation change, which is the cumulative effect of sediment deposition, sediment erosion, soil organic matter accumulation, and autocompaction, was monitored, and ΔE rates (i.e., vertical development) were calculated. The accuracy of the SET method is about 1 mm (Cahoon et al., 2002). Field data were collected from March 2006 (i.e. the start of tidal flooding of the CRT) up to December 2009.

Before the flooding started in the CRT, a topographic survey was conducted. Point elevations were measured on a 25 x 25 m grid with a DGPS (accuracy ± 2 cm). Based on these measurements the initial digital elevation model (DEM) of the Lippenbroek was constructed with a resolution of 1 by 1 m (see Figure 5.2a). In December 2009 a second survey was performed (about 10 x 10 m grid), allowing us to generate a second DEM of the Lippenbroek surface, with the same resolution of 1 by 1 m, after nearly 4 years of reduced tidal flooding. The difference between both DEMs provided spatially distributed ΔE rates.

5.3.1.2 Channel formation

Before the tide was introduced, the ditch morphology was determined by measuring xyz-coordinates with a total station (Sokkia SET510k, accuracy 1-3 mm). Measuring points were located along the length profile (stream threads) of the ditches and along 6 cross-sections. Along the length profile, points were measured every 10 m, along the cross-sections every 0.25 m. Measurements were repeated every year, and in this way the effect of tidal flooding and drainage on channel evolution was monitored. Data on channel morphology are available for March 2006 (before the start of flooding), November 2006, November 2007, December 2008 and December 2009.

During the monitoring period, new channels were formed and additional measurements were needed: (1) the stream threads of the new channels were measured (every 2-5 m one point) to follow up the planimetric evolution of the channel network and (2) 6 additional cross-sections were monitored. A new stream thread was only mapped when it incised the surface by more than 0.1 m, and this over a minimum distance of 10 m.

5.3.1.3 The tide

The water level in the CRT was measured by use of a diver (Schlumberger, type DIVER). This device contains a water pressure sensor and has an accuracy of ± 1 cm. To accurately cover the tidal movement, the measuring frequency was set at 5 minutes. The tide was monitored at one location in the main channel (Figure 5.2a). Tidal data of the Scheldt were provided by the Flemish Government (Flanders Hydraulics Research) and were measured in the same manner as in the CRT.

5.3.2 Modeling long-term elevation changes in a CRT

5.3.2.1. Building the model using empirical data

Spatio-temporal variations in sediment deposition on a tidal marsh platform are generally modeled as a function of tidal inundation (frequency, height, and/or duration), the distance from the creeks, and the distance from the marsh edge (D'Alpaos et al., 2007b; Kirwan and Murray, 2007; Temmerman et al., 2003b). By use of a stepwise multiple exponential regression analysis we found that the last two parameters explained very little variation in our empirical dataset (see results §5.4.2). We therefore built a simplified model, predicting ΔE rates uniquely as a function of tidal inundation, according to:

$$\Delta E = ah^b \qquad (1)$$

where ΔE = the rate in elevation change (m a^{-1}); a and b are regression coefficients; and h = the mean water depth (m), which is defined as:

$$h = \frac{1}{k}\sum_{j=1}^{k}(H_j - z_j) \qquad (2)$$

where k = the number of tides during the considered time period; H_j = the high water level for tide j (m TAW); and z_j = the platform elevation at tide j (m TAW). If $H_j < z_j$ there is no inundation and H_j-z_j = 0. Based on the ΔE measurements in the CRT and the tidal marsh (i.e. at the 13 SET locations, see Figure 5.2a), we performed a non-linear exponential regression analysis between ΔE rates and mean water depths over 4 periods of about one year (March 2006 to March 2007, March 2007 to March 2008, March 2008 to March 2009 and March 2009 to December 2009). Based on this regression analysis the model coefficients a and b (Equation (1)) were estimated. Hence the resulting equation explains both the spatial variation in ΔE rate (between the 13 SET locations) and the temporal variation (between the 4 periods).

Apart from elevation changes on the CRT platform, channel erosion has an effect on the changes in mean water depth. In order to account for channel erosion in the model, the observed total volumes of channel erosion were calculated and modeled as a function of time. Based on the yearly channel measurements, we quantified the volume of sediment eroded in the former ditches and in the new formed channels. First we performed a linear interpolation of elevation along the yearly measured stream threads (using ArcGis 9.2). In this way the change in elevation was determined for every point along the stream threads (length profiles). Secondly, using the cross-

sectional data, we calculated the change in cross-sectional area and related this to the change in stream thread elevation for all cross-sections. Based on this relationship, the changes in stream thread elevation (derived from the yearly interpolation along the length profile) were converted to changes in cross-sectional area, and allowed us to calculate the total volume of eroded sediment in the channels. The temporal evolution of the eroded channel volume was then modeled as:

$$V_e(t) = c\ln(t) + d \qquad (3)$$

where $V_e(t)$ = the eroded volume after t years (m^3); t = the number of years after the flooding started in the CRT; and c and d are regression coefficients. A logarithmic equation was used, simulating the initially fast erosion of channels directly after the introduction of the tide, followed by a decreasing rate of channel erosion, as the channels approached a dynamic equilibrium with the introduced tidal regime.

To obtain a representative distribution of high water levels in the CRT, we used the high water levels measured from March 2006 (start of flooding) till March 2007 (period of one year). In the model, these tidal data were used to calculate ΔE rates, with a yearly correction on the high water levels, a consequence of the CRT morphodynamics (see §5.3.2.2).

5.3.2.2 Spatial implementation of the model

We implemented the model spatially so that it predicts the elevation at the end of every year t (where t=1 for the first year after flooding started in the CRT, etc.), and for each grid cell in the DEM with coordinates (x,y), as:

$$z(x,y,t) = z(x,y,0) + \sum_{1}^{t} \Delta E(x,y,t) \qquad (4)$$

where z(x,y,t) is the elevation (m TAW) at the end of year t for each grid cell (x,y); z(x,y,0) is the initial grid cell elevation before flooding started (m TAW); and ΔE(x,y,t) is the grid cell change in elevation (m) during year t. The grid cell change in elevation is dependent on the mean water depth (see Equation (1)) and is written as:

$$\Delta E(x,y,t) = ah(x,y,t)^b \qquad (5)$$

where h(x,y,t) = the mean water depth (m) during year t for each grid cell (x,y); and a and b are the regression coefficients that were found based on our SET data. Equation (5) is only valid for the CRT platform, for the channels no change in elevation was assumed ($\Delta E = 0$). The grid cell mean water depth in Equation (5) is defined as:

$$h(x,y,t) = \frac{1}{k}\sum_{j=1}^{k}(H_j(t) - z(x,y,t-1)) \quad (6)$$

where k = the number of tides during year t; $H_j(t)$ = the high water level (m TAW) for a tide j during year t; and z(x,y,t-1) = the grid cell elevation (m TAW) at the end of year (t-1) (i.e., beginning of year t). If $H_j(t) < z(x,y,t-1)$ the grid cell is not inundated and $H_j(t) - z(x,y,t-1) = 0$.

The high water levels $H_j(t)$ within a CRT rise in accordance with the rise of surface elevation in the CRT. As explained earlier, the supply of water is here determined by the sluice dimensions. This is an important difference with natural tidal marshes where a rise in surface elevation has no effect on the high water levels. We defined in the CRT model the term $H_j(t)$ as:

$$H_j(t) = H_j(1) + \sum_{2}^{t} H_m(t) + \sum_{2}^{t} H_e(t) \quad (7)$$

where $H_j(1)$ = the high water level (m TAW) for tide j during year 1 (i.e. the observed tidal data within the CRT from March 2006 till March 2007, thus after one year of flooding in the CRT); $H_m(t)$ = the mean effect of net sediment volume changes (morphodynamics) on the high water levels during year t (m); and $H_e(t)$ = the effect of a rise in MHWL in the estuary, on the CRT high water levels during year t (m). The term $H_m(t)$ hereby is defined as:

$$H_m(t) = \frac{1}{k}\sum_{j=1}^{k} H_{m,j}(t) \quad (8)$$

where k = the number of tides in the input tidal dataset between March 2006 and March 2007; and $H_{m_j}(t)$ = the effect of net sediment volume changes on the high water level of tide j during year t (m). These sediment volume changes are the net result of platform elevation change and channel erosion at the end of year (t-1) (i.e. beginning of year t). First the volume change caused by platform elevation change below the high water level of tide j at the end of year (t-1) is written as:

$$V_{\Delta E,j}(t-1) = \Delta x \Delta y \sum \Delta E_j(t-1) \quad (9)$$

where $V_{\Delta E,j}$(t-1) = the change in volume caused by platform elevation changes (m³) below the high water level of tide j during year (t-1); $\Delta x \Delta y$ = the surface area of one grid cell in the DEM (m²); and $\sum \Delta E_j$(t-1) = the sum of the grid cell elevation changes (m), for the cells flooded by tide j during year (t-1). Including the volume of sediment eroded in the channels (see Equation (3)), we can now define the net effect of platform elevation change and channel erosion on the high water level in a CRT as:

$$H_{m,j}(t) = \frac{V_{\Delta E,j}(t-1) - V_e(t-1)}{A_j} \quad (10)$$

where V_e(t-1) = the volume of sediment eroded in the channels (m³) during year (t-1); and A_j = the surface area flooded by the high water level of tide j (m²). This effect is absent in the estuary, there sediment volume changes have no effect on the water level, and for a natural tidal marsh the term $\sum H_m(t)$ (see Equation (7)) is equal to zero.

5.3.2.3 Model validation

Subtracting the DEM of December 2009 with the DEM of the former polder (see Figure 5.2a) allowed us to calculate an ΔE rate map after nearly 4 years of reduced tidal flooding. From this raster map of ΔE rates (with 1 by 1 m raster cells) we overlaid analyses points (in a 10x10 m grid) and attributed to every point the observed elevation and observed ΔE rate, and the modeled elevation and modeled ΔE rate after 4 years. In this way, the observed data (based on the DEMs) are independent from the model (based on the SET data). We plotted the observed data against the modeled data and made a distinction between data points located in the vegetated and the unvegetated zones. Delineation of vegetation zones was based on satellite images of the CRT marsh in June 2010. The model was evaluated according to the model efficiency coefficient ME (Nash and Sutcliffe, 1970):

$$ME = 1 - \frac{\sum (OBS - SIM)^2}{\sum (OBS - MEAN)} \quad (11)$$

where OBS = the observed elevation or ΔE rate; SIM = the simulated elevation or ΔE rate; and MEAN = the mean of the observed elevations or ΔE rates. Values for ME range from -∞ to 1. The closer ME approaches 1, the better the model predicts observed values.

5.3.2.4 Model scenarios

Once the model was validated, it was used to simulate long-term trends of elevation change (75 years) under a scenario without MHWL rise, one with a constant MHWL rise and one with an accelerated MHWL rise. For each scenario we compared elevation changes within the CRT with the elevation changes of the natural tidal marsh. For natural tidal marshes, changes in sediment volume have no effect on the water level, and the term $\sum H_m(t)$ (Equation (7)) was always equal to 0. In the estuary, at the Lippenbroek study area, the MHWL rise over the last decades is 1.5 cm a^{-1} (Temmerman et al., 2004b). Based on the relationship between the high water levels in the CRT and the estuary, this corresponds with a MHWL rise of 1.176 cm a^{-1} in the CRT (reduced tide). These values were used to simulate the scenario with constant MHWL rise. Within 50 years, almost a doubling of the sea-level rise is expected (Intergovernmental Panel on Climate Change IPCC, 2007). To simulate our scenario with accelerated MHWL rise, a yearly value of 0.02 cm a^{-1} was added to the MHWL rise of 1.5 cm a^{-1}. After 50 years, the MHWL rise increased in this way from 1.5 cm a^{-1} towards 2.5 cm a^{-1}. In the CRT a corresponding value of 0.0157 cm a^{-1} was added to the value of 1.176 cm a^{-1}. The term $\sum H_e(t)$ in Equation (7) stands for all scenarios involving MHWL rise.

To evaluate the model scenarios and the differences between the CRT and the natural tidal marsh, 3 time parameters were introduced. First we define the term t_r, which is the time needed to reduce the platform elevation differences (morphological range) below a certain threshold value. The condition is written as:

$$(z_h - z_l) < \Delta z_{cr} \qquad (12)$$

with z_h = the highest site elevation (m); z_l = the lowest site elevation (m); and Δz_{cr} = the critical elevation difference that defines the time t_r, in this study Δz_{cr} = 0.1 m. Under a scenario with constant MHWL rise, an equilibrium is reached after a certain time t_e, where the ratio between the MHWL rise and the increase in platform elevation becomes very close to 1, and this for all sites on the platform (low, intermediate and high elevated sites). The condition to define the equilibrium time t_e is written as:

$$\left|1-\frac{H_r}{\Delta E}\right| < 0.05 \qquad (13)$$

where H_r = the rise in MHWL (m a^{-1}); and ΔE = the ΔE rate (m a^{-1}). Finally we introduce a condition that describes the ability of a platform to keep up with an accelerating MHWL rise. The condition is written as:

$$H_r > \Delta E_l \qquad (14)$$

with ΔE_l = the ΔE rate (m a^{-1}) of the lowest elevated site. Once this condition is true, after a certain time t_a, the platform is no longer able to keep up with an accelerated MHWL rise. In total we introduced 3 time parameters (t_r, t_e, and t_a) defined by the conditions in equation (12), (13) and (14), and which respectively describe: (1) the rate whereby elevation differences decrease, (2) the time needed for attaining an equilibrium level under a constant sea-level rise, and (3) the ability to keep up with an accelerating sea-level rise.

5.4 Results

5.4.1 Observed ΔE rates

At 10 sites in the CRT and 3 sites in the adjacent natural tidal marsh, elevation changes were monitored by use of surface elevation tables (SETs). In the Lippenbroek, 8 of the 10 sites are located on the CRT platform; the other 2 are located in a tidal pool. This tidal pool is a topographic depression that is surrounded by a higher elevated zone (Figure 5.2a), in this way the depression is not drained completely at low tide, and the supply of water to the depression only takes place during high tides that overtop the surrounding higher elevated zone (Figure 5.2a). Based on the initial elevation relative to MHWL, the CRT sites can be subdivided into low elevated sites (sites 4, 5 and 6), intermediate elevated sites (sites 1, 2 and 3), high elevated sites (sites 7 and 10), and tidal pool sites (sites 8 and 9) (Figure 5.3, right side). Of the 3 sites on the natural tidal marsh one can be considered as intermediate elevated site (site R1) and two as high elevated sites (R2 and R3) (Figure 5.3). Low marsh sites are almost not present in the natural tidal marshes (Figure 5.3), and were therefore not monitored.

The low CRT sites are initially characterized by a strong increase in surface elevation (Figure 5.4a) at rates of 0.109 to 0.134 m a^{-1} during the first year (Figure 5.4b). Consequently these low sites get less flooded with time, ΔE rates progressively decrease towards about 0.085 m

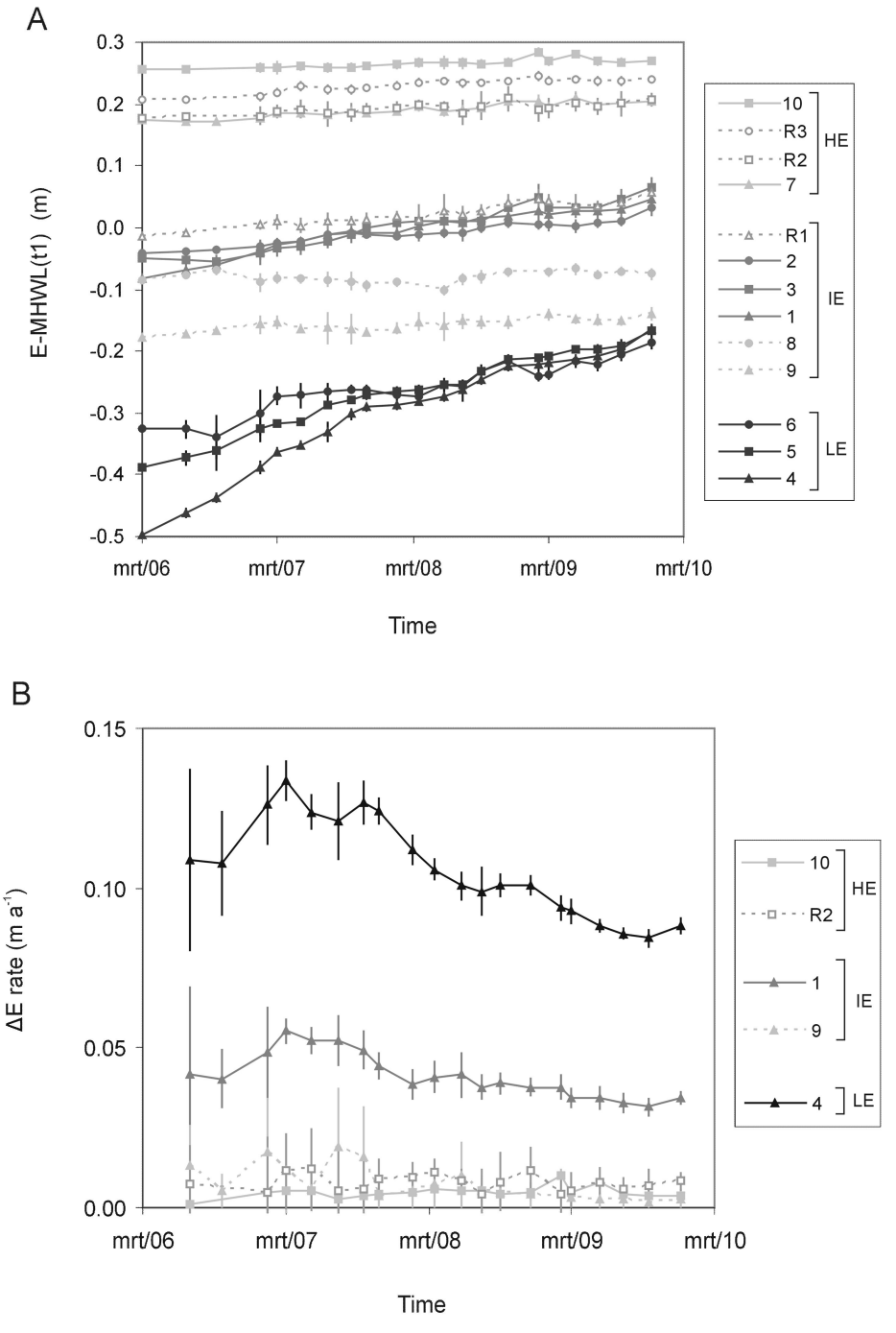

Figure 5.4 (a) Elevation changes (subtracted with the MHWL of the first year) over a period of nearly 4 years, represented for all measuring sites. (b) ΔE rates for a low elevated site (4), an intermediate elevated (1), two high elevated site (10 and R2), and a tidal pool site (9).

a^{-1} by the fourth year (site 4, Figure 5.4b), and the surface elevation increases less fast with time (Figure 5.4a). A similar pattern can be observed for the intermediate elevated sites, however, here the initially observed ΔE rates are lower (0.04 to 0.055 m a^{-1} for the first year), because these sites are located higher in the tidal frame, and consequently less frequently flooded. The decrease in ΔE rate with time is also slower on the intermediate elevated sites than on the low sites (cf. site 1 and 4, Figure 5.4b). For the high elevated sites, the ΔE rates are clearly lower (0.001 to 0.01 m a^{-1}), since they are less frequently flooded, and the ΔE rate at a site can be considered as constant (e.g. 0.005 m a^{-1} for site 10, see Figure 5.4b).

Although the tidal pool sites (sites 8 and 9) have an intermediate elevation, their ΔE rate is comparable with the high elevated sites (Figure 5.4a). This is because the tidal pool is a topographic depression, surrounded by a high elevated zone (Figure 5.2a), so that the depression is poorly drained at low tide, and is only flooded by the high tides that overtop the surrounding high elevated zone.

The tidal marsh sites have an initial elevation at MHWL (R1, Figure 5.4a) or above MHWL (R2 and R3, Figure 5.4a). For the high elevated marsh sites (R2 and R3) inundation frequencies are similar to the higher elevated zones of the Lippenbroek, and consequently ΔE rates and morphologic evolutions are very similar (e.g. cf. site 10 and R2, Figure 5.4a and 5.4b).

5.4.2 Explanatory variables for observed increase in elevation

The spatio-temporal variations in yearly ΔE rates at all sites (except from the tidal pool sites 8 and 9) were correlated to possible explanatory variables: mean water depth h (see Equation (2)), the distance D_c to the nearest tidal channel, and the distance D_e to the inlet sluice (for sites in the CRT) or marsh edge (for marsh sites). This was done by a stepwise multiple exponential regression analysis. The mean water depth h explains by far the largest part of the variations in ΔE rates (Figure 5.5, $R^2 = 0.72$, $p<0.0001$, $a = 0.245$ and $b = 1.269$), while the variables D_c and D_e have a negligible additional explanatory value (Table 5.1). Plotting the ΔE rates against the mean water depth showed no significant difference between the ΔE rates observed in the CRT and on the tidal marsh (Figure 5.5), hence both datasets were combined.

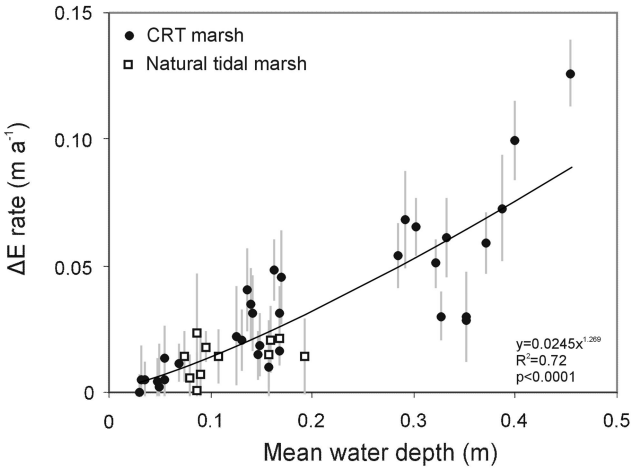

Figure 5.5 Relationship between mean water depth and ΔE rate.

Table 5.1 Contribution of the mean water depth h, distance D_c to the nearest tidal channel, and distance D_e from the inlet sluice (for the CRT sites) or tidal marsh edge (for the natural tidal marsh sites), to the rate in surface elevation change (ΔE rate).

Explanatory variables	R^2	p
h	0.72	<0.0001
D_c	0.01	0.62
D_e	0.31	0.001
h, D_c	0.35	0.002
h, D_e	0.57	<0.0001
D_c, D_e	0.57	<0.0001
h, D_c, D_e	0.58	<0.0001

5.4.3 Platform elevation increase versus channel erosion

In a CRT, both platform elevation changes and channel erosion will contribute to net volume changes of the CRT and will have an effect on the high water levels within the CRT: greater increase in surface elevation than erosion will cause an increase in high water levels, while more erosion than increase in surface elevation will cause a decrease (see Equation (10)). The total volume of platform elevation increase is significantly larger than the total volume of channel erosion (Figure 5.6). The temporal evolution of eroded channel volumes follows a logarithmic relationship, which we used to predict channel erosion in our model (see Equation (3); with c=517.663 and d=198.974).

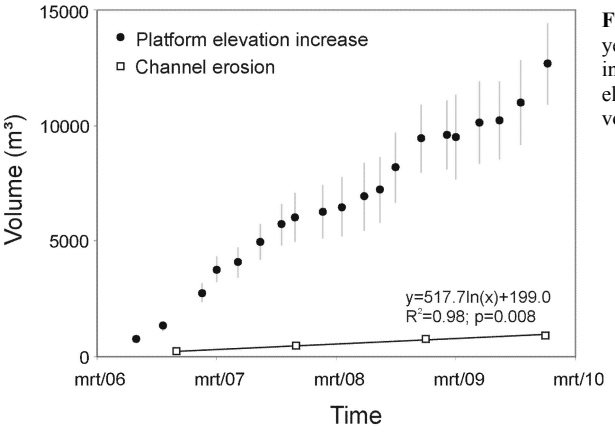

Figure 5.6 Time evolution (nearly 4 years) of the calculated sediment volumes induced by the increase in CRT platform elevation, and the eroded sediment volumes in the CRT channels.

5.4.4 Model validation

The model, which was built using the SET data (see Equations (1) and (2)), was validated against the independent DEM data, making a distinction between vegetated and unvegetated zones (delineation of these zones, Figure 5.7a). For the whole CRT platform, there is a strong correlation (R^2 = 0.84) between the observed and predicted elevations (Figure 5.7b). Only for the low elevations the model clearly overestimates observed elevations (data plot above 1:1 line). These elevation data are from locations in the unvegetated zones of the platform, indicating that for the same elevation, the increase in surface elevation is lower in the unvegetated than in the vegetated areas. The model efficiency ME = 0.74 when both vegetated and unvegetated areas were considered, and improves towards ME = 0.79 if only the vegetated area is considered. For the ΔE rates (Figure 5.7c), the correlation between observed and predicted data is less strong (R^2 = 0.31 for the whole platform; R^2 = 0.49 for only the vegetated zone), and the ME = -0.05 (for the whole platform), but significantly improves towards ME = 0.39 for the data in the vegetated area. If we only consider the lower elevations (< 2.9 mTAW, no unvegetated area above this threshold value, see Figure 5.7b), the ME for both vegetated and unvegetated areas is -0.22, and improves towards ME = 0.4 for the data in the vegetated area. Furthermore, there is an extremely highly significant difference between the observed and the predicted ΔE rates for the unvegetated area (Welch two sample t-test, $p<0.0001$), while the difference is clearly less significant for the vegetated area ($p=0.02$). Similar to the elevation, the overestimation of ΔE rates for the unvegetated areas is clearly demonstrated (Figure 5.7b and 5.7c), supported by the calculated ME and t-test values.

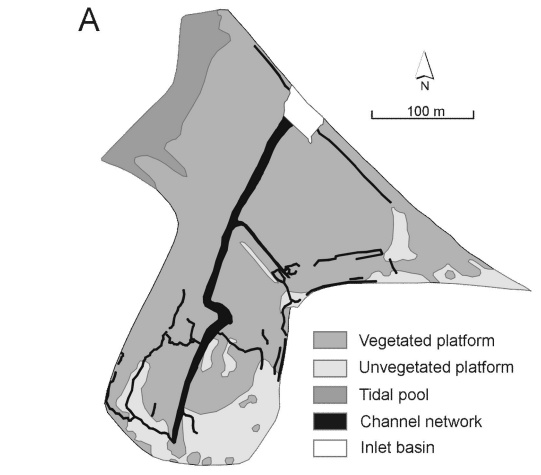

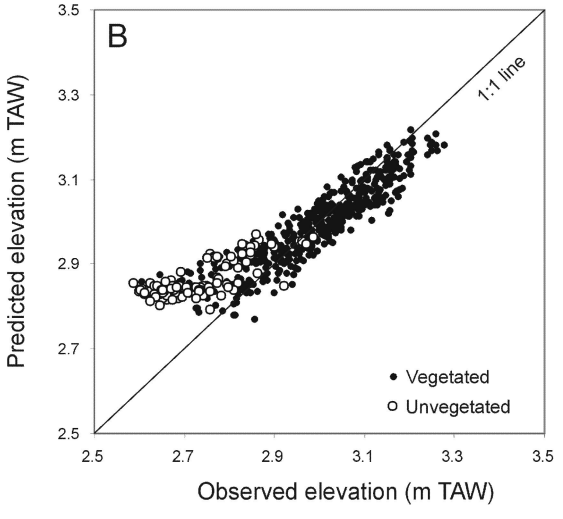

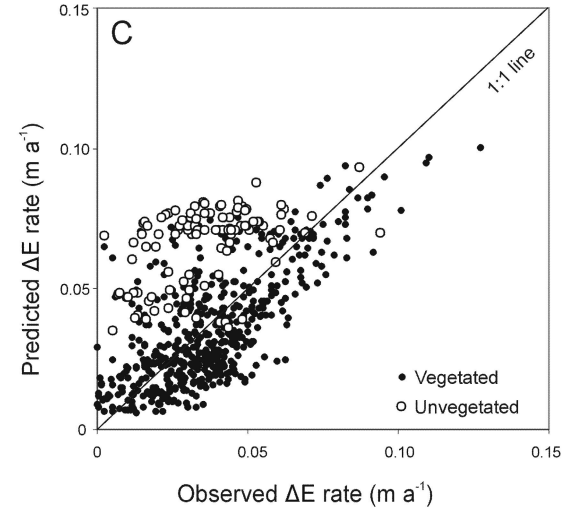

Figure 5.7 (a) Vegetated and unvegetated zones, and channel network after nearly 4 years of tidal working. (b-c) Comparison between the observed elevation and the predicted elevation (in m TAW = the Belgian ordnance level) (b), and the observed ΔE rate and the predicted ΔE rate (c), both over a period of 4 year.

5.4.5 Modeling long-term elevation changes in a CRT

The model describes the elevation change of a CRT platform and a natural tidal marsh platform over a period of 75 years, under a scenario with no MHWL rise, one with a constant MHWL rise and one with an accelerated MHWL rise. Without MHWL rise in the estuary, the MHWL within the CRT increases due to the net surface elevation increase within the CRT (Figure 5.8a). During the first years, ΔE rates are very comparable for the CRT platform and the natural tidal marsh platform. In time however, ΔE rates become higher for the CRT, caused by the increase in MHWL. In both systems, the spatial elevation-ΔE feedback, which refers to the faster increase in elevation for lower sites than for higher sites, causes a decrease in platform elevation range. For the CRT, the platform elevation range becomes less than 0.1 m after 17 years, whereas on the natural tidal marsh this occurs only after 40 years (see t_r, Figure 5.8a and Table 5.2). On a tidal marsh platform ΔE rates decrease in time for the entire platform: the higher the elevation of the marsh, the less it gets flooded and the smaller the rate in surface elevation increase. In a CRT this temporal elevation-ΔE feedback is absent, there the water supply is constant in time and the water depths become redistributed. As the CRT platform elevation range decreases, the mean water depth decreases for the low elevated sites resulting in a decrease in ΔE rate, and increases for the high elevated sites resulting in an increase in ΔE rate (Figure 5.8a, high elevated site, increase in ΔE rate at ~2015). After 75 years, the CRT platform no longer displays any spatial elevation differences, with the platform elevation 0.26 m above MHWL. Whereas in the natural tidal marsh the initially high elevated sites are still 0.06 m higher than the low elevated sites and with a platform elevation (from high elevated sites) 0.41 m above MHWL.

Under a scenario with a constant MHWL rise in the estuary of 1.5 cm a^{-1} (as observed in the past decades), which causes an additional MHWL rise within the CRT of 1.18 cm a^{-1} (in addition to the MHWL rise by increase in surface elevation), the time needed to reach a platform elevation range less than 0.1 m is 13 years for the CRT and 19 years for the natural tidal marsh, which is clearly faster compared to the scenario without MHWL rise (cf. Figure 5.8a and 5.8b, Table 5.2). In time, an equilibrium is reached with the rate in platform elevation increase equal to the constant rise in MHWL. Based on the condition in Equation (13), the time needed to reach this equilibrium (t_e) for the entire platform is 26 years for the CRT and 42 years for the natural tidal marsh (Figure 5.8b, Table 5.2). Importantly, the equilibrium platform elevation is hereby 0.06 m below MHWL for the CRT and 0.07 m above MHWL for the natural tidal marsh (Figure 5.8b).

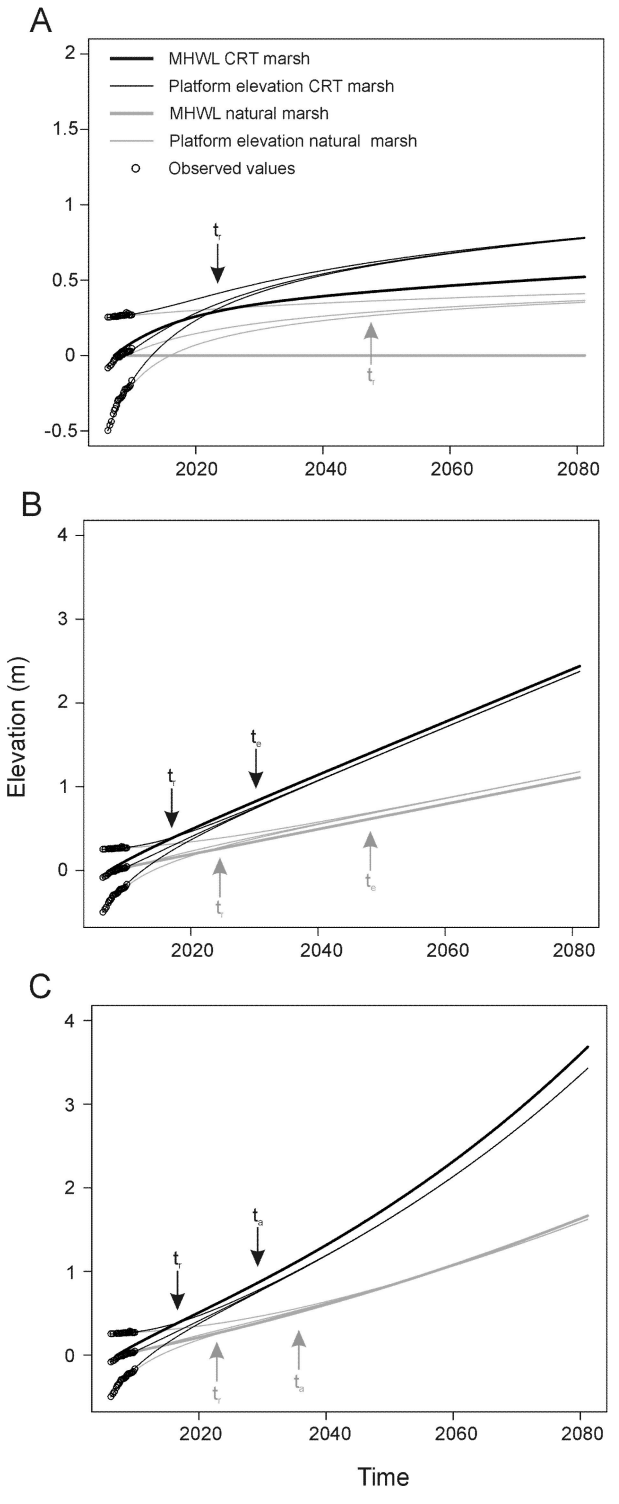

Figure 5.8 Simulation of the platform elevation changes (thin lines) for a low elevated site (LE), an intermediate elevated site (IE) and a high elevated site (HE), in a CRT marsh (black lines) and a natural tidal marsh (grey lines), over a period of 75 years, under 3 different scenarios of MHWL rise (bold lines): (a) no rise in MHWL, (b) constant MHWL rise (1.5 cm a^{-1}), and (c) an accelerated MHWL rise (additional acceleration of 0.02 cm a^{-1}). t_r is the time needed to reduce the spatial elevation differences below 0.1 m (Equation (12)), t_e the time needed to attain the equilibrium level (Equation (13)), and t_a the time after which the marsh is no longer able to keep up with an accelerated MHWL rise (Equation (14)). Observed values are plotted as circles and all elevations and MHWLs are relative to MHWL measured during the first year.

Table 5.2 Overview of the time (in years) needed to reduce the spatial elevation differences below 0.1 m (t_r) (Equation (12)), to attain the equilibrium condition (t_e) (Equation (13)), and after which the marsh is no longer able to keep up with an accelerated MHWL rise (t_a) (Equation (14)), compared for a CRT marsh and a natural tidal marsh, under a scenario without MHWL rise, with a constant MHWL rise and with an accelerated MHWL rise.

Scenario	CRT marsh			Natural tidal marsh		
	t_r	t_e	t_a	t_r	t_e	t_a
noMHWLr	17	-	-	40	-	-
cMHWLr	13	26	-	19	42	-
aMHWLr	13	-	24	18	-	30

In case of an accelerated MHWL rise (0.02 cm a^{-1} in the estuary, 0.0157 cm a^{-1} in the CRT), initially the MHWLs of the accelerated scenario versus the scenario with a constant MHWL rise are very similar, and the time needed to reduce the platform elevation is thus comparable for both (cf. Figure 5.8b and 5.8c, Table 5.2). After 24 years (t_a), the rate in platform elevation increase of the lowest elevated site in the CRT becomes lower, and remains lower, than the rise in MHWL (Figure 5.8c). At that point, the platform is no longer able to keep up with an accelerating MHWL rise. At t_a the platform elevation is 0.11 m lower than the MHWL, after 75 years this difference is already 0.25 m (Figure 5.8c). In the natural tidal marsh, after 30 years, the ΔE rate of the lowest elevated site becomes less than the rise in MHWL. At this point the site elevation is still 0.02 m above MHWL but in time becomes located below MHWL (0.04 m after 75 years, Figure 5.8c).

5.5 Discussion

On a natural tidal marsh, spatial variations in sediment deposition are explained by the tidal inundation (frequency, height, duration), the distance from the creeks and the distance from the marsh edge (Leonard, 1997; Temmerman et al., 2003b). In the studied CRT marsh, there is a relative large spatial variation in initial elevation (0.75 m, Figure 5.4a). Consequently the observed variations in ΔE rates are largely explained by the tidal inundation parameter (i.e. mean water depth), while distance from creeks and distance from marsh edge (i.e. inlet sluice) play a minor role (Table 5.1). However, due to the spatial elevation-ΔE feedback, elevation differences will decrease in time and the CRT marsh platform will progressively evolve towards a flattened platform. We expect that distance from the creeks and distance from the inlet sluice will become more important once the spatial elevation differences are strongly reduced (i.e. around t_a, Figure 5.8), resulting in the formation of levees along the channels, a typical feature observed in the natural tidal marshes (Allen, 2000; Temmerman et al., 2004a). Besides sediment deposition, organic matter accumulation contributes to ΔE (Nyman et al. 2006; Neubauer, 2008). Organic

matter accumulation can be expected to differ between the CRT sites and the natural tidal marsh due to the different vegetation species and colonization times (Jacobs et al., 2009). However, the large explanatory value of mean water depth (Table 5.1) suggests that these differences have no important effect on ΔE, and hence that the contribution of organic matter accumulation can be considered as rather limited.

Temporal variations in marsh sediment deposition are related to variations in tidal inundation (frequency, height, duration) and seasonal variations in suspended sediment supply (Hutchinson et al., 1995; Leonard, 1997; Temmerman et al., 2003a). The temporal elevation (~mean water depth)-ΔE feedback is clearly observed in our dataset. Low elevated sites (only in the CRT marsh) have initially high rates in surface elevation increase. Consequently these sites get less flooded with time, and ΔE rates progressively decrease. High elevated sites (in the CRT and natural marsh) have low rates in surface elevation increase, low mean water depths and ΔE rates do not change rapidly (Figures 5.4a and 5.4b). Although some variations are present in the bimonthly ΔE rates (Figure 5.4b), no significant changes are observed for the subsequent seasons, and we therefore consider the mean water depth as the most important parameter to explain temporal variations in ΔE rate (R^2=0.87 and $p<0.0001$ for the lowest elevated CRT site). Considering ΔE rates over a period of one year, rates in surface elevation increase are largely explained by the mean water depth (Figure 5.5). Despite the longer stagnant phase in a CRT marsh (Figure 5.2c), and the differences in vegetation cover and thus organic accumulation rate (pioneer vegetation in CRT, climax vegetation in natural tidal marsh (Jacobs et al., 2009), no significant differences are observed between ΔE in the CRT marsh and the natural tidal marsh (Figure 5.5). We therefore considered the strength of the temporal elevation-ΔE feedback equal for both systems. It is important to emphasize that the observed temporal CRT elevation-ΔE feedback is only applicable to the initial stage of the CRT marsh development. Once the spatial elevation differences are strongly reduced (by faster increase in surface elevation for the lower elevated sites) the temporal elevation-ΔE feedback disappears and the mean water depth remains constant in time (increase in surface elevation = increase in MHWL).

The effect of increase in the CRT platform elevation inducing a local increase in MHWL is absent for natural tidal marshes. There the temporal elevation-ΔE feedback is still present and an increase in elevation results in a decrease in mean water and thus a decrease in surface elevation rise. Consequently, as demonstrated by model simulations over a period of 75 years, ΔE rates become higher in a CRT marsh and spatial elevation differences are more rapidly reduced (Figure 5.8 and Table 5.2). This has important implications for the habitat diversity, since spatial elevation gradients in a tidal marsh are the most important cause of habitat diversity. Therefore, (1) loss in

diversity goes faster for a CRT marsh than for a natural tidal marsh (cf. t_r in Figure 5.8a) and (2) loss in diversity is faster under a scenario with constant MHWL rise or accelerated MHWL rise (cf. t_r in Figure 5.8a with Figures 5.8b and 5.8c). Once the platform elevation differences are strongly reduced for both systems, regardless of the scenario in MHWL rise, a CRT marsh platform is always more inundated than a natural tidal marsh (lower platform elevation compared to the MHWL, Figure 5.8a, 5.8b and 5.8c). Consequently a CRT marsh evolves in all scenarios towards a relative lower stage in marsh vegetation succession. The absolute stage in vegetation succession is however very different for the three scenarios. Without an increase in MHWL the platform elevation becomes for both systems clearly higher than the MHWL (Figure 5.8a), and the platform will evolve towards high stages in marsh vegetation. Under a constant MHWL rise, the platforms reach an equilibrium with the MHWL (see t_e Figure 5.8b and Table 5.2), with the platform elevation of the natural marsh being above MHWL and being below MHWL for the CRT marsh (Figure 5.8b). This is important for the restoration of tidal marshes along the Scheldt estuary: a platform elevation below MHWL implies the restoration of typical lower marshes, which is a habitat that is scarce along the Scheldt estuary (Jacobs et al., 2009). Under an accelerated sea-level rise, the platform for both the CRT and natural tidal marsh becomes lower elevated than MHWL, however for the CRT marsh this process goes much faster (Figure 5.8c).

In the Lippenbroek, we clearly observed lower rates in surface elevation increase for the unvegetated sites than for the vegetated sites (see Figure 5.7b and 5.7c). In general, vegetation is considered to reduce incoming flow and hence to promote sedimentation (e.g., Leonard and Luther, 1995; Nepf and Vivoni, 2000; Neumeier and Amos, 2006). However, due to the long phase with stagnant water in a CRT marsh, most of the sediment has sufficient time to settle down from suspension, so that the additional flow reduction effect is limited. A more important effect of vegetation probably occurs during the ebb phase. As the unvegetated sites are always in direct connection with channels (Figure 5.7a), flow velocities are not reduced during drainage, and the unvegetated sites may become subject to re-suspension. Meanwhile, flow velocities remain low on the vegetated sites (flow reduction) and mineral sediment deposition is further promoted. Apart from differences in mineral sediment deposition, the accretion of organic matter (above-ground litter and below-ground roots) also may contribute to the higher ΔE rates observed in vegetated areas as compared to unvegetated areas.

Our model simulates that after 75 years, the platform elevation of the CRT marsh would increase (compared to the initial MHWL) by 0.75 m for a scenario with no MHWL rise, by nearly 2.5 m for a scenario with a constant MHWL rise (historical rate of 1.5 cm a^{-1}), and by 3.4 m for a scenario with accelerated sea-level rise (additional 0.02 cm a^{-1}). To assess the impact of these

values on the flood buffering function of a CRT marsh, the following issues should be taken into account. First the model predicts well the increase in elevation for a vegetated CRT marsh platform, but makes a clear overestimation for unvegetated sites (Figure 5.7). Consequently the simulations of overall increase in elevation of the CRT marsh platform are overestimated. It is thus important to know how these unvegetated sites will evolve in the long-term. Increase in elevation could favor the establishment of vegetation, but on the other hand, the increase in MHWL may be too large and the surface elevation may not be able to follow, as observed for some intertidal areas (Reed, 1995; Ward et al., 1998). Secondly, autocompaction could become an important factor in the long term morphologic evolution. Although we directly measured surface elevation changes, which is considered to include effects of autocompaction (Cahoon et al., 1995), it is uncertain whether autocompaction was already important over the relatively short measuring period of 4 years. The evolution of low elevated sites towards the MHWL (Figure 5.4) and the further channel development probably leads to a better drainage of the area and dewatering of sediments. Moreover, at vegetated sites, the organic matter may start to decay, initiating a lowering of the surface elevation. All these aspects indicate that autocompaction will occur, however to what extent and over which time period remains unclear.

Between Antwerp and Ghent (Figure 5.1b), in total 1500 ha of embanked land will be restored using the CRT technique. The CRT areas are dispersed along the river and this may have implications for the platform elevation increase of the different areas. Along the Scheldt estuary, the increase in MHWL varies from 0.6 cm a^{-1} up to 1.5 cm a^{-1} (Temmerman et al., 2004b). At CRT marsh sites where the increase in MHWL is high, the morphological evolution will be more according to the scenario with the MHWL rise equal to 1.5 cm a^{-1} (as in this study) (Figure 5.8b). If the increase in MHWL is rather low, CRT marshes will evolve more according to the case without MHWL rise (Figure 5.8a). Increase in MHWL is not the only parameter that has a gradient along the estuary. Average suspended sediment concentration varies between 0.1 g l^{-1} and 0.15 g l^{-1} in the Belgian part of the estuary (Temmerman et al., 2004b), with the highest values close to the present study site. This implies less sediment input and a less powerful elevation-ΔE feedback mechanism for a CRT marsh located at sites with lower suspended sediment concentrations.

5.6 Conclusions

(1) The spatio-temporal variations in wetland vertical development were measured over a period of 4 years in a restored tidal marsh with controlled reduced tide (CRT). The observed variations in the rate in platform elevation change (ΔE) were explained by variations in the mean water depth.

This relationship was not significantly different in the CRT marsh compared to an adjacent natural tidal marsh.

(2) Based on the relationship between ΔE rate and mean water depth a 2-dimensional, time-stepping model was developed and validated against independently collected field data. The model simulates the long-term (10-100 year) platform elevation change in a CRT marsh and a natural tidal marsh, by incorporating the effect of platform elevation change on MHWL rise in the CRT marsh, an effect that is absent for a natural tidal marsh.

(3) Model results show higher ΔE rates in a CRT marsh than in a natural marsh. Under a scenario of no MHWL rise, and after 75 years, the platform elevation in a CRT marsh is 0.75 m higher than the initial MHWL in the first year. Under a constant MHWL rise (1.5 cm a^{-1}) this increase in elevation amounts to 2.5 m, while under accelerated MHWL rise (acceleration of 0.02 cm a^{-1}) this increase in elevation is 3.4 m, or about 2 to 2.5 times higher as for the natural tidal marsh. Furthermore, there is a faster reduction of spatial elevation differences (<0.1m) in a CRT marsh (13-17 years) than in a natural tidal marsh (18-40 years). Under a scenario with constant MHWL rise, the equilibrium condition for the CRT marsh is reached after 26 years with the platform elevation 0.07 m above MHWL, and for the natural tidal marsh after 42 years with platform elevation 0.06 m below MHWL. A CRT marsh is less able to keep up with an accelerated MHWL rise; after 75 years the platform elevation is 0.25 m below MHWL, where in a natural tidal marsh this is only 0.04 m below MHWL.

(4) Above described results should be taken into account for future restoration and management of CRT marshes. Managing sluice dimensions and volumes of water exchange can improve the safety function of a CRT marsh (e.g. by reducing volumes of water and sediment import) and may force the restoration of the CRT marsh towards a specific stage in marsh succession (e.g. the lost lower marshes of the Scheldt estuary).

Chapter 6:

High-resolution observations on tidal channel network formation within a constructed tidal marsh

W. Vandenbruwaene, P. Meire and S. Temmerman

Geomorphology (submitted)

Abstract

The morphogenesis of tidal channel networks that dissect intertidal flats and marshes has been studied especially by morphodynamic modeling, while relatively few empirical data exist on high-resolution field observations. Here we measured the spontaneous formation and evolution of a tidal channel network in a newly constructed tidal marsh (Schelde estuary, Belgium) over a period of 4 years, by high-accuracy topographic surveying with a temporal resolution of 1 year and high spatial resolution considering all channels deeper than 0.1 m. As a reference, topographic measurements with a similarly high resolution were performed in a nearby, mature natural tidal marsh network. Based on the field surveying and additional GIS processing, we derived several geometric parameters (channel width, depth, volumes, cross-sectional area, length profiles, drainage density, mainstream length and watershed area), and compared the evolution of geometric relationships in the constructed marsh with the natural tidal marsh, in this way evaluating how fast an equilibrium state was attained. We found that after 2 to 3 years of tidal working the cross-sectional areas of the former ditches in the constructed marsh were in equilibrium with the corresponding watershed areas. Furthermore we observed that the mainstream lengths and the drainage densities for the smaller watershed areas were comparable with the natural tidal marsh, demonstrating the rapid headward growth of newly forming channels and tributary channel formation near the channel heads. Newly formed channels preferentially developed in the low elevated zones of the constructed marsh and channel extension was not significantly influenced by the presence or absence of vegetation. However, the overall channel drainage density and channel cross-sectional areas of the newly formed channels were after 4 years still lower compared to the natural tidal marsh. This indicates that further channel network extension and continued channel deepening must be expected during the coming years.

6.1 Introduction

Tidal channel networks are important landscape features of tidal environments. They play an essential role in tidal ecosystem functioning since they are the major flow paths for water, sediments and nutrients between the intertidal zone and the subtidal estuarine or coastal area. The morphogenesis of tidal channel networks has been studied especially through morphodynamic modeling (e.g., Fagherazzi and Furbish, 2001; Fagherazzi and Sun, 2004; D'Alpaos et al., 2005; Marciano et al., 2005; Temmerman et al., 2007; Kirwan and Murray 2007; D'Alpaos et al., 2007b). Existing models typically considered the initial formation of tidal channel networks as a quick morphodynamic process (e.g., Fagherazzi and Sun, 2004; D'Alpaos et al., 2005). After the rapid network initiation, slower, more long-term (10-100 years) processes are considered to take place, like meandering of the tidal channels (Marani et al., 2002) and gradual channel infilling as channel discharges decrease in response to vertical accretion of the surrounding intertidal platform (D'Alpaos et al. 2006). Once a critical elevation is exceeded the intertidal platform becomes colonized by vegetation, leading to enhanced sediment accretion on the platform, prevention of erosion, and stabilization of channel banks. From this point the tidal network is considered in most models to be frozen, with only minor changes during further network development.

Apart from morphodynamic models, relatively few empirical field data exist on the initial formation and evolution of tidal channel networks. This is probably because most tidal channel networks observed in the field are already in an equilibrium state (e.g., Fagherazzi et al., 1999; Rinaldo et al., 1999a; Rinaldo et al., 1999b; Marani et al., 2003; Novakowski et al., 2004; Shi et al., 1995a). Therefore, the initial formation of tidal channel networks may be best studied after restoration or creation of new intertidal areas, since here the formation of tidal channel networks mostly must start from a non-channeled landscape state (D'Alpaos et al., 2007a; Wallace et al., 2005; Williams et al., 2002). D'Alpaos et al. (2007) studied the tidal network formation in a constructed salt marsh in the Venice lagoon (Italy). The planimetric form of channel networks was extracted from aerial photographs for two time steps (2 and 4 years after tide introduction). These authors solely focused on the evolution of channel drainage density and compared field data with model simulations. A more extensive field study was done in the Tijuana estuary (California, USA) by Wallace et al. (2005). Channel cross-sectional areas and channel lengths were monitored over a period of 5 years, with a high temporal resolution of 1 year. In San Francisco bay (USA) channel cross-sectional areas were monitored over a period of 13 years, with a temporal resolution of 2 or more years (Williams et al., 2002). Data were collected for several restoration sites and the relationship between tidal prism and cross-sectional area was compared with the equilibrium state from nearby mature marshes. Summarizing these existing studies, they focused either on the

planimetric formation and evolution of channel density (D'Alpaos et al., 2007) or the evolution of a number of channel cross-sections (Wallace et al., 2005; Williams et al., 2002). To our knowledge, no studies have been done on the synergistic planimetric expansion and cross-sectional formation of tidal channel networks with a high temporal and spatial resolution, covering all scales within the tidal network.

Along the Scheldt estuary (Belgium) tidal marsh area is being restored on formerly embanked land. This is done through the construction of a culvert or sluice system through the dyke, which allows a controlled reduced tidal regime (CRT) in the formerly embanked area (Cox et al., 2006; Maris et al., 2007). Due to the low position of the formerly embanked land in the tidal frame, complete de-embankment would solely lead to bare tidal flat development. A reduced tidal regime is therefore essential to obtain a partially vegetated tidal marsh ecosystem on the formerly embanked land. After introduction of the CRT we expect the incision and extension of a new tidal channel network. However it remains unclear how fast network development takes place, when network properties are comparable with the equilibrium state of a natural tidal marsh network, and which geometric properties or geometric relationships attain their equilibrium state first.

The objective of this study is to gain empirical field knowledge with a high spatial and temporal resolution, on the initial formation of a tidal channel network in a constructed CRT marsh. The developing network in a watershed of 8 ha was surveyed every year, over a period of 4 years, by measuring changes in network planimetry, channel cross-sections, length profiles, and calculating channel volumes. The geometric properties and relationships of the developing network, and their spatio-temporal evolution, were compared with a fully developed channel network in a nearby natural tidal marsh.

6.2 Study area

The Scheldt estuary is located in the northwest of Belgium and the southwest of the Netherlands (Figure 6.1a). The estuary is characterized by a semi-diurnal meso- to macrotidal regime, with at the mouth a mean tidal range of 4.46 and 2.97 m respectively during spring and neap tides. Further upstream, the mean tidal range increases towards respectively 5.93 and 4.49 m near Temse, and then progressively decreases to 2.24 and 1.84 m near Ghent (Claessens and Meyvis, 1994). Due to the salinity gradient along the estuary, the tidal marshes bordering the stream channel can be subdivided into salt, brackish and freshwater marshes (Figure 6.1b) (for more detailed information about the Scheldt estuary, see e.g. Meire et al., 2005).

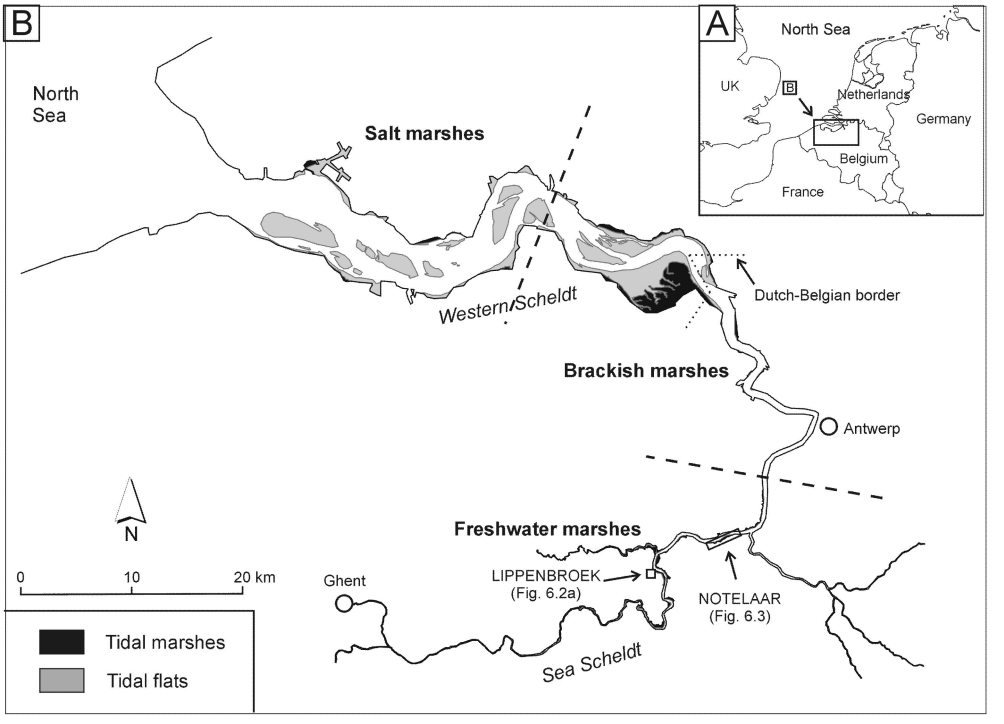

Figure 6.1 The Scheldt estuary. (a) Location within Western Europe. (b) Location of the salt, brackish and freshwater tidal marshes (separated by dashes lines), location of the Lippenbroek and Notelaar study areas.

The Lippenbroek and Notelaar study sites are located in the freshwater zone of the estuary, close to the maximum tidal range (~6 m) observed near Temse (Figure 6.1b). The Lippenbroek study site is a former polder area of 8 ha that has been restored into a tidal marsh, by the introduction of a so-called controlled reduced tide (CRT) in the former polder area since March 2006 (Cox et al., 2006; Maris et al., 2007). The Lippenbroek CRT marsh serves as a case study for much larger CRT areas (~100s of ha), currently under construction along the Scheldt estuary. Before March 2006, the study area was a polder area with a low elevation (2.3-3.2 m TAW, TAW = the Belgian Ordnance Level), with the higher elevated zones more close to the river dyke, and two artificial ditches (Figure 6.2a). As opposed to the embanked polder, the adjacent natural tidal marshes increased in elevation with rising MHWL, resulting nowadays in a marsh platform elevation around 5.7 m TAW. To create similar tidal conditions in the lower elevated polder (2.5 to 3.4 m lower), the principle of controlled reduced tide (CRT) was introduced (Cox et al., 2006; Maris et al., 2007).

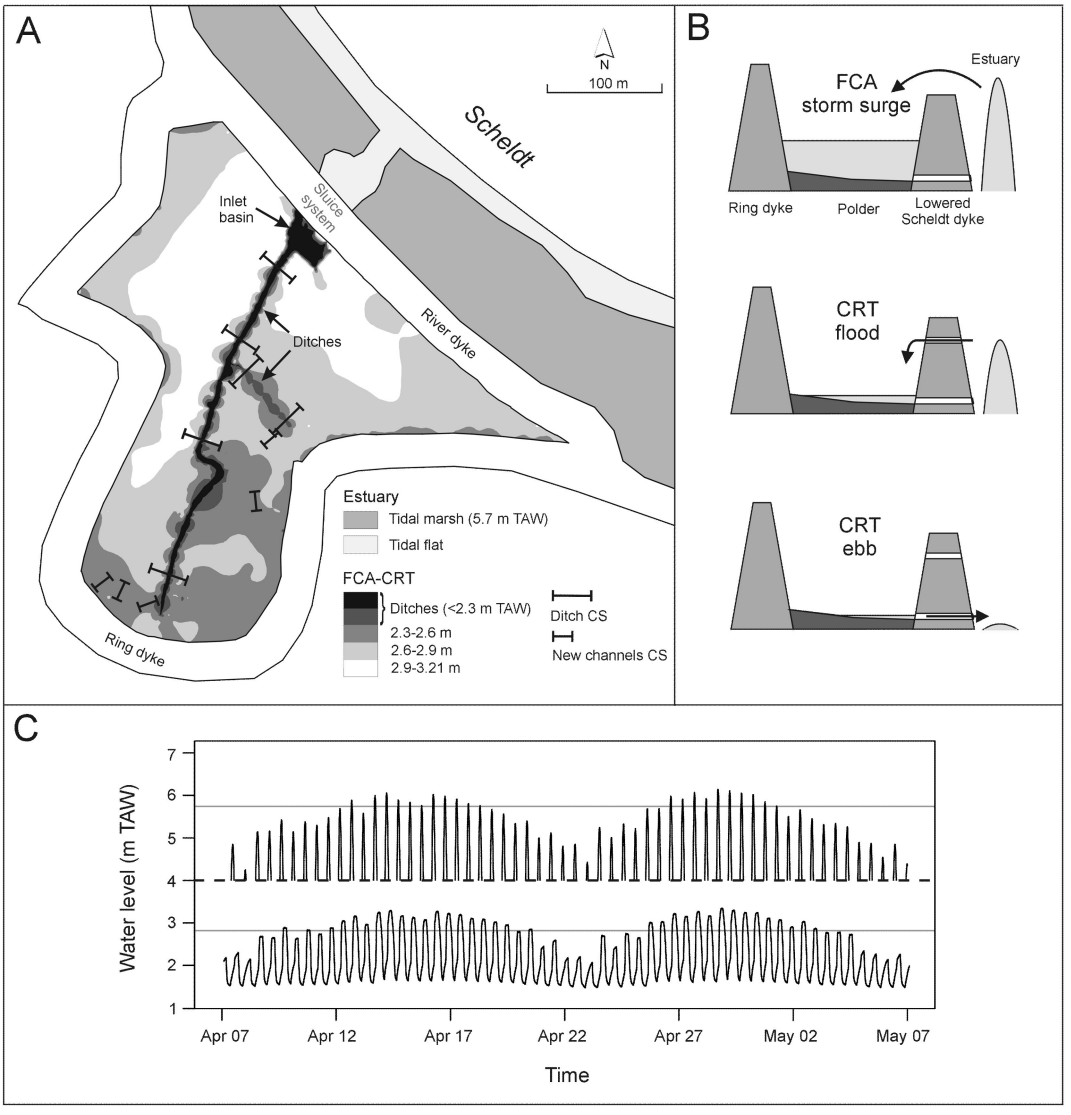

Figure 6.2 (a) The Lippenbroek flood control area (FCA) with controlled reduced tide (CRT), represented together with the former polder morphology and the measured channel cross-sections (CS). (b) Working principle of the FCA-CRT, illustrated for a storm surge (at the top), and for a mean tide during flood (in the middle) and during ebb (at the bottom). (c) Water levels in the Lippenbroek CRT (at the bottom) and in the estuary nearby the Lippenbroek (at the top) for two spring-neap tide cycles. For the estuary, only the water levels above 4 m TAW are presented (above the heavy dashed line). The two grey lines indicate the mean elevation of the Lippenbroek CRT marsh (bottom line) and the adjacent natural tidal marshes (top line).

To construct a marsh ecosystem in the low-elevated polder, with a controlled reduced tide (CRT), 3 major adaptations were necessary: (1) building a ring dyke to protect the surrounding land from flooding (Figure 6.2a), (2) lowering the river dyke for temporary storage of storm surge water, and (3) constructing an inlet (high in the river dyke) and an outlet sluice (low in the river dyke) to introduce the daily tidal regime (Figure 6.2b). By using a high inlet and a low outlet, the

spring-neap variations in tidal flooding frequency and height were successfully installed in the polder, however, with a clear longer stagnant phase as in the estuary (Figure 6.2c) (Cox et al., 2006; Maris et al., 2007). Already after a few years of tidal working in the CRT marsh, the former polder morphology was significantly altered by sedimentation and erosion processes (**Chapter 5**), and typical tidal freshwater vegetation colonized the area (Jacobs et al., 2009).

The Lippenbroek CRT marsh is compared here with the natural Notelaar tidal marsh, which is located more downstream in the estuary (Figure 6.1b). The Notelaar study site is a mature tidal marsh with a mean platform elevation 0.2 m above MHWL, and in equilibrium with the rise in MHWL observed in the estuary (Temmerman et al., 2004b). This typical high tidal marsh is morphologically characterized by a marsh platform with a levee-basin topography and a well-developed channel network (e.g. Temmerman et al., 2004a). The natural tidal marsh vegetation consists of typical freshwater tidal marsh plants and can be subdivided into a lower-elevated zone dominated by *Phragmites australis* and a higher-elevated zone dominated by *Salix* (Figure 6.3).

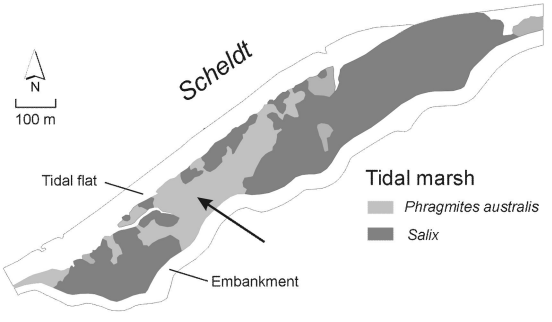

Figure 6.3 Notelaar tidal marsh study area with indication of the two dominant vegetation zones. The tidal network studied in this work is located in the *Phragmites australis* vegetation zone indicated by the black arrow.

6.3 Methods

6.3.1 Repeated measuring of channel morphology in the CRT marsh

Before the CRT was introduced in the Lippenbroek polder in March 2006, the morphology of the ditches, that were already present in the polder, was determined by measuring xyz-coordinates with a total station (Sokkia SET510k, accuracy 1-3 mm). Measuring points were located along the length profile (stream threads) of the ditches and along 6 cross-sections (Figure 6.2a). Along the length profile, points were measured every 10 m, along the cross-sections every 0.25 m. Measurements were repeated for the first time 8 months after the CRT was introduced, and since then with an interval of 1 year, so that the initial formation and temporal evolution of the channel network was monitored. Data on channel morphology are available for March 2006 (before the start of flooding, t0), November 2006 (t1), November 2007 (t2), December 2008 (t3)

and December 2009 (t4). In December 2008 additional measurements were performed to delineate the ditch edges (every 10 m one point).

During the monitoring period, new channels were formed and additional measurements were needed: (1) the stream threads of the new channels were measured (every 2-5 m one point) to follow up the planimetric evolution and extension of the channel network and (2) 6 additional cross-sections were monitored along the newly formed channels. A new channel was only mapped when its deepest point was at least 0.1 m deeper than the surrounding platform (within a radius of 2 m) over a channel length of minimum 10 m. All new channels were measured from November 2006 onwards, the additional cross-sections from December 2008.

6.3.2 Measuring the channel morphology of the natural tidal marsh

For the natural tidal marsh only the channel network located in the *Phragmites* vegetation zone (Figure 6.3) was measured. Channels in this area were determined by measuring xyz coordinates with a total station (Sokkia SET5F, accuracy 1-3 mm). Measuring points were located along the stream threads and edges of the channels. For every stream thread point (every 2-10 m one point), one accompanying edge point was measured on both sides of the channel. The greater part of the network was measured in February 2001 (with total station), a small part of the network, close to the mouth, was measured in April 2009 with a DGPS (Thales z-max, accuracy 1-2 cm).

6.3.3 Quantifying geometric parameters

6.3.3.1 Channel width w and channel depth d

As a first step to calculate channel widths and depths, the position and elevation of the channel edges had to be determined. In the CRT marsh, w and d were derived for each cross-section (Figure 6.2a) and for each measuring campaign, based on the curvature of the cross-sectional profile that was measured with a resolution of 0.25 m. The position of the channel edge was defined as the position where the curvature was above a critical threshold value. The channel width was calculated then as the horizontal distance between both edge points. The channel depth d was determined as the difference between the mean elevation of both edge points and the elevation of the deepest point in the channel (i.e. stream thread point).

In the natural tidal marsh, no detailed cross-sections were measured, but here about every 2-10 m one stream thread point and two accompanying edge points were measured (on both sides one). After plotting the points in a GIS (ArcGIS 9.2) first the channel edges were delineated by connecting the edge points with line features and secondly a distance raster was created (distance

from the created channel edges) which allowed us to attribute the channel width to each stream thread point. For the channel depth two interpolated raster files were created: one based on the elevation of the stream thread points and one based on the elevation of the edge points. The difference between both interpolated raster files resulted at the stream thread point locations into the channel depth.

6.3.3.2 Cross-sectional area Ω

For the cross-sections in the CRT marsh (Figure 6.2a), the cross-sectional area Ω was determined by connecting the fixed edge points by a straight line. In this way an enclosed polygon shape was created of which the area was calculated. For the natural marsh transects only channel widths and channel depths are known. To be able to calculate Ω for the natural tidal marsh, the Ω of the CRT marsh cross-sections was calculated alternatively based on the area of half an ellipse, according to:

$$\Omega = \frac{wd\pi}{6} \qquad (1)$$

with Ω = the cross-sectional area (m²); w = the channel width (m); and d = the channel depth (m). The half ellipse method was in good agreement with the more detailed polygon shape method ($R^2 = 0.99$; $p < 0.0001$). Hence cross-sectional areas for the natural marsh channels were calculated based on w and d values using Equation (1).

6.3.3.3 Channel drainage density

To evaluate the drainage density of tidal channel networks, previous studies have used the frequency distribution of so-called unchanneled flow lengths on the marsh platform (e.g., Marani et al., 2003; D'Alpaos et al., 2005; D'Alpaos et al., 2007b). The unchanneled flow lengths are calculated here as the shortest distance from any platform point to the nearest channel edge. The frequency distribution of unchanneled flow lengths is then a measure for the channel drainage density: the shorter the unchanneled flow lengths, the higher the drainage density. For the Lippenbroek ditches (Figure 6.2a), edge points were measured in December 2008 and channel edges were created for all 5 campaigns by connecting the December 2008 edge points. For the newly formed channels in the CRT marsh, channel edge points were only measured along the 6 cross-sections. To create channel edges for the newly formed channels, first the measured stream thread points (of the new channels) were connected by line features. Next a mean value for the

channel width of the newly formed channels was calculated based on the 6 cross-sections of the two campaigns (December 2008 and December 2009). Using the stream thread lines as input, two parallel lines (i.e. the channel edges) were created at half the channel width distance (i.e. mean value). This half width distance was than used to create the new formed channel edges for every campaign. For the natural tidal marsh, edge points were measured in the field about every 2-10 m and channel edges were created by connecting the edge points.

As a next step we evaluated the effect of the initial polder elevation and the vegetation development on the formation of new channels. First the distance to the new formed channel edges (exclusion of the ditches) was spatially calculated as a distance raster for every campaign (t1 till t4). By an overlay analysis of the Digital Elevation Model of the former polder surface (Figure 6.2a) and the created distance raster, the effect of initial polder elevation on the formation of new channels was examined. To assess the effect of vegetation, first the vegetated and non-vegetated zones were delineated using satellite images (July 2010, i.e. vegetation zones after about 3.5 years of tidal working). For both zones the same overlay analysis were done (DEM and distance raster for new formed channels), and by selecting three elevation classes, the effect of vegetation together with the combined effect of vegetation and elevation was evaluated.

6.3.3.4 Watershed area A, mainstream length L and total channel length ∑L

In terrestrial river networks watershed areas are exclusively delineated by elevation gradients, however, for tidal channel networks elevation differences are very limited and water flow is mainly determined by energy gradients (Rinaldo et al., 1999a; Marani et al., 2003). To determine watershed areas in the CRT marsh and the natural tidal marsh the following assumptions were made: (1) water over a platform always flows perpendicular away from the nearest stream thread (during flood tide) or perpendicular towards the nearest stream thread (during ebb tide) at flow velocities that are spatially homogeneous above the platform; (2) the contributing watershed area increases along channels with increasing distance from channel heads, measured along the channel network, and (3) channels not connected to the dendritic network were excluded (this only applies for the Lippenbroek networks). The watershed areas were calculated using the hydrology tools in the ArcGIS 9.2 software (Spatial Analyst extension). This algorithm is designed for terrestrial networks and requires as input a Digital Elevation Model. Based on the above described assumption (1), we first created a raster file representing the shortest distance between every platform raster cell and the nearest stream thread. For assumption (2), the distance from the mouth (measured along the network) was spatially represented by an allocation raster file. By summing both raster files, a virtual Digital Elevation Model (DEM) was made, incorporating

our postulated assumptions, which was used as input for the hydrology algorithm. As output a flow accumulation raster file was created returning the watershed surface areas along the stream threads. Finally the total channel length ∑L and the mainstream length L, for every location along the stream threads, were respectively determined by summing all channel lengths in the corresponding sub-watershed and then selecting the longest channel. Dividing ∑L with the watershed area A returned the channel drainage density. Data were analyzed by plotting the channel drainage density and the mainstream channel length L against the corresponding watershed area A. The L-A relationship is the so-called Hack's law which is used for analyzing terrestrial river networks (e.g., Rodriguez-Iturbe and Rinaldo, 1997).

6.3.3.5 Attributing channel properties to data points

To analyze channel properties through entire networks, data points were created every meter along the stream threads. For each data point the channel width, channel depth, the cross-sectional area (based on Equation (1)), mainstream length and watershed area were attributed. In the CRT marsh, channel width and channel depth are only attributed at the cross-sections (Figure 6.2a) and not through the entire network. Channels in the natural tidal marsh with a channel depth ≤ 0.1 m over a length < 10 m were excluded from the analysis according to the postulated criteria for measuring channels in the CRT marsh (§6.3.1).

6.3.4 Mainstream length profiles

To construct mainstream length profiles, we plotted the stream thread elevations of the measured mainstreams (CRT marsh: t0, t1, t2, t3, t4; and the natural tidal marsh), against the distance from the mainstream mouths, measured along the stream threads. On each length profile we applied a linear regression, allowing us to derive mean slopes based on the regression equations.

6.3.5 Changes in CRT channel volume

Based on the yearly channel measurements in the CRT marsh, we quantified the volume of sediment eroded in the former ditches and in the newly formed channels. First we performed a linear interpolation of elevation along the yearly measured stream threads (using ArcGis 9.2). In this way the change in elevation was determined for every point along the stream threads (length profiles). Secondly, using the cross-sectional data, we calculated the change in cross-sectional area and related this to the change in stream thread elevation for all cross-sections. Based on this relationship, the changes in stream thread elevation (derived from the yearly interpolation along

the length profile) were converted to changes in cross-sectional area, and allowed us to calculate the total volume of eroded or deposited sediment in the channels.

6.4 Results

6.4.1 Channel drainage density

6.4.1.1 Observed drainage density

Between t0 and t4 new channels were formed in the Lippenbroek CRT marsh (Figure 6.4a-6.4e) resulting in a decrease of the average unchanneled flow length (i.e. the shortest distance from any platform location to the nearest channel edge) (Figure 6.5a). The

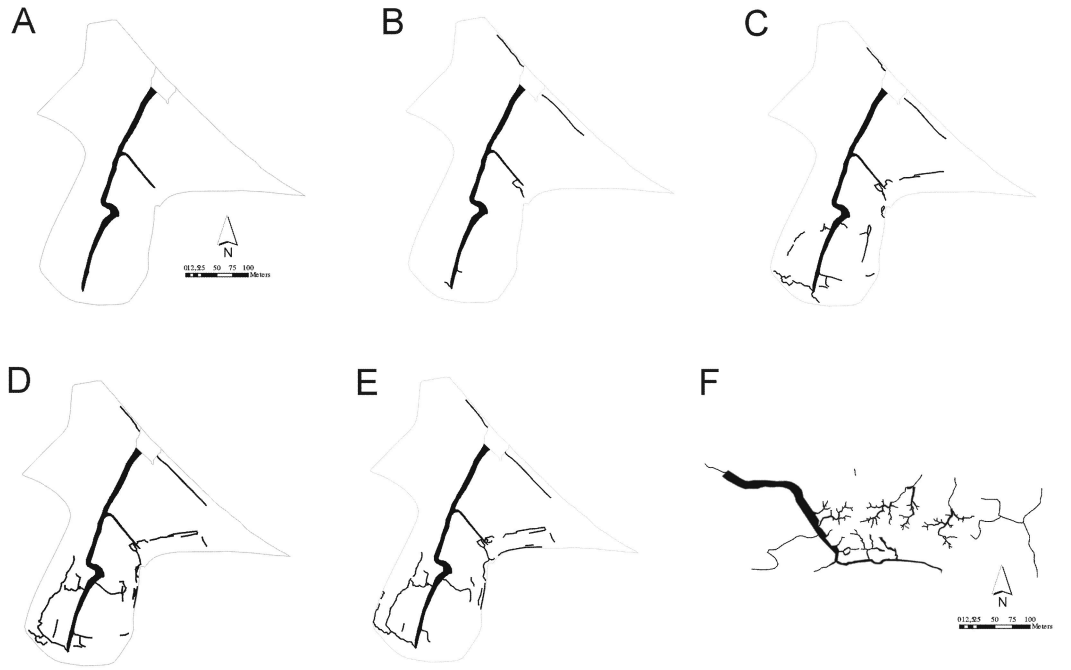

Figure 6.4 (a)-(e) Planimetric evolution of the CRT marsh network, t0 = before flooding started (March 2006), t1 = after nearly 1 year of tidal flooding (November 2006), t2 = after 2 years (November 2007), t3 = after 3 years (December 2008), and t4 = after 4 years (December 2009). (f) Channel network of the natural tidal marsh.

strongest decrease in unchanneled flow length is observed in the first 2 years between t0, t1 and t2. From then on the increase in drainage density is less rapidly with only minor changes between t2, t3 and t4. Despite the slower network development the last two years, the channel network in the CRT marsh has not reached yet the drainage density of the natural tidal marsh network (Figure 6.4f); at t4 larger unchanneled flow lengths are much more likely compared to the natural tidal marsh, with a maximum unchanneled flow length of 140 m in the CRT marsh, and of about 40 m in the natural tidal marsh (Figure 6.5a). The channel drainage density for the entire CRT marsh

area evolves from 0.0056 m/m² (t0), 0.0085 (t1), 0.0146 (t2), 0.0181 (t3) towards 0.0184 (t4) m/m² (Figure 6.5b). In the CRT marsh not all channels are yet connected (Figure 6.4a-6.4e). Excluding the non-connected channels (only for t2, t3 and t4) results in drainage densities of 0.0106 m/m² (t2), 0.0147 m/m² (t3) and 0.0142 m/m² (t4). In the natural tidal marsh the network is fully developed with a total channel drainage density of 0.0256 m/m² (Figure 6.5b).

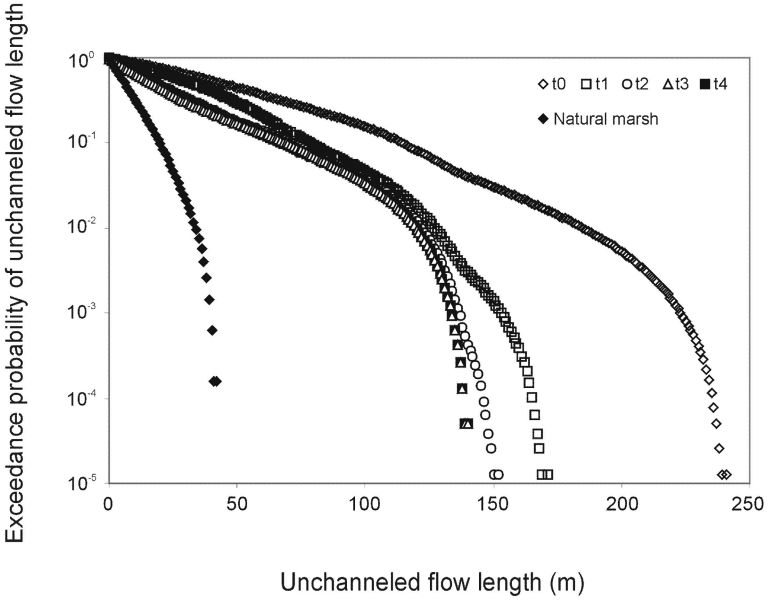

Figure 6.5 Probability density function of the unchanneled flow length (i.e., the distance of any platform location to the nearest channel), for t0 up to t4 at the constructed CRT marsh, and for the natural tidal marsh (NM).

6.4.1.2 Effect of initial platform elevation on the drainage density

After one year of tidal working (t1) there is not yet an effect of the initial platform elevation on the incision of new channels (Figure 6.6). Platform locations within all considered elevation classes have very comparable mean distances to newly formed channels, which means that the channel drainage density is not significantly different between the different platform elevation classes. After 2 years of tidal inundation (t2), the drainage density has become clearly higher at low elevated sites (less than about 0.4 m below MHWL), demonstrated by the significant decrease in mean distance to the newly formed channel edges (Figure 6.6). From then on, this effect of initial elevation remains more or less stable (Figure 6.6).

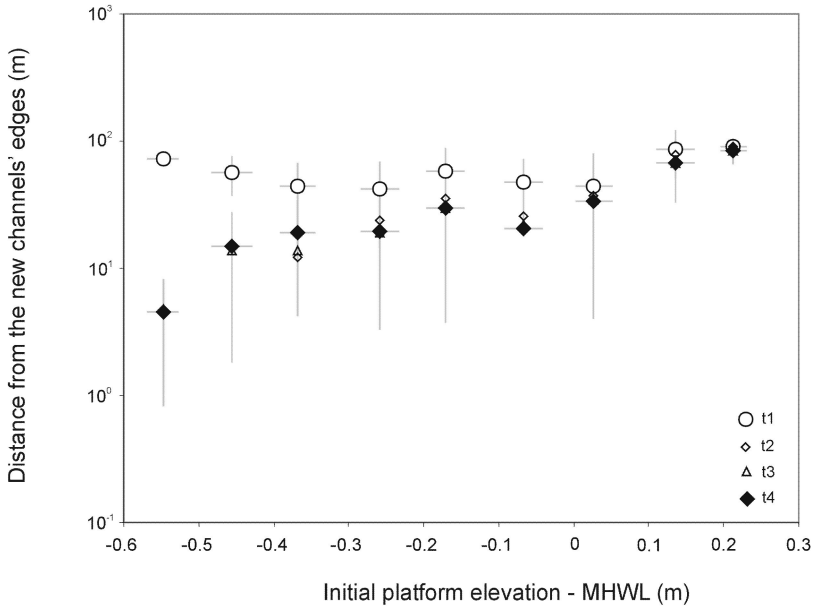

Figure 6.6 Effect of initial platform elevation on the drainage density of newly formed channels in a constructed CRT marsh. Drainage densities are calculated for elevation classes in steps of about 0.1 m.

6.4.1.3 Effect of vegetation on the drainage density

17% of the platform in the CRT marsh was not vegetated at t4 (Figure 6.7a) and almost the entire non-vegetated platform had an elevation less than 0.1 m below MHWL (Figure 6.7b). In order to distinguish between the effect of platform elevation and vegetation on the formation of new channels, three elevation classes were defined (Figure 6.7b) for which the distances to the newly formed channel edges were compared between vegetated and non-vegetated zones (Figure 6.7c). After 4 years of tidal working and vegetation growth, the mean distance to the newly formed channel edges was very comparable for the vegetated and non-vegetated elevation classes (Figure 6.7c).

6.4.1.4 Watershed area versus mainstream length (Hack's law) and channel drainage density

Applying Hack's law shows that the relationship between watershed area, A, and mainstream channel length, L, is different between the initial CRT marsh channel network at t0 and the equilibrium situation at a natural tidal marsh (Figure 6.8a). At t1 and t2 Hack's relationship in the CRT marsh evolves to the natural marsh relation. At t3 and t4 Hacks's relationship has become comparable for the CRT and natural tidal marsh (Figure 6.8a). This evolution demonstrates a quick elongation of the mainstream channel lengths in the CRT marsh until they reach an equilibrium condition after about 3 years of tidal flooding.

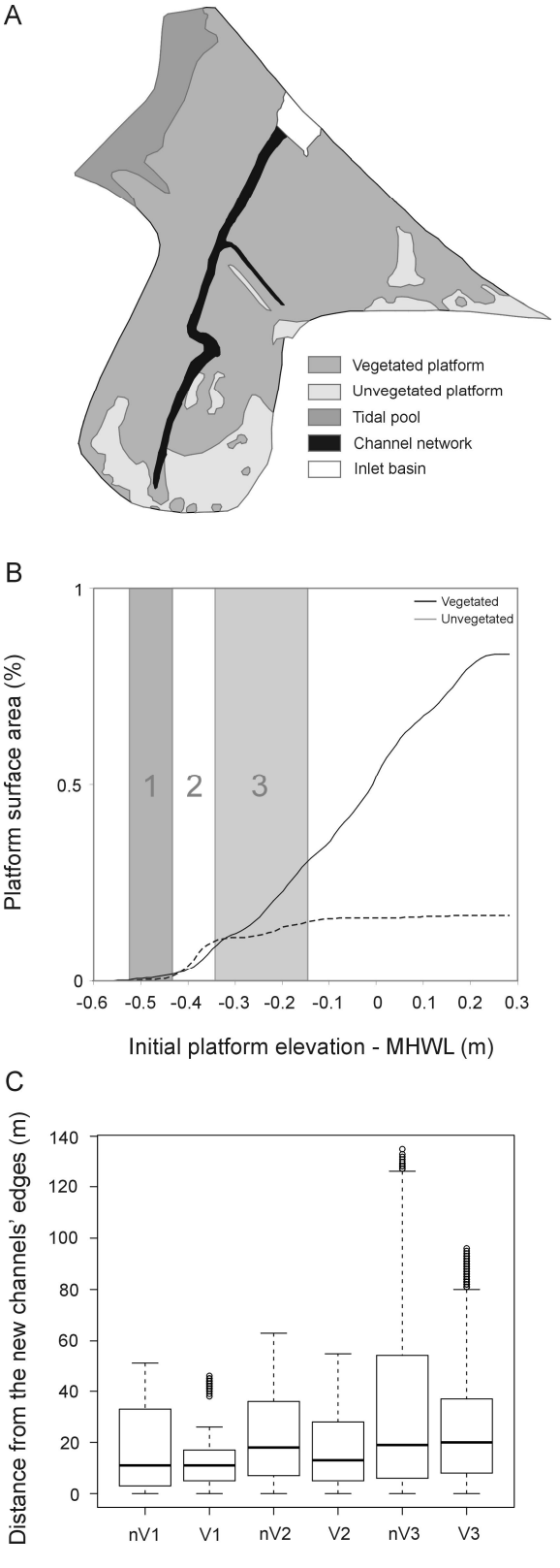

Figure 6.7 (a) Vegetated and unvegetated zones in the Lippenbroek CRT marsh at t4. (b) Elevation distribution of the former polder platform, according to the vegetation zones at t4. (c) Whisker boxplots of the distance to the newly formed channel edges (at t4), according to the 3 elevation zones defined in Figure 6.7b.

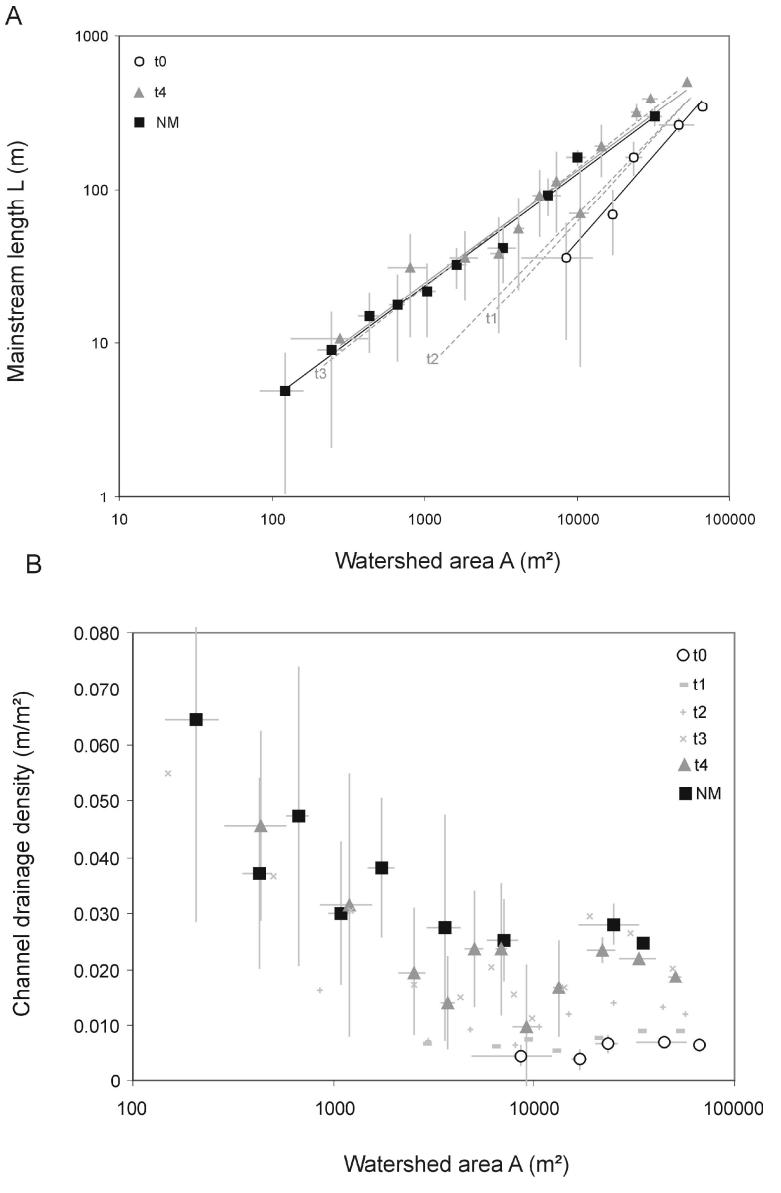

Figure 6.8 (a) Relationship between watershed area and mainstream length (Hack's law).For t1, t2 and t3 only trendlines are added to enhance figure clarity. NM in legend = natural marsh (b) Relationship between watershed area and channel drainage density.

The channel drainage density of the two CRT marsh ditches at t0 (Figure 6.4a) does not exceed the value of 0.010 m/m² (circles, Figure 6.8b). At t1 and t2 channel extension is rather limited and channel drainage density just attains values up to 0.015 m/m². After 3-4 years the increase in channel drainage density becomes however clearly pronounced, with values around 0.020 m/m² for the largest watershed areas, and values around 0.050 m/m² for the smallest watershed areas. This increase in channel drainage density with decreasing watershed area is also

observed for the natural tidal marsh. There, for the smallest watershed areas, channel drainage densities are comparable with the CRT marsh (t4), however for the larger watershed areas (> 2000 m²) the drainage densities are still higher on the natural marsh than on the CRT marsh (t4), indicating that the formation of more new tributary channels may be expected in the CRT marsh.

6.4.2 Channel cross-sections

6.4.2.1 Watershed area versus cross-sectional area

As for all channel networks (terrestrial and tidal) the cross-sectional area in the natural tidal marsh is in proportion with the watershed area (Figure 6.9). This A-Ω relationship evolves differently in the CRT marsh for the former ditches (grey symbols in Figure 6.9) versus the newly formed channels (white symbols in Figure 6.9). At t0 some of the cross-sectional areas of the former ditches are divergent from the natural A-Ω relationship (Figure 6.9). Over time, A and Ω change at the considered transects, so that data points shift towards the equilibrium line and after 4 years (t4) all cross-sectional areas are in equilibrium, or close to the equilibrium, with the corresponding watershed areas (Figure 6.9). As opposed to the ditches, most cross-sections of the newly formed channels plot below the equilibrium line (white symbols, Figure 6.9). To attain the equilibrium state under constant watershed area, an important increase in cross-sectional area would be necessary, by channel deepening and/or widening. Under a scenario with decreasing watershed areas (due to channel network extension), no important changes in cross-sectional area would be needed.

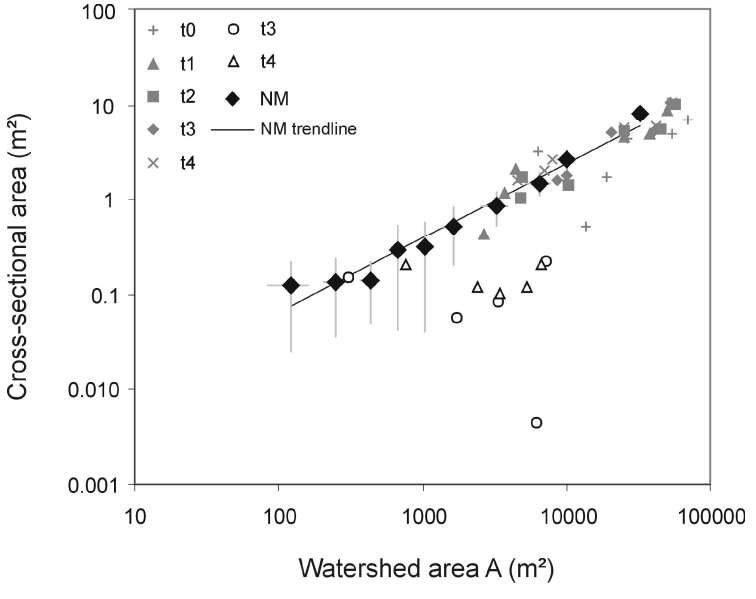

Figure 6.9 Watershed area versus cross-sectional area. Grey symbols represent the ditch cross-sections of the CRT marsh, white symbols the cross-sections of the new formed channels in the CRT marsh, NM = the natural marsh.

6.4.2.2 Width to depth ratio

In the natural tidal marsh the width to depth ratio β (=w/d) varies between 2.5 and 5.5 (Figure 6.10); only for the largest channel width (w ~ 10 m) the width to depth ratio is larger (β = 7.6). The mean β value over the entire natural channel network is 4.5. For the CRT marsh, the data are scattered around the equilibrium line and clearly not all width to depth ratios (both for ditches as for newly formed channels) are comparable with the natural marsh (Figure 6.10). At t4 the mean β value for the ditch cross-sections is 5.2, for the newly formed channel cross-sections this is 6.1, indicating that channel deepening would be necessary to obtain the β values observed in the natural tidal marsh (between 2.5 and 5.5).

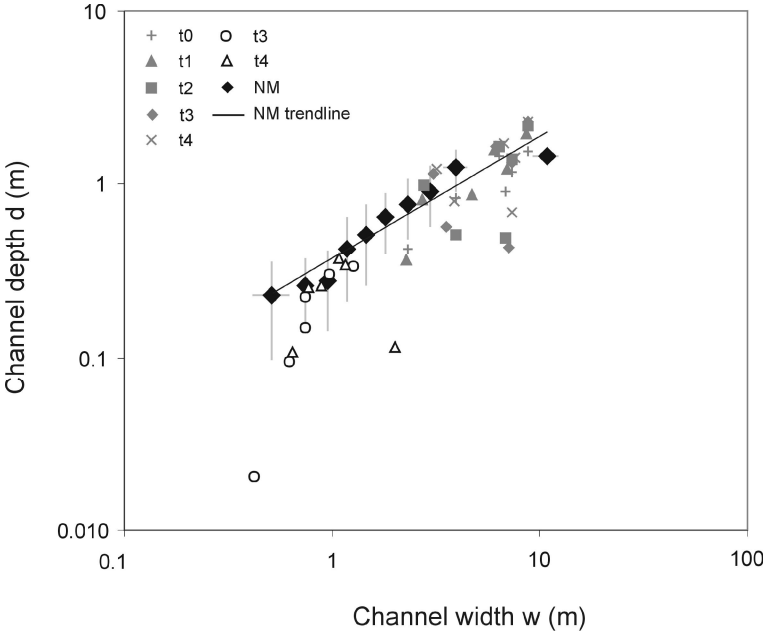

Figure 6.10 Channel width versus channel depth. Grey symbols represent the ditch cross-sections of the CRT marsh, white symbols the cross-sections of the new formed channels in the CRT marsh, NM = the natural marsh.

6.4.3 Mainstream length profile

At t0 the length profile of the former ditch is characterized by an increase in stream thread elevation (away from the inlet sluice) under a mean slope of 0.13 % (Figure 6.11a and b). During the first year of tidal working, erosion causes channel deepening along the first 200 m of the length profile (t1, Figure 6.11a). Moreover we observe channel extension at the head of the former ditch over a distance of 10 m. Between t1 and t2 there is continued erosion along the proximal parts of the length profile, while along the distal parts (between 250 and 370 m) sedimentation causes channel infilling. At the channel head, the newly formed channel further

extends over a distance of 28 m (Figure 6.11a). Between t2, t3 and t4, the changes in stream thread elevation (both proximal and distal) are rather limited. The most important change is observed at the channel head where the newly formed channel further extends over a distance of 130 m (Figure 6.11a). Changes in stream thread elevation along the former ditch and further channel extension have their impact on the mean slope of the mainstream length profile. During the first two years of tidal working there is a clear increase in mean slope, whereas the following two years only small changes are observed (Figure 6.11b). At t4 the mainstream slope in the CRT marsh has not reached yet the mainstream slope in the natural tidal marsh (0.34 % vs. 0.43 %) (Figure11b). Furthermore we observe that the stream thread elevation in the natural tidal marsh (compared to MHWL) is ~0.5-1 m lower than the stream thread elevation in the CRT marsh (at t4) (Figure 6.11a).

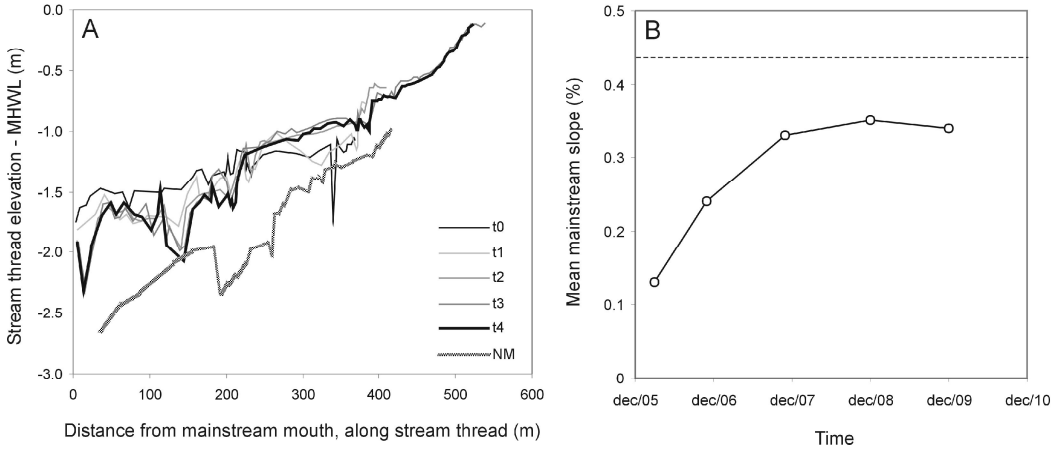

Figure 6.11 (a) Evolution of the mainstream length profile in the CRT marsh (t0 till t4), compared to the mainstream length profile of the natural tidal marsh (NM). (b) Evolution of the mainstream mean slope in the CRT marsh. Horizontal dashed line represents the mainstream mean slope in the natural marsh.

6.4.4 Eroded channel volumes

As demonstrated by the mainstream length profile development (Figure 6.11), the former ditch volumes change both by erosion and sedimentation processes. In time there is an increase in the amount of sediment eroded in the former ditches, however the erosion rate decreases in time and tends to zero by t4, indicating that an equilibrium has been reached (Figure 6.12). The amount of sediment deposited in the former ditches is clearly smaller compared to the eroded volumes and has attained an equilibrium already after 2 years (Figure 6.12). Whereas erosion in the former ditches is limited to channel incision, eroded volumes in the newly formed channels are determined by both channel incision and channel extension. Hence, as opposed to the former

ditches, erosion rates for the newly formed channels are constant in time, and have not reached an equilibrium yet after 4 years (Figure 6.12). Sedimentation in the newly formed channels is of minor importance.

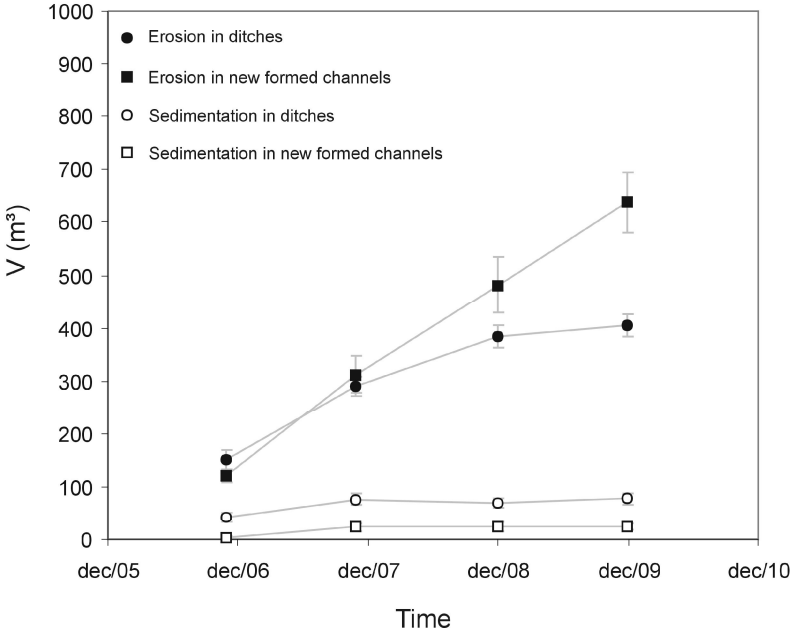

Figure 6.12 Evolution of the volumes of sediment eroded and deposited in the ditches and the new formed channels in the CRT marsh.

6.5 Discussion

The initial formation and evolution of tidal channel networks has recently attained much attention, especially based on numerical modeling (e.g., Fagherazzi and Furbish, 2001; Fagherazzi and Sun, 2004; D'Alpaos et al., 2005; D'Alpaos et al., 2007b; Kirwan and Murray 2007; Temmerman et al., 2007). However, empirical field data on initial channel formation are relatively scarce (D'Alpaos et al., 2007a; Wallace et al., 2005; Williams et al., 2002). Particularly few analyses exist on both the planimetric and cross-sectional evolution of an entire tidal channel network, covering the evolutionary stages from initial channel network formation up to a dynamic equilibrium stage. As a consequence, the rate at which channel networks form and evolve towards an equilibrium state, for example in restored or newly created intertidal areas, is difficult to predict.

In this study we looked at the evolution of several geometric parameters and relationships in a newly constructed intertidal area (CRT marsh). Some of these relationships already quickly attained (after a few years) an equilibrium state comparable with a mature, natural tidal marsh. In

the CRT marsh we observe that the cross-sectional area Ω of the former ditches is currently (after 4 years) in equilibrium with the corresponding watershed areas, whereas for the newly formed channels a further increase in Ω is still necessary (Figure 6.9). The equilibrium state of the former ditches is supported by the decrease in net erosion and sedimentation rates towards zero after 4 years, while erosion in the newly formed channels continues in time at a relatively constant rate (Figure 6.12). Besides the cross-sectional area of the former ditches, also the mainstream lengths of the newly formed channels have already reached an equilibrium state (after 3 years) with their corresponding watershed areas (Figure 6.8a). With regard to the channel drainage density, an equilibrium state is reached for the smaller watershed areas (< 2000 m²), but not for the larger ones (Figure 6.8b). This indicates that the formation of new channels initially takes place by a quick increase in mainstream length (through headward growth), together with the formation of some tributary channel branches relatively close to the mainstream heads (i.e., the smaller watershed areas). For the larger watershed areas, tributary channel formation still can be expected, especially for the watershed areas between 2000 and 10000 m² (Figure 6.8b).

That new channel formation is still an ongoing process is clearly illustrated by the evolution of unchanneled flow lengths, channel drainage density, and the volumes of sediment eroded by the newly formed channels. The unchanneled flow lengths decreased rapidly in the first 2 years and more slowly thereafter (Figure 6.5a), but note that this corresponds to a rather steady linear increase of channel drainage density with time (Figure 6.5b). Both the unchanneled flow length (max. 140 m at t4) and the channel drainage density (0.0184 m/m² at t4) are still far away from the values observed in a nearby natural tidal marsh (max. 40 m and 0.0256 m/m² respectively), suggesting that there is still much potential for channel network extension. Considering the eroded volumes in the newly forming channels (i.e. the combined effect of channel extension and incision), the erosion rates remain constant in time (Figure 6.12), implying that continued extension and incision of new channels may be expected the coming years. Despite the rapid channel initiation, after 4 years, the CRT marsh drainage density is still clearly lower than the drainage density of the natural tidal marsh (Figures 5a and 5b). An explanation for this is given by the fact that new channels develop first at more low elevated sites (Figure 6.6). These sites are characterized by concentration of flood and ebb flows, combined with higher inundation frequencies, and are thus subject to more intensive erosion processes. Also a second explanation may be brought forward: low elevated sites in (restored) tidal marshes are typically characterized by high sedimentation rates (Leonard et al., 1997; Temmerman et al., 2003a). In the CRT marsh we measured sedimentation rates up to 13.4 cm/yr in the lowest elevation zone (-0.5 m relative to MHWL) (**Chapter 5**), where the increase of channel drainage density was largest. These rapidly

deposited sediments are extremely water saturated and not consolidated (illustrated by the fact that you sink down into the mud very easily when walking in the field), so that they must have a low resistance against erosion and channel initiation. Once incision takes place, flow becomes increasingly concentrated towards the incipient channel, and the underlying high erosion-resistant polder clay (in case of restored sites) may start to erode. For the high elevated sites in restoration sites, channel incision is much more difficult. There, only few fresh sediment is deposited (only 0.5 cm/yr on the highest locations; **Chapter 5**), so that initial channel incision has to start almost immediately into the consolidated and hence erosion-restistant polder clay. Additionally, the high elevated sites in the CRT marsh were initially covered by dense terrestrial vegetation already from the beginning (Jacobs et al., 2009). Typically, vegetation reduces flow velocities and erosion (e.g. Leonard and Luther, 1995; Leonard and Croft, 2006; Neumeier and Amos, 2006), and hence channel initiation is less likely. Nevertheless for the lower elevated sites, the drainage density of newly formed channels was not significantly different between the vegetated sites, which are colonized by pioneer freshwater marsh vegetation (Jacobs et al., 2009), and the non-vegetated sites (Figure 6.7c). The preferential development of new channels at the low elevated sites is also observed for other marsh restoration sites (Wallace et al., 2005).

Besides the channel drainage density, the cross-sectional area of the newly formed channels in our study site has also not yet reached an equilibrium state (Figure 6.9). Although the main width-to-depth ratio for the newly formed channels (β=6.1) is comparable with width-to-depth ratios observed in other tidal marsh networks (β=5-7) (Marani et al., 2002), some cross-sections are not yet comparable to the natural tidal marsh (Figure 6.10). This is also reflected in the natural marsh mean width-to-depth ratio which has a lower value (β=4.5) compared to newly formed CRT channels (β=6.1). In the short-term it is most likely that the new channels in the CRT marsh will evolve towards an equilibrium cross-sectional area, mainly by channel deepening. In general, the temporal changes of channel depth (because of changes in tidal prism/watershed area) are considered to be more likely than the changes of channel width (D'Alpaos et al., 2006). However, in our specific case, the underlying erosion-resistant compacted polder clay may slow down this process of channel deepening and hamper the new channels to quickly attain their cross-sectional equilibrium state. This implication is not applicable to the former ditches. There, cross-sectional area quickly reached an equilibrium state (Figure 6.9) mainly by changes in stream thread elevation (Figure 6.11). Channel deepening is hereby more important in the proximal parts of the ditches (largest watershed areas), whereas channel infilling prevails in the distal parts (smaller watershed areas) (Figure 6.11). Deepening of the former ditches can be quickly because the former ditch bed does not consist of compacted polder clay but more of loose sediments. Also

channel infilling can occur rapidly due to the high suspended sediment concentrations in this part of the estuary (on average 150 mg/l; Temmerman et al., 2004b). Although the ditch cross-sectional area has attained an equilibrium state, this does not automatically imply that future changes are no longer possible. We observe that some of the ditch cross-sections are still divergent from the natural tidal marsh (Figure 6.9), and that the mean width-to-depth ratio for the ditches is still higher (β=5.2) than the mean width-to-depth ratio for the natural tidal marsh (β=4.5). Additionally, the evolution of the mainstream length profile (i.e. the mainstream for the entire CRT basin) suggests some possible changes in channel depth and/or channel width. At t4 the mainstream slope in the CRT marsh has not yet attained the mainstream slope of the natural tidal marsh (Figure 6.11b). However, through further erosion in the proximal parts of the former ditch, continued sedimentation in the more distal parts, or further channel extension at the channel head, the slope of the CRT mainstream may increase.

This study focused on channel formation in a freshwater tidal marsh environment. To further explore the effect of vegetation on tidal channel formation, it might be interesting to compare tidal channel properties (e.g., drainage density) for different tidal marsh systems (freshwater and brackish tidal marshes, salt marshes). The channel drainage density of the natural tidal freshwater marsh in this study (0.0256 m/m², maximum unchanneled flow length 40 m), is generally higher compared to values for salt marsh and brackish tidal marshes. Typically, tidal channel networks from salt marshes and brackish tidal marshes are extracted from aerial photographs, and reported values on channel drainage density and maximum unchanneled flow lengths respectively vary between 0.01 and 0.02 m/m², and 50 and 150 m (e.g., **Chapter 3**; Marani et al., 2003; Novakowski et al., 2004; Rinaldo et al., 1999a). However, the used aerial photographs have mostly spatial resolutions between 0.5 and 1 m, and as opposed to this study where entire channel networks are observed (topographic survey), the smallest tidal channels are not extracted, leading to an underestimation of the channel drainage density, and hence making it difficult to compare different tidal marshes. With regard to constructed tidal marshes, some other studies were able to extract entire tidal channel networks based on very high resolution aerial photographs (0.16 m) (D'Alpaos et al., 2007a), or topographical data (Wallace et al., 2005). In these studies values are reported for constructed salt marshes with a still developing tidal channel network (maximum unchanneled flow length 13 m after 2 years of network development, D'Alpaos et al., 2007a; channel drainage density 0.022 m/m² after 5 years of network development, Wallace et al., 2005). In the constructed freshwater tidal marsh of this study the channel drainage density and the maximum unchanneled flow length are respectively 0.0184 m/m² and 140 m after 4 years of network development. The clearly higher density of tidal channels in the constructed salt marsh

(maximum unchanneled flow length 13 m, D'Alpaos et al., 2007a) compared to the constructed freshwater tidal marsh (maximum unchanneled flow length 140 m, **this Chapter**) and the mature, natural tidal freshwater marsh (maximum unchanneled flow length 40 m, **this Chapter**) may be due to the difference in vegetation type. As discussed in **Chapter 2**, vegetation structures with higher vegetation densities will have stronger effects on bio-geomorphic landscape evolution (e.g., stronger flow concentration and channel erosion in between growing vegetation patches). Moreover, salt marsh vegetation has more extensive root networks compared to the vegetation in freshwater tidal marshes, resulting in more protection against erosive forces due to soil binding, and a higher capability to freeze tidal channel networks (Garofalo, 1980). To fully assess the role of salt marsh vegetation versus freshwater tidal marsh vegetation, more data on channel drainage density of entirely extracted tidal channel networks are necessary.

6.6 Conclusions

After introducing a controlled reduced tide (CRT) in a former polder area, spontaneous channel formation already took place after one year of tidal action. After two years, the cross-sectional area of the former ditches was already in equilibrium with the corresponding watershed areas. At the third year, the mainstream lengths and the channel drainage densities of smaller watersheds attained an equilibrium with the corresponding watershed areas, demonstrating the rapid headward growth of newly formed channels and tributary channel formation near the channel heads. New channels preferable developed at more low elevated sites because flood and ebb flows concentrated towards these low elevated zones, and because relatively thick deposits of fresh unconsolidated sediments enabled fast channel incision there. Within the low elevated zone, vegetation had no significant influence on the channel extension. Not all geometric properties already attained an equilibrium after 4 years of tidal working. The larger watershed areas, which also contain the high elevated zones, were featured by lower drainage densities. There, within the high elevated zone, channel formation was not common because incision almost immediately had to start into the compacted polder clay. The overall drainage density of the CRT marsh is thus not yet comparable with the drainage density of a natural tidal marsh and further tributary channel formation can be expected during the coming years. Additionally, for the existing newly formed channels, an increase in channel cross-sectional area may be necessary before they reach an equilibrium cross-section.

Chapter 7:

Synthesis

W. Vandenbruwaene

The synthesis of this PhD work summarizes the most important findings on tidal channel development according to the evolution of an intertidal landscape, i.e. from an unvegetated tidal flat towards a vegetated, high tidal marsh. Special attention goes out to the role of vegetation. The results are largely based on field observations in the natural tidal environment of the Scheldt estuary, but also include data on a restored tidal marsh. Tidal channel initiation and platform evolution in a restored tidal marsh site are compared to a natural tidal marsh.

7.1 Tidal channel development – from tidal flat to tidal marsh

Based on the results reported in the different chapters of the PhD thesis, we present now a general conceptual model (Figure 7.1) describing the changes in flow patterns and evolution of tidal channel networks, for the different stages of intertidal landscape evolution from an initially low-elevated non-vegetated tidal flat towards a high-elevated vegetated tidal marsh.

At an initial stage the intertidal landscape is characterized by an unvegetated tidal flat, dissected by a discrete channel network. Based on the channel morphogenesis in restoration sites (**Chapter 6**; D'Alpaos et al., 2007a; Wallace et al., 2005; Williams et al., 2002), it can be assumed that network initiation on a tidal flat is a rapid process (in the order of years). The channel drainage density D_c on tidal flats is low (0.004 m/m², **Chapter 3**) and the width-to-depth ratio (=β) is about 8.5 and does not alter with changing channel width (**Chapter 4)**. During flooding of the tidal flat platform, flow patterns are not concentrated to the channel network, but instead sheet flow occurs with flow velocities that are very similar in the tidal channels and above the non-vegetated platform (**Chapter 4)** (Figure 7.1a and 7.1e).

As a next step in the intertidal landscape evolution, the tidal flat becomes colonized by vegetation patches of pioneer species, which is in our study area especially *Spartina anglica*. The establishment of patchy vegetation has important implications on the flow hydrodynamics: at a small-scale, within the vegetation patches, flow velocities are reduced because of the friction

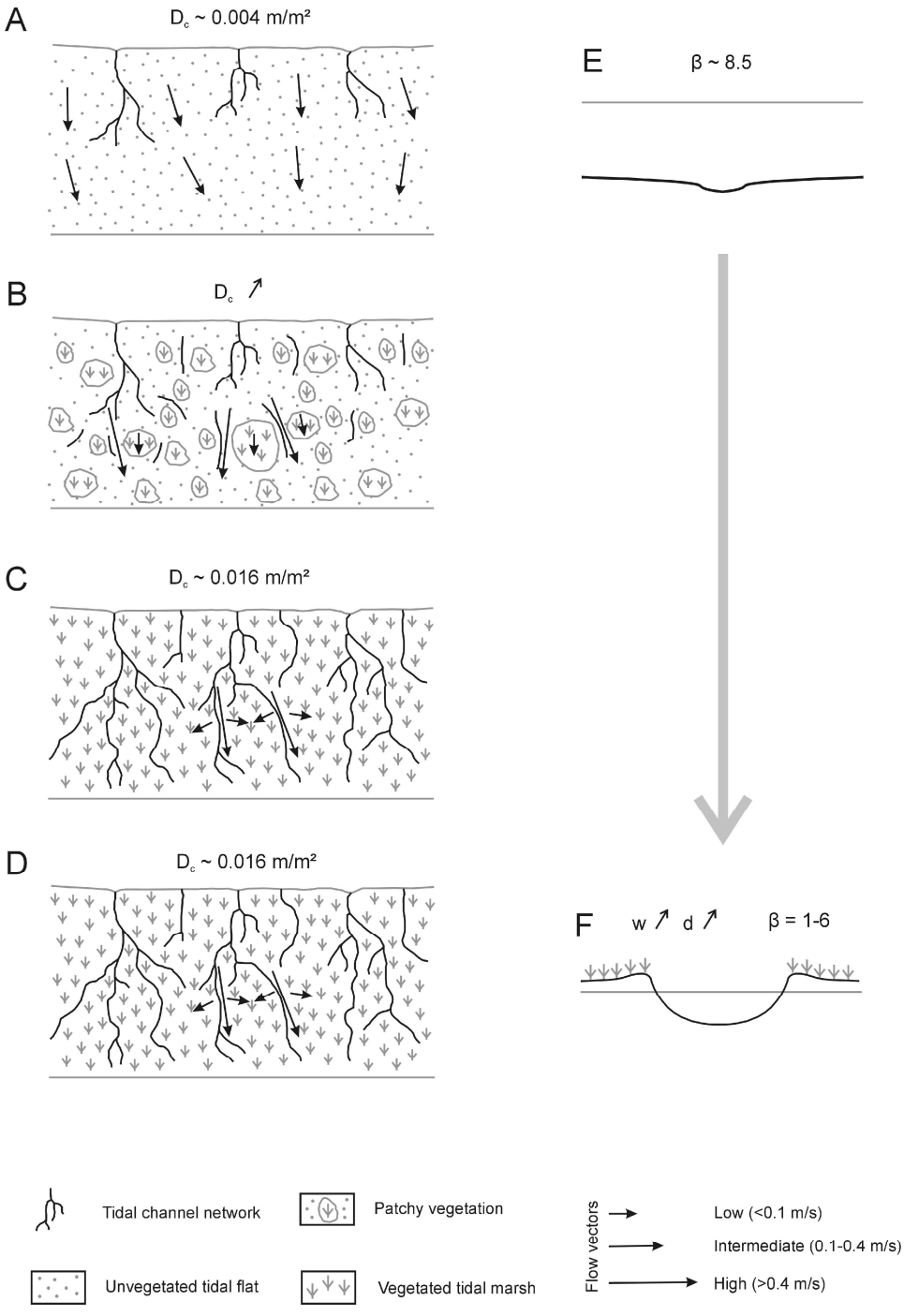

Figure 7.1 Conceptual model on tidal channel evolution illustrating the evolution of tidal channel networks and changes in flow patterns for (a) an unvegetated tidal flat, (b) an intertidal landscape with patchy vegetation, (c) a low elevated, vegetated tidal marsh, and (d) a high elevated, vegetated tidal marsh. (e-f) Tidal channel cross-sections for comparable watershed areas in (e) a tidal flat and (f) a high elevated tidal marsh.

exerted by the vegetation on the flow; but at a larger scale, this vegetation friction causes the water to flow partly around the vegetation patches, leading there to increased flow velocities (**Chapter 2**; Bouma et al., 2009; Temmerman et al., 2007; van Wesenbeeck et al., 2008). Moreover, the vegetation patches are dynamic in time. The flow in between two expanding vegetation patches starts to interact once the ratio between patch diameter (D) and inter-patch distance (d) exceeds a critical value ($D/d \geq$ 0.43-0.67 for two *Spartina anglica* patches) (**Chapter 2**). At a certain point in time, the increased flow velocities next to and in between growing vegetation patches may lead to more erosion (Bouma et al., 2009; Temmerman et al., 2007; van Wesenbeeck et al., 2008), the initiation of tidal channels (and prevention of further patch growth), and consequently an increase in channel drainage density (Figure 7.1b). If incoming flow velocities are too low, flow acceleration around patches may not induce erosion, and moreover, flow acceleration becomes suppressed once expanding vegetation patches become so big and so close to each other that a second critical D/d value is exceeded ($D/d \geq$ 6.67-10, for two *Spartina anglica* patches). Vegetation patches may start to merge with each other and eventually form closed vegetation fields that are dissected by non-vegetated channels.

Hence, the intertidal landscape has evolved from an initially bare tidal flat state, over a transitional state with patchy vegetation, towards a low tidal marsh with a continuous vegetation cover that is only dissected by non-vegetated tidal channels. This evolution is associated with a shift from sheet flow on the initially bare tidal flow, over increasingly concentrated flow in between the growing vegetation patches, and finally concentrated flow that is confined to the channels that dissect the vegetated tidal marsh platform (Figure 7.1).

Due to the shift from sheet flow to concentrated flow, tidal marshes are characterized by much higher channel drainage densities than tidal flats (0.016 m/m² to 0.004 m/m², **Chapter 3**) (Figure 7.1c and 7.1a). Moreover, the vegetated platform of tidal marshes has an important control on the flow hydrodynamics compared to the tidal flats. First, flow patterns on the tidal marsh are clearly concentrated to the tidal channel network, whereas on the tidal flat sheet flow prevails. On a tidal marsh sheet flow only occurs when the vegetation becomes overtopped (**Chapter 4**). Secondly, there is a strong reduction in flow on the vegetated platform of the tidal marsh, and consequently maximum platform flow velocities (up to 0.07 m/s) are much smaller than maximum channel flow velocities (0.3-1 m/s). On the tidal flat no significant differences in flow velocity are observed between the platform and the channel network, and the maximum flow velocities on the tidal flat are intermediate (0.1-0.4 m/s) between the marsh platform velocities (up to 0.07 m/s) and marsh channel velocities (0.3-1 m/s) (**Chapter 4**) (cf. Figure 7.1c/d and 7.1a). These differences in flow hydrodynamics between the tidal marsh and the tidal flat have important implications towards

the channel properties. For comparable watershed areas, larger discharges are forced to flow through tidal marsh channels and consequently these channels are wider and deeper (larger cross-sectional area) compared to tidal flat channels (Figure 7.1e and 7.1f). Additionally, the width-to-depth ratio (=β) of tidal marsh channels has a value between 1 and 6, where β increases with increasing channel width. For tidal flat channels β is around 8.5 and remains constant with increasing channel width. It should be noted that these channel properties only apply to watershed areas up to 22000 m² (**Chapter 4**).

During the subsequent long-term evolution of the marsh platform (10-100 years), the platform elevation rises in the tidal frame due to sediment accretion and consequently the tidal prism decreases. Due to the presence of vegetation there is partitioning of the tidal prism: the part below the vegetation top is forced to flow through the channel network, the part that overtops the vegetation is transported as sheet flow (**Chapter 4**). Therefore, for a low marsh the volumes of water transported as sheet flow are larger compared to a high marsh, however the concentrated flow through the channel network is comparable for both systems. Hence, the relationship between watershed area and channel width does not change as the marsh platform accretes to a higher position in the tidal frame, and moreover, no differences in channel drainage density are observed between low and high marshes (**Chapter 3**) (Figure 7.1c and 7.1d).

This PhD thesis demonstrates that (1) intertidal vegetation has a major impact on flow patterns and on the evolution of channel network dimensions, and (2) that changes in tidal prism only play a minor role. These new findings should form the basis for improvement of existing models of intertidal hydrodynamics and morphodynamics. The best available models at this moment (e.g., D'Alpaos et al., 2005; D'Alpaos et al., 2006; D'Alpaos et al., 2007b; Fagherazzi and Furbish, 2001; Fagherazzi and Sun, 2004; Kirwan and Murray, 2007), assume that entire tidal prisms are forced to flow through the channel network. As a consequence, these models predict that channel dimensions (width, depth) evolve in response to changes of the tidal prism. This means that when the tidal prism decreases due to sediment accretion on the surrounding platform, these models simulate that channel dimensions (width, depth) decrease by channel infilling (e.g., D'Alpaos et al., 2006). However this was not confirmed by our empirical observations (**Chapter 3**). Similarly, when platform accretion cannot keep up with sea level rise, the tidal prism increases and the models simulate that channel dimensions would increase by erosion. In contrast with these models, our empirical findings demonstrate that tidal channels are not likely to respond much to an increasing tidal prism due to sea level rise, as long as the intertidal platform stays in a vegetated state. Our work suggests that large-scale die-back of the vegetation, which may be caused by sea-

level rise, will have a particularly important effect as channel flow velocities will decrease and channels will silt up, and platform flow velocities will increase.

7.2 Restoration of intertidal areas and implications towards safety

After the major inundations along the Flemish part of the Scheldt estuary in 1976, the Belgian government launched the so-called Sigmaplan in 1977 to protect the estuary from flood disasters, by proposing (1) the heightening and strengthening of the dykes, (2) the building of a storm surge barrier, and (3) the construction of so-called flood control areas (FCA's) on formerly embanked land. A more recent revision of the Sigmaplan proposed to extent the number of FCA's, and foresees that an important part of these FCA's will be installed as FCA's with a controlled reduced tide (CRT). In this way the objective is to combine the protection against storm surges with the restoration of tidal marsh ecosystem functions (**Chapter 5**; Cox et al., 2006; Maris et al., 2007).

Introducing a controlled reduced tide induces important morphological changes on the formerly embanked land (**Chapters 5 and 6**). After 4 years of tidal working in the Lippenbroek FCA-CRT (a pilot project of 8 ha), a new tidal channel network developed by which the mainstream lengths and the channel drainage densities of smaller watersheds attained an equilibrium (i.e., compared to a mature, natural tidal freshwater marsh), demonstrating the rapid headward growth of newly formed channels and rapid tributary channel formation near the channel heads. New channels preferentially developed at more low elevated sites, resulting in drainage densities comparable to a natural tidal marsh, both for the vegetated as for the unvegetated CRT zones (**Chapter 6**). Similar drainage densities between vegetated and unvegetated zones are also observed in the natural tidal environment (i.e., for comparable watershed areas), however on the larger landscape scale tidal flats have clearly lower drainage densities (Figure 7.1a and 7.1c) (**Chapter 3**). Although some tidal channel properties in the CRT already attained an equilibrium state, we may say that new channel formation is still an ongoing process, based on: (1) the lower drainage densities in the higher elevated CRT zones, (2) the constant erosion rates (in time) in the channels, and (3) the lower cross-sectional areas of the new channels (**Chapter 6**). So we may expect the further spatial extension of new channels and further deepening of new channels.

On the CRT platform there is an overall increase in surface elevation, with a higher increase in surface elevation for the more lower elevated sites, resulting in a decrease in spatial elevation differences (**Chapter 5**). Once spatial elevation differences are strongly reduced, changes in platform elevation on natural tidal marshes are typically determent by a temporal feedback mechanism. Rising marsh elevation hereby results in a decrease in inundation depth, and

consequently the decrease of sediment accretion rate. However, in the CRT area this temporal feedback mechanism is absent because the mean high water level (MHWL) follows the overall increase in surface elevation (**Chapter 5**). Hence a decrease of sediment accretion rates may be not expected in a CRT.

The CRT areas along the Scheldt estuary have two main objectives: (1) protection against storm surges, and (2) restoration of tidal marsh ecosystem functions. During 4 years of tidal working, the morphological evolution of the Lippenbroek CRT can be considered as favorable for the restoration of tidal marsh area. First, a tidal channel network rapidly developed which is essential for the transport of sediment and nutrients. Secondly, there is increase in platform elevation which is crucial for the colonization and evolution of tidal marsh ecosystems. Indeed after a few years, tidal freshwater vegetation was restored in the CRT, with restoration of species typical for the lower freshwater marsh zones, a habitat which is entirely lost along the Scheldt estuary (Jacobs et al., 2009). Although these short-term morphological changes are important for the restoration of tidal marsh area, the long-term changes in platform elevation may not endanger the first objective of a CRT area, i.e. protection against storm surges. Based on the assumption that in a CRT MHWL follows the overall increase in surface elevation, conceptual modeling demonstrated that on the long term (75 years): (1) the platform elevation gain in a CRT marsh is 2-2.5 times larger compared to a natural tidal marsh, and the reduction of spatial elevation differences is faster; (2) under a scenario of constant MHWL rise, the equilibrium elevation (relative to MHWL) is lower in the CRT marsh and is reached almost 2 times faster; and (3) under a scenario of accelerated MHWL rise, the CRT marsh is much less able to keep up with the MHWL rise (**Chapter 5**). Although this larger elevation gain in the CRT marsh can be considered as unfavorable for the safety objective of a CRT area, the model does not include long-term effects such as autocompaction (Cahoon et al., 1995). Moreover, the strength of the relationship between mean water depth and accretion rate (used for the model calculations) can be considered as strong due to the high suspended sediment concentrations in this part of the estuary (Temmerman et al., 2004b). Other planned CRTs are located along areas with lower corresponding suspended sediment concentrations. Although the long-term increase in platform elevation might be a problem, a major advantage of the CRT concept is that sluice dimensions and thus water volumes can be managed. In this way, the safety function of a CRT marsh can be improved by for example reducing volumes of water and sediment import, and moreover, managing sluice dimensions offers the option to force the restoration of a CRT marsh towards a specific stage in marsh succession.

References

Allen, J.R.L., 1990. Salt-marsh growth and stratification: a numerical model with special reference to the Severn Estuary, southwest Britain. Marine Geology, 95: 77-96.

Allen, J.R.L., 1999. Geological impacts on coastal wetland landscapes: some general effects of sediment autocompaction in the Holocene of northwest Europe. Holocene, 9: 1-12.

Allen, J.R.L., 2000. Morphodynamics of Holocene salt marshes: a review sketch from the Atlantic and Southern North Sea coasts of Europe. Quaternary Science Reviews, 19(12): 1155-1231.

Ataie-Ashtiani, B. and Beheshti, A.A., 2006. Experimental investigation of clear-water local scour at pile groups. Journal of Hydraulic Engineering-Asce, 132(10): 1100-1104.

Baas, A.C.W. and Nield, J.M., 2007. Modelling vegetated dune landscapes, Geophysical Research Letters, pp. L06405.

Bakker, J.P., Esselink, P., Dijkema, K.S., van Duin, W.E. and de Jong, D.J., 2002. Restoration of salt marshes in the Netherlands. Hydrobiologia, 478(1-3): 29-51.

Balke, T., 2009. Biogeomorphology of *Spartina anglica* tussocks. GIS based comparison of contrasting sites at the Westerschelde and Blackwater estuary, University of Hannover, Hannover.

Bayliss-Smith, T.P., Healey, R., Lailey, R., Spencer, T. and Stoddart, D.R., 1979. Tidal flow in salt marsh creeks. Estuarine Coastal and Shelf Science, 9: 235-255.

Bochet, E., Poesen, J. and Rubio, J.L., 2000. Mound development as an interaction of individual plants with soil, water erosion and sedimentation processes on slopes. Earth Surface Processes and Landformes, 25: 847-867.

Bouma, T.J., De Vries, M.B., Low, E., Kusters, L., Herman, P.M.J., Tanczos, I.C., Temmerman, S., Hesselink, A., Meire, P. and van Regenmortel, S., 2005. Flow hydrodynamics on a mudflat and in salt marsh vegetation: identifying general relationships for habitat characterisations. Hydrobiologia, 540: 259-274.

Bouma, T.J., Van Duren, L.A., Temmerman, S., Claverie, T., Blanco-Garcia, A., Ysebaert, T. and Herman, P.M.J., 2007. Spatial flow and sedimentation patterns within patches of epibenthic structures: combining field, flume and modelling experiments. Continental Shelf Research, 27: 1020-1045.

Bouma, T.J., Friedrichs, M., van Wesenbeeck, B.K., Temmerman, S., Graf, G. and Herman, P.M.J., 2009. Density-dependent linkage of scale-dependent feedbacks: a flume study on the intertidal macrophyte Spartina anglica. Oikos, 118(2): 260-268.

Byrne, R.J., Bullock, P. and Tyler, D.G., 1975. Response characteristics of a tidal inlet: a case study In: L.E. Cronin (Editor), Estuarine research, Volume II: Geology and Engineering. Academic press, New York, pp. 201-216.

Cahoon, D.R., Reed, D.J. and Day, J.W., 1995. Estimating shallow subsidence in microtidal salt marshes of the southeastern United States: Kaye and Barghoorn revisisted. Marine Geology, 128: 1-9.

Cahoon, D.R., Lynch, J., Perez, B., Segura, B., Holland, R.D., Stelly, C., Stephenson, G. and Hensel, P., 2002. High-Precision measurements of Wetland sediment elevation: II. The Rod surface elevation table. U.S.Geological Survey: 734

Callaway, J.C. and Josselyn, M.N., 1992. The introduction and spread of smooth cordgrass (Spartina alterniflora) in South San Francisco Bay. Estuaries, 15: 218-226.

Castellanos, E.M., Figueroa, M.E. and Davy, A.J., 1994. Nucleation and facilitation in saltmarsh sucssession: interactions between *Spartina maritima* and *Arthrocnemum perenne*. Journal of Ecology, 82(2): 239-248.

Claessens, J. and Meyvis, L., 1994. Overzicht van de tijwaarnemingen in het Zeescheldebekken gedurende het decennium 1981-1990, Ministerie van de Vlaamse Gemeenschap AWZ Afdeling Maritieme Schelde, Antwerpen.

Collins, D.B.G., Bras, R.L. and Tucker, G.E., 2004. Modeling the effects of vegetation-erosion coupling on landscape evolution, Journal of Geophysical Research, pp. F03004.

Corenblit, D., Gurnell, A.M., Steiger, J. and Tabacchi, E., 2008. Reciprocal adjustments between landforms and living organisms: Extended geomorphic evolutionary insights. Catena, 73(3): 261-273.

Costanza, R., d'Arge, R., de Groot, R., Farber, S., Grasso, M., Hannon, B., Limburg, K., Naeem, S., O'Neill, R.V., Paruelo, J., Raskin, R.G., Sutton, P. and Van den Belt, M., 1997. The value of the world's ecosystem services and natural capital. Nature, 387: 253-260.

Costanza, R., Perez-Maqueo, O., Martinez, M.L., Sutton, P., Anderson, S.J. and Mulder, K., 2008. The value of coastal wetlands for hurricane protection. Ambio, 37(4): 241-248.

Cotton, J.A., Wharton, G., Bass, J.A.B., Heppell, C.M. and Wotton, R.S., 2006. The effects of seasonal changes to in-stream vegetation cover on patterns of flow and accumulation of sediment. Geomorphology, 77 320-334.

Coulthard, T.J., 2005. Effects of vegetation on braided stream pattern and dynamics, Water Resources Research, pp. W04003.

Cox, T., Maris, T., De Vleeschauwer, P., De Mulder, T., Soetaert, K. and Meire, P., 2006. Flood control areas as an opportunity to restore estuarine habitat. Ecological Engineering, 28(1): 55-63.

D'Alpaos, A., Lanzoni, S., Marani, M., Fagherazzi, S. and Rinaldo, A., 2005. Tidal network ontogeny: channel initiation and early development. Journal of Geophysical Research, 110: F02001.

D'Alpaos, A., Lanzoni, S., Mudd, S.M. and Fagherazzi, S., 2006. Modeling the influence of hydroperiod and vegetation on the cross-sectional formation of tidal channels. Estuarine Coastal and Shelf Science, 69: 311-324.

D'Alpaos, A., Lanzoni, S., Marani, M., Bonornetto, A., Cecconi, G. and Rinaldo, A., 2007a. Spontaneous tidal network formation within a constructed salt marsh: Observations and morphodynamic modelling. Geomorphology, 91(3-4): 186-197.

D'Alpaos, A., Lanzoni, S., Marani, M. and Rinaldo, A., 2007b. Landscape evolution in tidal embayments: modeling the interplay of erosion, sedimentation, and vegetation dynamics. Journal of Geophysical Research, 112: 1-17.

D'Alpaos, A., Lanzoni, S., Marani, M. and Rinaldo, A., 2010. On the tidal prism - channel area relations. Journal of Geophysical Research-Earth Surface, 115: -.

Fagherazzi, S., Bortoluzzi, A., Dietrich, W.E., Adami, A., Lanzoni, S., Marani, M. and Rinaldo, A., 1999. Tidel networks 1. Automatic network extraction and preliminary scaling features from digital terrain maps. Water Resources Research, 35(12): 3891-3904.

Fagherazzi, S. and Furbish, D.J., 2001. On the shape and widening of salt marsh creeks. Journal of Geophysical Research-Oceans, 106: 991-1003.

Fagherazzi, S. and Sun, T., 2004. A stochastic model for the formation of channel networks in tidal marshes. Geophysical Research Letters, 31(21): L21503.

French, J.R. and Stoddart, D.R., 1992. Hydrodynamics of salt marsh creek systems: implications for marsh morphological development and material exchange. Earth Surface Processes and Landforms, 17: 235-252.

French, J.R., 1993. Numerical simulation of vertical marsh growth and adjustment to accelerated sea-level rise, north Norfolk, U.K. Earth Surface Processes and Landforms, 18(1): 63-81.

French, J.R., Spencer, T., Murray, A.L. and Arnold, N.S., 1995. Geostatistical analysis of sediment deposition in two small tidal wetlands, Norfolk, United Kingdom. Journal of Coastal Research, 11(2): 308-321.

French, J.R., 2006. Tidal marsh sedimentation and resilience to environmental change: exploratory modelling of tidal, sea-level and sediment supply forcing in predominantly allochthonous systems. Marine Geology, 235: 119-136.

Gardner, L.R. and Bohn, M., 1980. Geomorphic and Hydraulic Evolution of Tidal Creeks on a Subsiding Beach Ridge Plain, North-Inlet, Sc. Marine Geology, 34(3-4): M91-M97.

Gran, K. and Paola, C., 2001. Riparian vegetation controls on braided stream dynamics. Water Resources Research, 37: 3275-3283.

Gribsholt, B., Boschker, H.T.S., Struyf, E., Andersson, M., Tramper, A., De Brabandere, L., van Damme, S., Brion, N., Meire, P., Dehairs, F., Middelburg, J.J. and Heip, C.H.R., 2005. Nitrogen processing in a tidal freshwater marsh: A whole-ecosystem N-15 labeling study. Limnology and Oceanography, 50(6): 1945-1959.

Hack, J., 1957. Studies of longitudinal stream profiles in Virginia and Maryland. U.S. Geological Survey Professional Paper, 294-B.

Hubbard, J.C.E., 1965. Spartina marshes in southern England. VI. Pattern of invasion in Poole Harbour. Journal of Ecology, 53: 799-813.

Hutchinson, S.E., Sklar, F.H. and Roberts, C., 1995. Short term sediment dynamics in a Southeastern USA Spartina marsh. Journal of Coastal Research, 11(2): 370-380.

Intergovernmental Panel on Climate Change IPCC, 2007. Climate Change 2007: The Scientific Basis. Contribution of Working Group I to the Fourth Assesment Report of the Intergovernmental Panel on Climate Change. Cambridge University Press, Cambridge, 1056 pp.

Istanbulluoglu, E. and Bras, R.L., 2005. Vegetation-modulated landscape evolution: effects of vegetation on landscape processes, drainage density, and topography, Journal of Geophysical Research, pp. F02012.

Jacobs, S., Struyf, E., Maris, T. and Meire, P., 2008. Spatiotemporal aspects of silica buffering in restored tidal marshes. Estuarine Coastal and Shelf Science, 80(1): 42-52.

Jacobs, S., Beauchard, O., Struyf, E., Cox, T., Maris, T. and Meire, P., 2009. Restoration of tidal freshwater vegetation using controlled reduced tide (CRT) along the Schelde Estuary (Belgium). Estuarine Coastal and Shelf Science, 85(3): 368-376.

Jarrett, J.T., 1976. Tidal Prism-Inlet Area Relationship, CERC-WES General Investigation of Tidal Inlets, Dept. of the Army, U.S. Corps of Engineering.

Kirwan, M. and Temmerman, S., 2009. Coastal marsh response to historical and future sea-level acceleration. Quaternary Science Reviews, 28(17-18): 1801-1808.

Kirwan, M.L. and Murray, A.B., 2007. A coupled geomorphic and ecological model of tidal marsh evolution. Proceedings of the National Academy of Sciences of the United States of America, 104(15): 6118-6122.

Kirwan, M.L., Guntenspergen, G.R., D'Alpaos, A., Morris, J.T., Mudd, S.M. and Temmerman, S., 2010. Limits on the adaptability of coastal marshes to rising sea level. Geophysical Research Letters, 37: -.

Leonard, L.A. and Luther, M.E., 1995. Flow hydrodynamics in tidal marsh canopies. Limnology and Oceanography, 40(8): 1474-1484.

Leonard, L.A., 1997. Controls on sediment transport and deposition in an incised mainland marsh basin, southeastern North Carolina. Wetlands, 17(2): 263-274.

Leonard, L.A. and Croft, A.L., 2006. The effect of standing biomass on flow velocity and turbulence in Spartina alterniflora canopies. Estuarine Coastal and Shelf Science, 69 325-336.

Lotze, H.K., Lenihan, H.S., Bourque, B.J., Bradbury, R.H., Cooke, R.G., Kay, M.C., Kidwell, S.M., Kirby, M.X., Peterson, C.H. and Jackson, B.C., 2006. Depletion, degradation, and recovery potential of estuaries and coastal seas. Science, 312 1806-1809.

Marani, M., Lanzoni, S., Zandolin, D., Seminara, G. and Rinaldo, A., 2002. Tidal meanders. Water Resources Research, 38(11): Art. No. 1225.

Marani, M., Belluco, E., D'Alpaos, A., Defina, A., Lanzoni, S. and Rinaldo, A., 2003. On the drainage density of tidal networks. Water Resources Research, 29(2): Art. No. 1040.

Marani, M., D'Alpaos, A., Lanzoni, S., Carniello, L. and Rinaldo, A., 2007. Biologically-controlled multiple equilibria of tidal landforms and the fate of the Venice lagoon, Geophysical Research Letters, pp. L11402.
Marciano, R., Wang, Z.B., Hibma, A., De Vriend, H.J. and Defina, A., 2005. Modeling of channel patterns in short tidal basins. Journal of Geophysical Research, 110: F01001.
Maris, T., Cox, T., Temmerman, S., De Vleeschauwer, P., Van Damme, S., De Mulder, T., Van den Bergh, E. and Meire, P., 2007. Tuning the tide: creating ecological conditions for tidal marsh development in a controlled inundation area. Hydrobiologia.
Mason, D.C., Scott, T.R. and Wang, H.J., 2006. Extraction of tidal channel networks from airborne scanning laser altimetry. Isprs Journal of Photogrammetry and Remote Sensing, 61(2): 67-83.
McLusky, D.S. and Elliot, M., 2004. The Estuarine Ecosystem; ecology, threats and management, 3rd Edn. OUP, Oxford, 216 pp.
Meire, P., Ysebaert, T., Van Damme, S., Van den Bergh, E., Maris, T. and Struyf, E., 2005. The Scheldt estuary: a description of a changing ecosystem. Hydrobiologia, 540 1-11.
Melville, B.W., 1997. Pier and abutment scour: Integrated approach. Journal of Hydraulic Engineering-Asce, 123(2): 125-136.
Melville, B.W. and Chiew, Y.M., 1999. Time scale for local scour at bridge piers. Journal of Hydraulic Engineering-Asce, 125(1): 59-65.
Mitsch, W.J. and Gosselink, J.G., 2000. The value of wetlands: importance of scale and landscape setting. Ecological Economics, 35(1): 25-33.
Murray, A.B. and Paola, C., 2003. Modelling the effect of vegetation on channel pattern in bedload rivers. Earth Surface Processes and Landforms, 28: 131-143.
Murray, A.B., Knaapen, M.A.F., Tal, M. and Kirwan, M.L., 2008. Biomorphodynamics: Physical-biological feedbacks that shape landscapes, Water Resources Research, pp. W11301.
Myrick, M. and Leopold, L.B., 1963. Hydraulic geometry of a small tidal estuary. U.S. Govt. Print Off Washington, 18 pp.
Nash, J.E. and Sutcliffe, J.V., 1970. River flow forecasting through conceptual models. Part I. A discussion of principles. Journal of Hydrology, 10: 282-290.
Nepf, H.M. and Vivoni, E.R., 2000. Flow structure in depth-limited, vegetated flow. Journal of Geophysical Research, 105: 547-557.
Neubauer, S.C., 2008. Contributions of mineral and organic components to tidal freshwater marsh accretion. Estuarine Coastal and Shelf Science, 78(1): 78-88.
Neumeier, U. and Amos, C.L., 2006. The influence of vegetation on turbulence and flow velocities in European salt-marshes. Sedimentology, 53 (2): 259-277.
Novakowski, K.I., Torres, R., Gardner, L.R. and Voulgaris, G., 2004. Geomorphic analysis of tidal creek networks. Water Resources Research, 40.
Nyman, J.A., Walters, R.J., DeLaune, R.D. and Patrick Jr, W.H., 2006. Marsh vertical accretion via vegetative growth. Estuarine Coastal and Shelf Science, 69: 370-380.
O'Brien, M.P., 1931. Estuary tidal prisms related to entrance areas Civil Engineering, 1(8): 738-739.
O'Brien, M.P., 1969. Equilibrium flow areas of inlets on sandy coasts Journal of the Waterway and Harbour Divisions, ASCE, 95(WW1): 43-52.
Oliveto, G. and Hager, W.H., 2002. Temporal evolution of clear-water pier and abutment scour. Journal of Hydraulic Engineering-Asce, 128(9): 811-820.
Pethick, J., 2002. Estuarine and tidal wetland restoration in the United Kingdom: Policy versus practice. Restoration Ecology, 10(3): 431-437.
Pethick, J.S., 1980. Velocity surges and asymmetry in tidal channels. Estuarine Coastal and Shelf Science, 11: 331-345.
Pethick, J.S., 1981. Long-term accretion rates on tidal salt marshes. Journal of Sedimentary Petrology, 51: 571-577.
Reed, D.J., 1995. The response of coastal marshes to sea-level rise: survival or submergence? Earth Surface Processes and Landforms, 20(1): 39-48.
Reed, D.J., Spencer, T., Murray, A.L., French, J.R. and Leonard, L., 1999. Marsh surface sediment deposition and the role of tidal creeks: implications for created and managed coastal marshes. Journal of Coastal Conservation, 5: 81-90.
Reinhardt, L., Jerolmack, D., Cardinale, B.J., Vanacker, V. and Wright, J., 2010. Dynamic interactions of life and its landscape: feedbacks at the interface of geomorphology and ecology. Earth Surface Processes and Landforms, 35(1): 78-101.
Rietkerk, M. and Van de Koppel, J., 2008. Regular pattern formation in real ecosystems. Trends in Ecology & Evolution, 23(3): 169-175.
Rinaldo, A., Fagherazzi, S., Lanzoni, S., Marani, M. and Dietrich, E., 1999a. Tidal networks 3. Landscape-forming discharges and studies in empirical geomorphic relationships. Water Resources Research, 35(12): 3919-3929.
Rinaldo, A., Fagherazzi, S., Lanzoni, S., Marani, M. and Dietrich, E., 1999b. Tidal networks 2. Watershed delineation and comparative network morphology. Water Resources Research, 35(12): 3905-3917.
Rodriguez-Iturbe, I. and Rinaldo, A., 1997. Fractal River Basins: Chance and Self-Organization. Cambridge University Press, New York.
Sanchez, J.M., SanLeon, D.G. and Izco, J., 2001. Primary colonisation of mudflat estuaries by Spartina maritima (Curtis) Fernald in northwest Spain: vegetation structure and sediment accretion. Aquatic Botany, 69(1): 15-25.

Schnauder, I. and Moggridge, H., 2009. Vegetation and hydraulic-morphological interactions at the individual plant, patch and channel scale. Aquatic Sciences, 71(3): 318-330.
Shi, Z., Lamb, H.F. and Collin, R.L., 1995a. Geomorphic change of saltmarsh tidal creek networks in the Dyfi Estuary, Wales. Marine Geology, 128(1-2): 73-83.
Shi, Z., Pethick, J.S. and Pye, K., 1995b. Flow structure in and above the various heights of a saltmarsh canopy: a laboratory flume study. Journal of Coastal Research, 11: 1204-1209.
Shi, Z., Pethick, J.S., Burd, F. and Murphy, B., 1996. Velocity profiles in a salt marsh canopy. Geo-Marine Letters, 16: 319-323.
Steel, T.J. and Pye, K., 1997. The development of saltmarsh tidal creek networks: evidence from the UK, Guelph, Ontario, pp. 267-280.
Struyf, E., Dausse, A., Van Damme, S., Bal, K., Gribsholt, B., Boschker, H.T.S., Middelburg, J.J. and Meire, P., 2006. Tidal marshes and biogenic silica recycling at the land-sea interface. Limnology and Oceanography, 51(2): 838-846.
Tal, M. and Paola, C., 2007. Dynamic single-thread channels maintained by the interaction of flow and vegetation. Geology, 35: 347-350.
Temmerman, S., Govers, G., Meire, P. and Wartel, S., 2003a. Modelling long-term tidal marsh growth under changing tidal conditions and suspended sediment concentrations, Scheldt estuary, Belgium. Marine Geology, 193(1-2): 151-169.
Temmerman, S., Govers, G., Wartel, S. and Meire, P., 2003b. Spatial and temporal factors controlling short-term sedimentation in a salt and freshwater tidal marsh, Scheldt estuary, Belgium, SW Netherlands. Earth Surface Processes and Landforms, 28(7): 739-755.
Temmerman, S., Govers, G., Meire, P. and Wartel, S., 2004a. Simulating the long-term development of levee-basin topography on tidal marshes. Geomorphology, 63(1-2): 39-55.
Temmerman, S., Govers, G., Wartel, S. and Meire, P., 2004b. Modelling estuarine variations in tidal marsh sedimentation: response to changing sea level and suspended sediment concentrations. Marine Geology, 212: 1-19.
Temmerman, S., Bouma, T.J., Govers, G. and Lauwaet, D., 2005a. Flow paths of water and sediment in a tidal marsh: relations with marsh developmental stage and tidal inundation height. Estuaries, 28(3): 338-352.
Temmerman, S., Bouma, T.J., Govers, G., Wang, Z.B., De Vries, M.B. and Herman, P.M.J., 2005b. Impact of vegetation on flow routing and sedimentation patterns: Three-dimensional modeling for a tidal marsh, Journal of Geophysical Research, pp. F04019.
Temmerman, S., Bouma, T.J., Van de Koppel, J., Van der Wal, D., De Vries, M.B. and Herman, P.M.J., 2007. Vegetation causes channel erosion in a tidal landscape. Geology, 35(7): 631-634.
Torres, R. and Styles, R., 2007. Effects of topographic structure on salt marsh currents. Journal of Geophysical Research, 112: F02023.
Van Hulzen, J.B., Van Soelen, J. and Bouma, T.J., 2007. Morphological variation and habitat modification are strongly correlated for the autogenic ecosystem engineer Spartina anglica (common cordgrass). Estuaries and Coasts, 30(1): 1-19.
van Wesenbeeck, B.K., van de Koppel, J., Herman, P.M.J. and Bouma, T.J., 2008. Does scale-dependent feedback explain spatial complexity in salt-marsh ecosystems? Oikos, 117(1): 152-159.
Wallace, K.J., Callaway, J.C. and Zedler, J.B., 2005. Evolution of tidal creek networks in a high sedimentation environment: A 5-year experiment at Tijuana Estuary, California. Estuaries, 28(6): 795-811.
Wamsley, T.V., Cialone, M.A., Smith, J.M., Atkinson, J.H. and Rosati, J.D., 2010. The potential of wetlands in reducing storm surge. Ocean Engineering, 37(1): 59-68.
Ward, L.G., Kearney, M.S. and Stevenson, J.C., 1998. Variations in sedimentary environments and accretionary patterns in estuarine marshes undergoing rapid submergence, Chesapeake Bay. Marine Geology, 151: 111-134.
Williams, P.B. and Faber, P.M., 2001. Salt marsh restoration experience in the San Francisco Bay Estuary. Journal of Coastal Research, Special issue, 27: 203-211.
Williams, P.B., Orr, M.K. and Garrity, N.J., 2002. Hydraulic geometry: A geomorphic design tool for tidal marsh channel evolution in wetland restoration projects. Restoration Ecology, 10(3): 577-590.
Wolters, M., Bakker, J.P., Bertness, M.D., Jefferies, R.L. and Moller, I., 2005. Saltmarsh erosion and restoration in south-east England: squeezing the evidence requires realignment. Journal of Applied Ecology, 42(5): 844-851.